



SOCRAT (Seismic Simulation of Overhead Crane on Shaking Table) International Benchmark Final Report

**NUCLEAR ENERGY AGENCY
COMMITTEE ON THE SAFETY OF NUCLEAR INSTALLATIONS**

**SOCRAT (Seismic Simulation of Overhead Crane on Shaking Table)
International Benchmark Final Report**

JT03562460

ORGANISATION FOR ECONOMIC CO-OPERATION AND DEVELOPMENT

The OECD is a unique forum where the governments of 38 democracies work together to address the economic, social and environmental challenges of globalisation. The OECD is also at the forefront of efforts to understand and to help governments respond to new developments and concerns, such as corporate governance, the information economy and the challenges of an ageing population. The Organisation provides a setting where governments can compare policy experiences, seek answers to common problems, identify good practice and work to co-ordinate domestic and international policies.

The OECD member countries are: Australia, Austria, Belgium, Canada, Chile, Colombia, Costa Rica, Czechia, Denmark, Estonia, Finland, France, Germany, Greece, Hungary, Iceland, Ireland, Israel, Italy, Japan, Korea, Latvia, Lithuania, Luxembourg, Mexico, the Netherlands, New Zealand, Norway, Poland, Portugal, the Slovak Republic, Slovenia, Spain, Sweden, Switzerland, Türkiye, the United Kingdom and the United States. The European Commission takes part in the work of the OECD.

OECD Publishing disseminates widely the results of the Organisation's statistics gathering and research on economic, social and environmental issues, as well as the conventions, guidelines and standards agreed by its members.

NUCLEAR ENERGY AGENCY

The OECD Nuclear Energy Agency (NEA) was established on 1 February 1958. Current NEA membership consists of 34 countries: Argentina, Australia, Austria, Belgium, Bulgaria, Canada, Czechia, Denmark, Finland, France, Germany, Greece, Hungary, Iceland, Ireland, Italy, Japan, Korea, Luxembourg, Mexico, the Netherlands, Norway, Poland, Portugal, Romania, Russia (suspended), the Slovak Republic, Slovenia, Spain, Sweden, Switzerland, Türkiye, the United Kingdom and the United States. The European Commission and the International Atomic Energy Agency also take part in the work of the Agency.

The mission of the NEA is:

- to assist its member countries in maintaining and further developing, through international co-operation, the scientific, technological and legal bases required for a safe, environmentally friendly and economical use of nuclear energy for peaceful purposes;
- to provide authoritative assessments and to forge common understandings on key issues, as input to government decisions on nuclear energy policy and to broader OECD policy analyses in areas such as energy and sustainable development.

Specific areas of competence of the NEA include the safety and regulation of nuclear activities, radioactive waste management and decommissioning, radiological protection, nuclear science, economic and technical analyses of the nuclear fuel cycle, nuclear law and liability, and public information. The NEA Data Bank provides nuclear data and computer program services for participating countries.

This document, as well as any data and map included herein, are without prejudice to the status of or sovereignty over any territory, to the delimitation of international frontiers and boundaries and to the name of any territory, city or area.

Corrigenda to OECD publications may be found online at: www.oecd.org/about/publishing/corrigenda.htm.

© OECD 2025



Attribution 4.0 International (CC BY 4.0).

This work is made available under the Creative Commons Attribution 4.0 International licence. By using this work, you accept to be bound by the terms of this licence (<https://creativecommons.org/licenses/by/4.0>).

Attribution – you must cite the work.

Translations – you must cite the original work, identify changes to the original and add the following text: *In the event of any discrepancy between the original work and the translation, only the text of original work should be considered valid.*

Adaptations – you must cite the original work and add the following text: *This is an adaptation of an original work by the OECD. The opinions expressed and arguments employed in this adaptation should not be reported as representing the official views of the OECD or of its Member countries.*

Third-party material – the licence does not apply to third-party material in the work. If using such material, you are responsible for obtaining permission from the third party and for any claims of infringement.

You must not use the OECD logo, visual identity or cover image without express permission or suggest the OECD endorses your use of the work.

Any dispute arising under this licence shall be settled by arbitration in accordance with the Permanent Court of Arbitration (PCA) Arbitration Rules 2012. The seat of arbitration shall be Paris (France). The number of arbitrators shall be one.

Committee on the Safety of Nuclear Installations (CSNI)

The Committee on the Safety of Nuclear Installations (CSNI) addresses Nuclear Energy Agency (NEA) programmes and activities that support maintaining and advancing the scientific and technical knowledge base of the safety of nuclear installations.

The Committee constitutes a forum for the exchange of technical information and for collaboration between organisations, which can contribute, from their respective backgrounds in research, development and engineering, to its activities. It has regard to the exchange of information between member countries and safety R&D programmes of various sizes in order to keep all member countries involved in and abreast of developments in technical safety matters.

The Committee reviews the state of knowledge on important topics of nuclear safety science and techniques and of safety assessments, and ensures that operating experience is appropriately accounted for in its activities. It initiates and conducts programmes identified by these reviews and assessments in order to confirm safety, overcome discrepancies, develop improvements and reach consensus on technical issues of common interest. It promotes the co-ordination of work in different member countries that serve to maintain and enhance competence in nuclear safety matters, including the establishment of joint undertakings (e.g. joint research and data projects), and assists in the feedback of the results to participating organisations. The Committee ensures that valuable end-products of the technical reviews and analyses are provided to members in a timely manner, and made publicly available when appropriate, to support broader nuclear safety.

The Committee focuses primarily on the safety aspects of existing power reactors, other nuclear installations and new power reactors; it also considers the safety implications of scientific and technical developments of future reactor technologies and designs. Further, the scope for the Committee includes human and organisational research activities and technical developments that affect nuclear safety.

Acknowledgements

The members of the Nuclear Energy Agency (NEA) Committee on the Safety of Nuclear Installations (CSNI) Working Group on Integrity and Ageing of Components and Structures (WGIAGE) acknowledge the significant contributions of those individuals who had a key role in the SOCRAT (Seismic Simulation of Overhead CRANE on shaking Table) international benchmark and the preparation of this report. Additional thanks are extended to leading authors, steering committee members and expert committee members for supporting the SOCRAT workshops and contributing to the preparation of this report.

This report was approved at the 73rd meeting of the NEA Committee on the Safety of Nuclear Installations (CSNI) on 6 June 2023. (as recorded in the “Summary Record of the 73rd Meeting of the CSNI” [NEA/SEN/SIN(2023)1] [not publicly available]).

Leading authors

Ibrahim BITAR	Institut de radioprotection et de sûreté nucléaire (IRSN), France
Charles DROSZCZ	Géodynamique et Structure (GDS), France
Fabien GRANGE	Electricité de France (EDF), France

Contributors

Bastien BOUDY	Framatome, France
Michael BRUN	Université de Lorraine, France
Pierre LABBE	Ecole Spéciale des Travaux Publique (ESTP), France
Ioannis POLITOPOULOS	French Alternative Energies and Atomic Energy Commission (CEA), France
Jean-Mathieu RAMBACH	Géodynamique et Structure (GDS), France
Benjamin RICHARD	Institut de radioprotection et de sûreté nucléaire (IRSN), France
Emmanuel VIALLET	Electricité de France (EDF), France

Table of contents

List of abbreviations and acronyms.....	8
Executive summary	9
1. Introduction	12
1.1. Objectives and scope	12
1.2. Procedure	12
1.3. Organising committees	12
1.4. Key dates in terms of benchmark communication.....	13
1.5. Organisation of the report.....	14
2. The reference experimental campaign	15
2.1. The mock-up.....	15
2.2. Shaking table AZALEE	17
2.3. Test campaign.....	17
3. Overview of the teams participating in the benchmark.....	19
3.1. Participating teams.....	19
3.2. General information on participants’ models	21
4. Stage 1: Modelling assumptions and initial structural calibration	27
4.1. Main contents.....	27
4.2. Exercise 1: Modal calibration of the load cell block	27
4.3. Exercise 2: Modal calibration of runway beam 1	29
4.4. Exercise 3: Modal calibration of the crane	34
4.5. Exercise 5: Calibration of friction coefficients.....	39
4.6. Exercise 6: Seismic analysis – RUN 117.....	47
4.7. Exercise 7: Seismic analysis – RUN 53.....	50
5. Stage 2: Nonlinear blind simulations.....	54
5.1. Main content	54
5.2. Displacements.....	55
5.3. Accelerations – Response spectra.....	68
5.4. Support reactions	83
5.5. Comments on the results.....	95
6. Assessment of anchor capacity	97
7. Concluding remarks and recommendations	101
7.1. Conclusions.....	101
7.2. Recommendations.....	101
References.....	103

List of tables

Table 1.1. Key dates that marked the benchmark in terms of communication	13
Table 2.1. Masses of the mock-up	17
Table 3.1. Overview of the participants	19
Table 3.2. Software – numbers of nodes and elements	22

Table 3.3. Type of finite elements	23
Table 3.4. Number of models by finite element types used for beams and rails	23
Table 3.5. Damping models used by participants	24
Table 3.5. Damping models used by participant (Continued)	25
Table 4.1. Modal analysis – Load cell block A fixed – Without one-tonne mass. Exercise 1	29
Table 4.2. Modal analysis – Load cell block A fixed – With one-tonne mass. Exercise 1	29
Table 4.3. Runway beam frequencies provided by the participants for exercise 2	31
Table 4.4. Crane frequencies provided by the participants for exercise 3	36
Table 4.5. X displacements of the trolley in cm- RUN 64	42
Table 4.6. Friction coefficients	46
Table 4.7. Z displacements of Girder beams in cm- RUN 117	49
Table 5.1. Exercises of Stage 2	54

List of figures

Figure 1.1. SOCRAT benchmark agenda	12
Figure 2.1. Top view of the mock-up model of the bridge crane on the AZALÉE table	15
Figure 2.2. Components of the mock-up	15
Figure 3.1. The various fields of the participants	20
Figure 3.2. Breakdown of industrial sector participation	21
Figure 3.3. Software used by the participants	21
Figure 3.4. Number of nodes by type of elements (for the runway and girder beams) and by participants	24
Figure 3.5. Number of responses per exercise	26
Figure 4.1. Load cell block with its two plates and four cells	27
Figure 4.2. RUN 1-4-8 impact force	28
Figure 4.3. Runway beam	30
Figure 4.4. The different acceleration sensors on the runway beam	30
Figure 4.5. Experimental modal shapes of the runway beam	30
Figure 4.6. Boxplots of the frequency values provided by the participants for the runway beam	31
Figure 4.7. Reading of a box plot	32
Figure 4.8. Response spectra calculated from accelerations [g] given by participants at the AxProule location with a damping of 2%, RUN 17	32
Figure 4.9. Response spectra calculated from accelerations given by participants at the AZProule location with a damping of 2%, RUN 19	33
Figure 4.10. Bridge crane – Centred configuration	34
Figure 4.11. Distribution of the tri-axial accelerometers on the shaking tabletop	35
Figure 4.12. Sensors AxyzChariot, AxyzProule1H3, AxyzPcharge1H1	35
Figure 4.13. Experimental mode-shapes of the crane	36
Figure 4.14. Boxplots of the frequency values provided by the participants for the crane	37
Figure 4.15. Response spectra [m/s ²] of the Trolley – Run 33	38
Figure 4.16. Response spectra of the Girder beam [m/s ²] - RUN 33	38
Figure 4.17. Response spectrum on the Runway beam [m/s ²] - RUN 33	39
Figure 4.18. Sliding configuration	40
Figure 4.19. Mixed wheels configuration	40
Figure 4.20. Input pulses for Exercise 5	41
Figure 4.21. Displacement of the four wheels of the trolley, RUN 64	42
Figure 4.22. Boxplots of maximum values of wheel displacements of the trolley obtained by the participants	43
Figure 4.23. Analysis of the experimental results of RUN 64	43
Figure 4.24. Y displacement of the four wheels of the end-truck beams, RUN 62	44
Figure 4.25. Boxplots of maximum and minimum (final values) values of wheel displacements of the end-truck beams obtained by the participants, RUN 62	45
Figure 4.26. Y displacement of the four wheels of the end-truck beams, RUN 82	45
Figure 4.27. Boxplots of maximum and minimum values (final values) of wheel displacements of the end-truck beams obtained by the participants, RUN 82	46
Figure 4.28. Friction coefficients for RUNs 64-62-82	47
Figure 4.29. Decentred configuration	48
Figure 4.30. Input signal and crane configuration for RUN 117	48
Figure 4.31. Vertical displacement of the girder beams and boxplots of the max and min values, RUN 117	50
Figure 4.32. Input signal and crane configuration for RUN 53	50

Figure 4.33. Response spectra of tri-axial accelerations calculated by the participants at the trolley for RUN 53	51
Figure 4.34. Response spectra of tri-axial accelerations calculated by the participants on the girder beam for RUN 53	51
Figure 4.35. Response spectra of tri-axial accelerations calculated by the participants on the runway beam for RUN 53	52
Figure 5.1. Location of the sensors and the four load cell blocks	55
Figure 5.2. RUN 42 – Displacements of the trolley	56
Figure 5.3. RUN 42 – Displacements of the end-truck beams	57
Figure 5.4. Trolley’s trajectory - RUN 42	57
Figure 5.5. RUN 42 – Vertical displacements of the Girder beams	58
Figure 5.6. RUN 80 – Displacements of the trolley	58
Figure 5.7. RUN 80 – Displacements of the end-truck beams	59
Figure 5.8. Trolley’s trajectory - RUN 80	59
Figure 5.9. RUN 80 – Vertical displacements of the Girder beams	60
Figure 5.10. RUN 112 – Displacements of the trolley	60
Figure 5.11. RUN 112 – Displacements of the end-truck beams	61
Figure 5.12. Trolley’s trajectory - RUN 112	61
Figure 5.13. RUN 112 – Vertical displacements of the girder beams	62
Figure 5.14. RUN 128 – Displacements of the trolley	63
Figure 5.15. RUN 128 – Displacements of the end-truck beams	64
Figure 5.16. Trolley’s trajectory - RUN 128	64
Figure 5.17. RUN 128 – Vertical displacements of the girder beams	65
Figure 5.18. RUN 100 – Displacements of the trolley	65
Figure 5.19. RUN 100 – Displacements of the end-truck beams	66
Figure 5.20. Trolley’s trajectory - RUN 100	66
Figure 5.21. RUN 100 – Vertical displacements of the girder beams	67
Figure 5.22. RUN 42 – Acceleration spectra - trolley	69
Figure 5.23. RUN 42 – Acceleration spectra – Girder beam	70
Figure 5.24. RUN 42 – Acceleration spectra – Runway beam	71
Figure 5.25. RUN 80 – Acceleration spectra - Trolley	72
Figure 5.26. RUN 80 – Acceleration spectra – Girder beam	73
Figure 5.27. RUN 80 – Acceleration spectra – Runway beam	74
Figure 5.28. RUN 112 – Acceleration spectra – Girder beam	75
Figure 5.29. RUN 112 – Acceleration spectra – Runway beam	76
Figure 5.30. RUN 128 – Acceleration spectra - Trolley	77
Figure 5.31. RUN 128 – Acceleration spectra – Girder beam	78
Figure 5.32. Acceleration spectra – Runway beam	79
Figure 5.33. RUN 100 – Acceleration spectra - Trolley	80
Figure 5.34. RUN 100 – Acceleration spectra – Girder beam	81
Figure 5.35. RUN 100 – Acceleration spectra – Runway beam	82
Figure 5.36. Co-ordinate systems of load cells	83
Figure 5.37. RUN 42 – Support reactions – min/max	84
Figure 5.38. RUN 42 – Support reactions	85
Figure 5.39. RUN 80 – Support reactions – min/max	86
Figure 5.40. RUN 80 – Support reactions	87
Figure 5.41. RUN 112 – Support reactions – min/max	88
Figure 5.42. RUN 112 – Support reactions	89
Figure 5.43. RUN 128 – Support reactions – min/max	90
Figure 5.44. RUN 128 – Support reactions	91
Figure 5.45. RUN 100 – Support reactions – min/max	92
Figure 5.46. RUN 100 – Support reactions	93
Figure 5.47. All RUNs – Centred crane configurations - Support reactions	94
Figure 5.48. All RUNs – Decentred crane configurations - Support reactions	94
Figure 5.49. Final position of the crane for RUN 80	96
Figure 5.50. Support reactions in load cell blocks B and C in X and Z directions	96
Figure 6.1. Types of anchoring	99
Figure 6.2. Anchorage verifications	100

List of abbreviations and acronyms

AFPS	Association Française de génie Parasismique (France)
ASN	Autorité de sûreté nucléaire (French Nuclear Safety Authority)
CAPS	CSNI activity proposal sheet
CEA	Commissariat à l'énergie atomique et aux énergies alternatives (Alternative Energies and Atomic Energy Commission, France)
CSNI	Committee on the Safety of Nuclear Installations (NEA)
EDF	Electricité de France
EDP	Engineering demand parameters
FFT	Fast Fourier Transform
GDS	Géodynamique et Structure (Consultant engineering firm specialising in civil and earthquake engineering, France)
IRSN	Institut de Radioprotection et de Sûreté Nucléaire (French Institute for Radiological Protection and Nuclear Safety [ASNR since January 2025])
NEA	Nuclear Energy Agency
PSA	Probabilistic safety assessment
SOCRAT	Seismic Simulation of Overhead CRANE on shaking Table
WGIAGE	Working Group on Integrity and Ageing of Components and Structures (NEA)

Executive summary

Background

Bridge cranes, which are components that handle devices designed to lift and transfer heavy loads, are widely used in the nuclear sector. Assessing the dynamic behaviour of bridge cranes is essential for nuclear safety. Indeed, despite favorable seismic experience feedback (EPRI, 2005a; EPRI, 2005b) within the context of seismic level 1 probabilistic safety assessment (PSA) studies, these devices have been identified as significant contributors to the probability of core meltdown in case of failure.

Moreover, modelling the mechanical behaviour of such a device under seismic load is a challenging scientific and engineering exercise due to the importance of accounting for nonlinearities such as frictional sliding and local shocks. The behaviour of the anchoring system seems to be one of the possible causes of failure of this component when loading is assumed beyond the design conditions. Consequently, it is necessary to enhance knowledge on the dynamic behaviour of this component to fully understand its response to earthquakes and to assess the efforts transmitted by the crane to the anchors.

Objective

Within this scope, the SOCRAT (Seismic Simulation of Overhead CRANE on shaking Table) international benchmark, organised by the Institute for Radiological Protection and Nuclear Safety (France's Institut de radioprotection et de sûreté nucléaire, or IRSN) and Electricity of France (EDF) under the umbrella of the Nuclear Energy Agency (NEA), was launched in June 2020. Its initial objectives were: (i) to identify best modelling practices of bridge crane devices in the beyond design domain; and (ii) to identify relevant failure criteria. Due to the tight schedule and the heavy content of the benchmark, the second objective was just partially addressed by evaluating the forces transmitted to the anchor as they seem to be one of the primary causes of failure.

Work performed

An experimental campaign on a scaled model of an overhead bridge crane was carried out in 2015 on the AZALEE shaking table operated by CEA in Saclay, France, the outputs of which are now encompassed in a large experimental database. These experimental data were used to perform a series of exercises as part of the benchmark. On the one hand, some of these data were used by the participants to characterise and calibrate their models. On the other hand, other data were used to evaluate the predictive capacity of their models.

More precisely, the SOCRAT benchmark consisted of two major stages, each lasting approximately six to seven months. Stage 1 was focused on the development and characterisation of the numerical models. General information on the numerical models developed by the participants as well as specific information on how the models describe local contacts and shocks was collected. Thus, six exercises were proposed to guide the participants in calibrating their models at the component level (load cell blocks, runway beams) and at the crane scale. Each exercise is related to a run test and the experimental results of that run have been made available to the participants. At the end of Stage 1, an online workshop was organised for the participants to share their results and prepare Stage 2. After calibrating their models, participants were requested to perform five prediction exercises, without the experimental results. Hence, Stage 2 aimed at evaluating,

by blind simulations, the nonlinear response of the crane models under high intensity seismic loads.

Twenty participants officially registered in teams and nineteen sent results for at least one exercise. Most participants came from European countries, while three came from Asian countries. The participants spanned a variety of fields, from academia to general industry and the nuclear sector.

The benchmark concluded with a workshop, at EDF Lab Saclay (France), on 21-23 March 2022, in which the participating teams exchanged views and discussed their modelling assumptions and results. The steering committee collected all the results submitted by the participants and compared and analysed them. The findings were shared with the participants during the workshop and led to fruitful discussions. As a result, some of the best practices for modelling overhead bridge cranes under seismic loading were identified. The participants were also invited to contribute to a special session dedicated to the SOCRAT benchmark at the occasion of SMiRT26 conference in Berlin, Germany, in July 2022 (Brun et al., 2022; Rodriguez et al., 2022; Borgerhoff et al., 2022; Bahr et al., 2022; Ghadimi et al., 2022; Colomb et al., 2022).

Results and their significance

The global dynamics of overhead cranes can be captured with different models, from the simplest to the most complex. Indeed, a fine description of the crane geometry does not seem necessary when a good description of the physics is reached (local shocks, sliding), if the goal of the exercise is to obtain accelerations, displacements or support reactions. However, it was not possible to reproduce exactly the dynamic response of the crane, especially the final position of each component, since this problem is highly nonlinear. Indeed, considering the different models and methodologies used by the participants, scattering in the engineering demand parameters (EDPs) (maximum accelerations, support reactions, displacements) was assessed, and appeared to be significant. Moreover, linear calculations appeared to be conservative since sliding and shock are the main sources of energy dissipation.

Recommendations

Following this benchmark, some recommendations can be drawn.

It appears that friction between wheels and rails has a significant influence; therefore, it is recommended that a sensitivity study be performed considering: (1) a range of values for the friction coefficients; and (2) the asymmetry of the friction coefficients (between two rails facing each other, and between the rails of the girder beam and of the runway beams).

In addition, given the significant influence of gaps between the wheels and the lateral faces of the rails, and the lack of knowledge of the initial position of the crane, it is recommended to carry out a sensitivity study taking into account (1) different lateral gaps between faces of the wheels and rails (symmetric and non-symmetric for two rails facing each other), and (2) different initial positions of the crane (centred, decentred).

Since reduced models (fewer elements, discrete elements) can provide relevant results, sensitivity/statistical studies should be performed to consider the uncertain quantities (friction coefficients, gaps [wheels/rails], initial position, material properties, damping).

Also, regarding the differential motion of the crane supports, which have an impact on the crane behaviour and can lead to the uplift of the trolley, it is recommended to consider the vertical motion imposed on the supports: at least by considering rigidly connected supports (rigid body) and imposing the rotational motion and the vertical motion (in addition to the

horizontal motion) to the rigidly connected supports; at best by imposing the differential motion on each support (multi-supported analysis).

Finally, regarding the question of damping, if the modelling of viscous damping is done with a global Rayleigh model, and if the computations are done in the absolute reference frame, the use of a damping proportional to the mass can induce an overdamping of the rigid body modes caused by the sliding between the moving parts of the crane. In this case, the damping matrix should be only proportional to the stiffness matrix.

1. Introduction

1.1. Objectives and scope

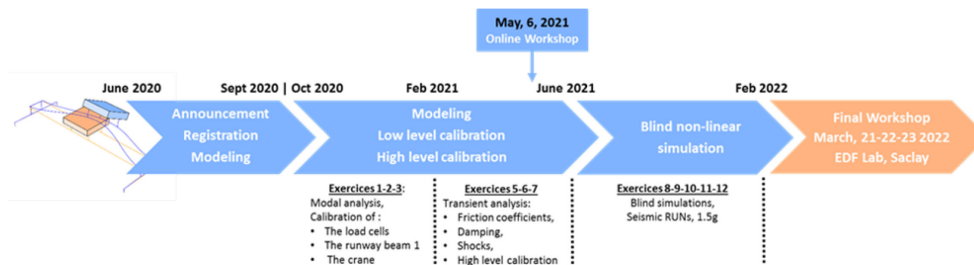
The objective of the SOCRAT international benchmark, launched in June 2020 and organised by the Institut de Radioprotection et de Sûreté Nucléaire (IRSN) and Electricité de France (EDF), under the umbrella of the NEA, is: (i) to identify best modelling practices for bridge crane devices beyond the design domain and; (ii) to identify relevant failure criteria.

An experimental campaign on a scaled model of an overhead bridge crane was carried out in 2015 on the AZALEE shaking table of CEA in France and the results have allowed to create a large experimental database. Some of these data have been used by participants to characterise and calibrate their models and in Stage 1 of the benchmark; other data have been used to assess the predictive capacity of their models in Stage 2. The benchmark was concluded by a workshop in which the different participants gathered to exchange views and discuss their modelling assumptions and results. In this way, some best practices for modelling overhead cranes bridge under seismic loading were identified.

1.2. Procedure

The SOCRAT international benchmark consisted of two major stages, namely Stage 1 and Stage 2, and two scientific workshops. The participants' results remained anonymous. Figure 1.1 gives an overview of the benchmark schedule.

Figure 1.1. SOCRAT benchmark agenda



1.3. Organising committees

To ensure the successful conduct of the benchmark, two committees were set: a steering committee and an expert committee.

Steering committee

The main tasks of the committee are to organise the benchmark, both scientifically and logistically, and to interact with the participants to answer their questions. The committee met regularly to discuss progress and decide on next steps.

This committee is composed of:

- Fabien GRANGE – EDF
- Ibrahim BITAR – IRSN
- Benjamin RICHARD – IRSN
- Charles DROSZCZ – Géodynamique & Structure
- Jean-Mathieu RAMBACH – Géodynamique & Structure

Expert committee

The main tasks of the expert committee are to participate in the technical exchange meetings that follow each computation stage with the benchmark steering committee to provide technical expertise and advice on how to interpret the different results. Essentially, this has consisted of participating in three to four meetings along the benchmark.

- Michael BRUN – Université de Lorraine
- Bastien BOUDY – Framatome
- Pierre LABBE – ESTP
- Pierre Alain NAZE – Géodynamique & Structure
- Ioannis POLITOPOLOUS – CEA
- Emmanuel VIALLET – EDF

1.4. Key dates in terms of benchmark communication

The key dates that marked the benchmark in terms of communication are summarised in Table 1.1.

Table 1.1. Key dates that marked the benchmark in terms of communication

Date	Title	Reference
25 March 2019	The first CAPS submission to the WGIAGE seismic subgroup	-
20 September 2019	Early announcement of the benchmark at the French national conference organised by the French Association of Earthquake Engineering (AFPS)	Bitar et al., 2019
10 June 2020	Early announcement of the benchmark to the Scientific and Technical Committee of the French Association of Earthquake Engineering (AFPS)	-
6 June 2021	First online workshop gathering the two organising committees and the participants	-
2 October 2021	Presentation of the benchmark at the 17 th World Conference on Earthquake Engineering (17WCEE)	Bitar et al., 2021
21-23 March 2022	Final workshop of the SOCRAT benchmark	-
11 July 2022	Special session on the work done in the SOCRAT benchmark at the SMiRT26 conference	Brun et al., 2022; Rodriguez et al., 2022; Borgerhoff et al., 2022; Bahr et al., 2022; Ghadimi et al., 2022; Colomb et al., 2022

In addition to these events, it is worth mentioning the various reports to the NEA Working Group on Integrity and Ageing of Components and Structures (WGIAGE) made on the following dates:

- 28 May 2019
- 1 October 2019
- 12 March 2020
- 24 September 2020

- 16 March 2021
- 7 September 2021
- 15 March 2022
- 15 September 2022

1.5. Organisation of the report

This report is constructed as follows. Chapter 2 provides a brief presentation of the experimental campaign of the bridge crane mock-up. Chapter 3 presents an overview of the teams participating in the benchmark. Statistical studies of the participants and of the software used as well as on the main characteristics of their models are presented. Chapter 4 offers an overview of the first stage of the benchmark focusing on model characterisation exercises based on the experimental results provided to the participants. The statements of the exercises one to seven are recalled and the results of the participants are presented, compared and analysed. Chapter 5 describes the results of the second stage of the benchmark concerning the blind prediction of the models. Chapter 6 compares the demand in terms of force at the anchorages of the crane and the resistant capacity of common types of anchors. Finally, Chapter 7 outlines the topics of interest discussed during the closing workshop as well as the conclusions and recommendations resulting from the benchmark.

2. The reference experimental campaign

2.1. The mock-up

The mock-up is a simplified 1/5 scaled model of a 22.5 m long overhead bridge crane; see Figure 2.1. Its dimensions were derived from the dimensions of an actual bridge crane at the Phenix research reactor (Feau et al., 2015). Given that the shake table is a 6 m x 6 m table, this scale is the biggest scale that could have been considered.

Figure 2.1. Top view of the mock-up model of the bridge crane on the AZALÉE table



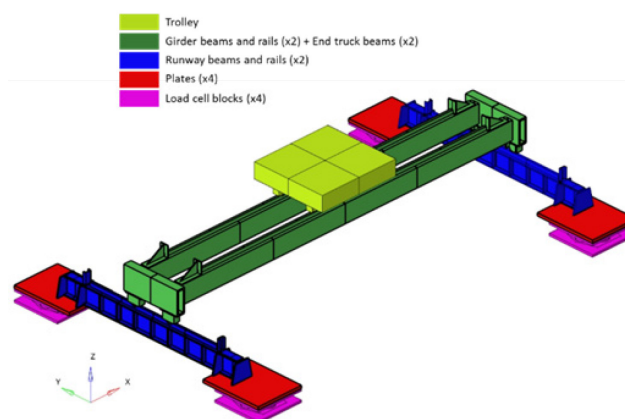
The crane is composed of the following components:

- a trolley
- rails and wheels
- two girder beams
- two end-truck beams
- two runway beams
- four load cell blocks

Each load cell block is composed of four load cells.

These different components are shown in the following pictures:

Figure 2.2. Components of the mock-up



One important issue for the design of the model was the determination of the similarity law presented in (EPRI, 2005a). The mock-up of the bridge crane is made up of several components: a trolley, rails, wheels, girder beams, end-truck beams, runway beams, and load cell blocks included in the supports between the shaking table upper plate and the bridge crane mock-up.

The trolley is a large metal basket on wheels, used for transporting heavy or large items. It has been made by assembling three metal plates 1 015 mm x 1 100 mm of thick 70 mm.

The girder beams are reconstituted welded beams supporting the trolley. They have the following characteristics:

- a rectangular hollow section of 110 mm x 250 mm x 30 mm;
- a length of 5 m;
- central axes that are separated by a distance equal to 50 cm.

The runway beams are reconstituted welded beams supporting the whole bridge. They have the following characteristics:

- IPN 240 beams stiffened by 15 mm thick plates positioned every 23.5 cm;
- a length of 2 m;
- runway beams that are each supported on two stiffening plates of thickness 15 mm at their ends.

The end trucks are reconstituted welded beams linking the two main girder beams. They have the following characteristics:

- a hollow rectangular section of 110 mm x 320 mm x 20 mm;
- a length of 0.8 m;
- a thickness of the section flanges and vertical walls of 30 mm.

Rails (girder beams/trolley and runway beams/end-truck beams) are also included with the mock-up to reproduce rolling and sliding nonlinearities, but they are not representative of industrial bridges as they are not industrial components, and they are made from unhardened steel. The girder rails are used to ensure the runway of the trolley. They have a rectangular cross-section of 60 x 40 mm. On the other hand, the runway rails are used to ensure the runway of the end trucks. They have a rectangular cross-section of 50 mm x 30 mm.

The trolley and the end trucks beams are equipped with single-piece track wheels with a diameter of 105 mm and a width of 35 mm. The trolley is supported by four wheels. Each end-truck beam is supported by two wheels. The wheels can be used in two different configurations. They can be fixed so that they cannot anymore rotate on the rails. In this case, they are called “fixed wheels” or “false wheels”. In real bridge cranes, the drive wheels (those connected to the motor) are considered as fixed wheels when the motor is turned off. Otherwise, the wheels can roll, and, in this case, they are called “roller wheels”.

For the trolley, the wheels are placed in such a way as to face the inner side of the rails. On the contrary, for the end-truck beams, the wheels are placed opposite to the outside face of the rails.

The wheels boxes are fixed under the trolley by M10 bolts and under the end-truck beams by M10 threaded rods. The false wheels and the wheels boxes are made of 42CD4 steel. Otherwise, only the roller wheels are made of 100Cr6 steel.

To accurately determine the reaction forces on the runway beams, six-axis load cells are put between the runway beam supports and the shaking table to record the forces at the interface between the bridge and its supporting structure. Each support is equipped with four suitably designed load cells. Each load cell can measure the three forces as well as the three moments. A load cell has a diameter of 175 mm and a height of 116 mm. It is made of stainless steel. Each group of four load cells is called ‘load cell block’. The load cells are fixed by means of two 30 mm thick plates. The first is fixed to the table and the second is fixed to the runway beam supports by means of four screws.

The reference system of axis is defined as follows:

- Ox is the horizontal axis parallel to the girder beams.
- Oy is the horizontal axis parallel to the runway beams.
- Oz is the vertical axis.

The total weight on board, which is the sum of the weights of the trolley, the girder beams, the runway beams, and the four load cell blocks, is 5 656 kg.

Table 2.1. Masses of the mock-up

Component	Mass (Kg)
Trolley	1880
2 × Girder beams + end trucks + rails	1820
2 × Runway beams + rails	980
4 × Load cell blocks	976
Total	5656

2.2. Shaking table AZALEE

The AZALEE shaking table can be considered as a semi-rigid block with a total mass of 25 tonnes fixed to eight hydraulic actuators, four in the horizontal directions and four in the vertical. The distance between two vertical actuators is 4 m. The distance between two horizontal actuators is 7.06 m. The axis of horizontal actuators is located at 0.52 m below the upper face of the shaking table. It can be assumed that there is no need to consider the shaking table model since the accelerations measured at the table are considered to be the input accelerations for the mock-up.

2.3. Test campaign

The test campaign was carried out in several phases, including modal identification of the mock-up and of each component and seismic tests in different mock-up configurations. Hammer shocks and white noise tests were performed for initial modal characterisation of the bridge crane mock-up and its components. Impulsion tests were conducted for friction characterisation. Bi-axial and tri-axial seismic tests were conducted to study the dynamic behaviour of the bridge crane mock-up.

Several configurations of the entire bridge crane are considered. There are three factors which determine the nature of the mock-up configuration: the initial position, the different wheel condition and the general state.

1. Initial positions: the initial position of the trolley on the girder beams and the initial position of the end trucks on the runway beams:

- a) Centred initial position: it consisted in positioning the girder beams and the trolley in the middle of the length of the rails that support them.
 - b) Decentred initial position: it consisted in positioning the girder beams and the trolley at a quarter of the length of the rails supporting them.
2. Different wheel conditions (roller or sliding):
- a) Sliding wheels: all wheels are fixed. They can only move by frictional sliding.
 - b) Mixed wheels: half of the wheels are rollers, and the other half are fixed.
3. General state:
- a) Blocked state: it consists in making the system linear by immobilising all the moving elements in all directions, each element being centred on its rail track. The girder beams were therefore connected to the runway beams laterally by clamps and vertically by straps. The trolley was connected to the girder beams by lateral clamps.
 - b) Free state: no blocking conditions are applied on the moving components of the mock-up.

To ensure that the seismic loading is representative of the type of excitation seen in practice by bridge cranes during earthquakes, narrowband seismic signals were selected for this campaign. They are based on recordings made during the Chüetsu-oki earthquake in July 2007 at the Kashiwazaki-Kariwa nuclear power plant. The signals were measured at a height of 22 metres in the turbine building of unit five of the power plant, during the main impact. The accelerograms have been adapted to coincide with the main frequency of the crane mock-up in the Y direction which is 8.3 Hz. They also have been filtered to lower energy beyond 20 Hz.

Seismic loads were applied in horizontal biaxial (X, Y) as well as tri-axial (X, Y, Z) mode. Seismic tests were conducted either incrementally, by increasing the level of acceleration until extreme displacements (blocking of the wheels on the rails, reaching the maximum displacement on the wire sensors) or until wheel shocks occur on the rails, or by repeating the same signal to study the dispersion of the system's response. In the latter case, the moving parts of the mock-up (trolley and end-truck beams) are systematically returned to their initial position for each new RUN.

3. Overview of the teams participating in the benchmark

3.1. Participating teams

The table below presents the 19 participants who sent results for at least one exercise. Among the registered participants, three sent nothing and thus their participation was not considered. The participants are mainly from European countries, and three participants are from Asian countries. Seven countries had participants from different areas, from academia to general industry and nuclear industry - most participants were consulting companies, some represent nuclear power plant operators or energy producers, and there were also participants from nuclear regulatory authorities and from a software company (see Figure 3.1 and Figure 3.2).

Table 3.1. Overview of the participants

Society	Country	Continent	Field 1	Field 2	Field 3	Software 1	Software 2
Atomic Energy Regulatory Board (AERB)	India	Asia	Industrial - Nuclear	Nuclear regulatory authority	-	ABAQUS	-
Atomic Energy Regulatory Board (AERB)	India	Asia	Industrial - Nuclear	Nuclear regulatory authority	-	ABAQUS	-
ATR	France	Europe	Industrial - General	Eng. - Consulting company	-	OPTISTRUCT	RADIOSS
CETIM Senlis	France	Europe	Industrial - Nuclear	-	-	CODE_ASTER	-
CKTI-Vibroseism Ltd.	Russia	Europe	Industrial - General	-	-	ANSYS	-
CNAM - Conservatoire national des arts et métiers	France	Europe	Academic	-	-	MATLAB	-
EGIS	France	Europe	Industrial - General	Eng. - Consulting company	-	ANSYS	-
ENSI Team B&H - Basler & Hofmann AG	Switzerland	Europe	Industrial - Nuclear	Nuclear regulatory authority	Eng. - Consulting company	LS-DYNA	-
ENSI Team Principia/SPI	Spain	Europe	Industrial - Nuclear	Nuclear regulatory authority	Eng. - Consulting company	ABAQUS	-
ENSI Team SPI - Stangenberg & Partners Consulting Engineers	Germany	Europe	Industrial - Nuclear	Nuclear regulatory authority	Eng. - Consulting company	SOFiSTiK	-
ESI	France	Europe	Industrial - General	Eng. - Consulting company	Software company	VPS	-
ESTP - Ecole Spéciale des Travaux Publics	France	Europe	Academic	-	-	LS-DYNA	ANSYS
F4E - ESTEYCO	Spain	Europe	Industrial - Nuclear	Eng. - Consulting company	-	ABAQUS	-
GRS - Gesellschaft für Anlagen und Reaktorsicherheit	Germany	Europe	Industrial - Nuclear	-	-	LS-DYNA	-
INSA Lyon / Laboratoire GEOMAS	France	Europe	Academic	-	-	MATLAB	-
Nuclear Power Corporation of India Ltd.	India	Asia	Industrial - Nuclear	Nuclear power plant operator	-	-	-
OKG Aktiebolag	Sweden	Europe	Industrial - Nuclear	Nuclear power plant operator	-	ANSYS	-
ORANO	France	Europe	Industrial - Nuclear	Eng. - Consulting company	-	ANSYS	-
TECHNIA (Formerly Scanscot Technology AB)	Sweden	Europe	Industrial - Nuclear	Eng. - Consulting company	-	ABAQUS	-

Each of the 19 teams consists of the following organisations:

- AERB - Atomic Energy Regulatory Board - Team 1 (India)
- AERB - Atomic Energy Regulatory Board - Team 2 (India)
- ATR (France)
- CETIM Senlis (France)
- CKTI - Vibroseism Ltd. (Russia)
- CNAM - Conservatoire National des Arts et Métiers (France)
- EGIS (France)
- ENSI Team B&H - Basler & Hofmann AG (Switzerland)
- ENSI Team Principia (Spain)
- ENSI Team SPI - Stangenberg & Partners Consulting Engineers (Germany)
- ESI (France)
- ESTP - Ecole Spéciale des Travaux Publics (France)
- F4E – ESTEYCO (Spain)
- GRS - Gesellschaft für Anlagen und Reaktorsicherheit (Germany)
- INSA Lyon / Laboratoire GEOMAS (France)
- Nuclear Power Corporation of India Ltd. (India)
- OKG Aktiebolag (Sweden)
- ORANO (France)
- TECHNIA (Scanscot Technology formerly) (Sweden)

Figure 3.1. The various fields of the participants

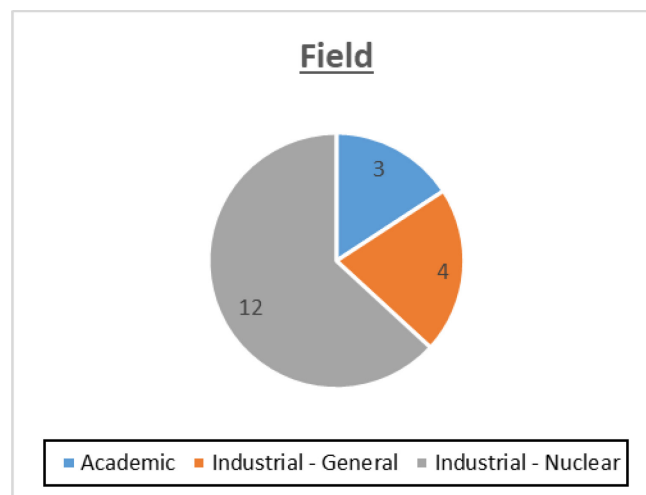
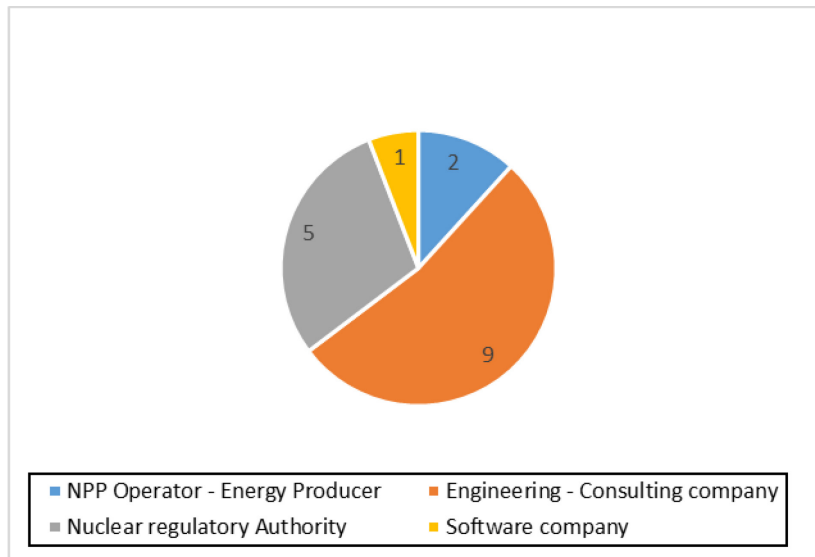
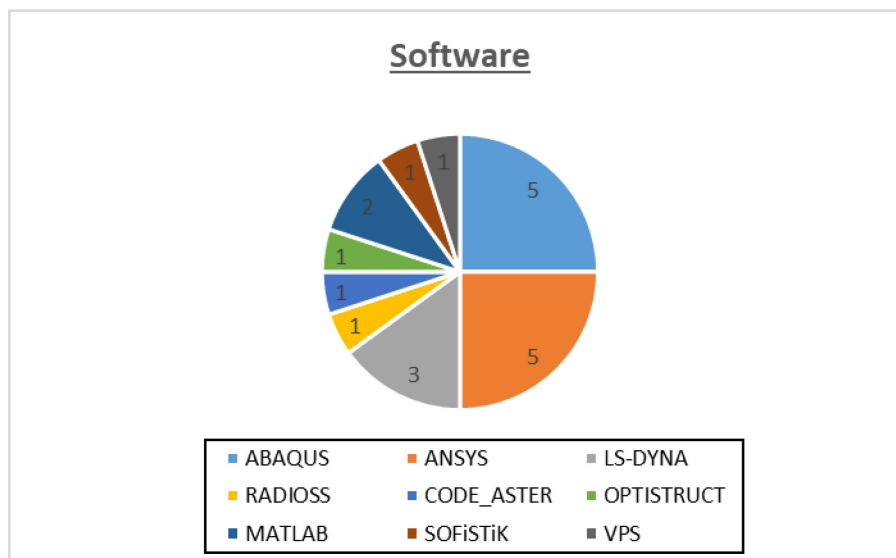


Figure 3.2. Breakdown of industrial sector participation

Regarding the software used (see Figure 3.3) it is worth mentioning that nine different software packages were used, which reflects a rich diversity. The two main pieces of software are ANSYS and ABAQUS, followed by LS-DYNA, Code aster and others.

Figure 3.3. Software used by the participants

3.2. General information on participants' models

The following tables sum up general information about the participants' models. They are intended to facilitate the analysis of participants' results.

This information was provided during the benchmark (mostly during Stage 1 calibration), but some participants provided information only at the end of the benchmark, during the final workshop. Some participants provided results but incomplete information on their model; they still appear in these tables.

3.2.1. Software and number of nodes and elements

Table 3.2 summarises the available information on the models and software used by each participant.

Table 3.2. Software – numbers of nodes and elements

N° Team	Software	Type	Analyse type	Contact model	Number of dof	Number of elements	Number of nodes	Total mass
1	ANSYS	Commercial			81597	15065	20676	5.680
2*	ABAQUS	Commercial	Explicit	Abaqus connector friction	320142-X	52149-12976	53433-13532	5.600
3	SOFiSTiK	Commercial	Implicit	Moving Springs	43754	8468	8854	5.647
4	MATLAB	Commercial			606	74	101	5.700
5	LS-DYNA	Commercial	Explicit	Automatic surf. to surf. contact**	113142	20168	21841	5.915
6	ANSYS	Commercial			24981	3070	5071	5.672
7	LS-DYNA	Commercial	Explicit	Automatic single surface		95084	145564	5.641
8	ABAQUS	Commercial	Implicit			10000	11500	
9	ANSYS	Commercial			47202	9711	9779	5.656
10	CODE ASTER	Open source				146000	573000	
11	ABAQUS							
12	RADIOSS + OptiStruct	Commercial	Explicit	Contact TYPE 7 - Stiffness formulation	484230	181307	143626	5.668
13	LS-DYNA	Commercial				16078	18770	5.645
14	ANSYS		Implicit	conta174 - targe170		9912		
15	Cast3m + MATLAB	Commercial	Implicit/Explicit	Lagrange multipliers (non-smoothed contact dynamics)	2544 (explicit)/119976 (implicit)	355 (explicit)/22788 (implicit)	836 (explicit)/39964 (implicit)	5.076 (without load cell blocks)
16	ABAQUS	Commercial			290000	56000	77000	5.656
17								
18	ABAQUS					10000	10436	

* Participant n°2 worked with two models, one with a refined mesh for modal analyses, with more nodes and elements, and another one with a larger mesh for transient analyses. Hence the two numbers of nodes/elements/dof.

** LS-DYNA contact algorithm based on the penalty method.

3.2.2. Type of finite elements

Table 3.3 summarises the available information on the finite element types by bridge crane component.

Table 3.3. Type of finite elements

N° Team	Runway beam finite element	Runway rail finite element	Girder beam finite element	Girder rail finite element	End-truck finite element	Wheels finite element	Wheels supp finite element	Load cell finite element	Trolley finite element
1	shell + solid (plates)	solid	shell	solid	shell	solid	shell	solid + shell (plates)	solid
2	shell	shell	shell	shell	shell	connector	shell	connector	shell
3	shell	beam	shell	beam	shell	not modelled	moving spring	spring	shell
4	beam (Euler-Bernoulli)	mass nodes	beam (Euler-Bernoulli)	mass nodes	beam (Euler-Bernoulli)	mass node	beam (Euler-Bernoulli)	springs (12 dof)	stiff structure + nodal mass
5	shell	solid	shell	solid	shell	not modelled	beam	beam	shell
6	shell (181)	shell (181)	shell (181)	shell (181)	shell (181)	solid (186) + shell (181)	shell (181)	shell (181)	solid (186)
7	solid	solid	solid	solid	solid	solid	solid	discrete beam	solid
8	beam		beam		beam			shell (plates)	mass
9	shell	solid	shell	solid	shell	solid	rigid beam + mass	rigid beam + springs	rigid beam + mass
10	solid (H20)	solid (H20)	solid (H20)	solid (H20)	solid (H20)	contact only	rigid	bushing	solid (H20)
11									
12	shell	solid	solid	solid	solid	solid	solid	shell	solid
13	shell	solid	shell	solid	shell	solid	shell	discrete	solid
14	shell (281)	not modelled	shell (281)	not modelled	shell (281)		rigid	matrix27	shell (281)
15	solid	solid	solid	solid	solid	solid	solid	beam	solid
16	shell	solid	shell	solid	shell	solid	solid	shell + connectors	solid
17									
18	shell	shell	shell	shell	shell				

Considering only the beams and the rails (in blue, all the crane except load cells, wheels, trolley), the table below sums up the elements chosen by the participants with an increasing level of complexity, and the number of participants who have chosen these kinds of elements.

Table 3.4. Number of models by finite element types used for beams and rails

Runway and girder beams		Runway and girder rails	
Numbers of participants	Type of elements	Numbers of participants	Type of elements
2	Beam	2	Not modelled (or mass nodes)
10	Shell	1	Not modelled
		1	Beam
		3	Shell
		5	Solid
3	Solid	3	Solid

Most of the participants used shell elements for the beams (10) and most of these participants used solid elements for the rails (5).

Participant n°12, who used both shell and solid elements for the beams (shell for the runway beams and solids for the girder beams), does not appear in the table.

Two participants used only beam elements, three only shell elements and three only solid elements.

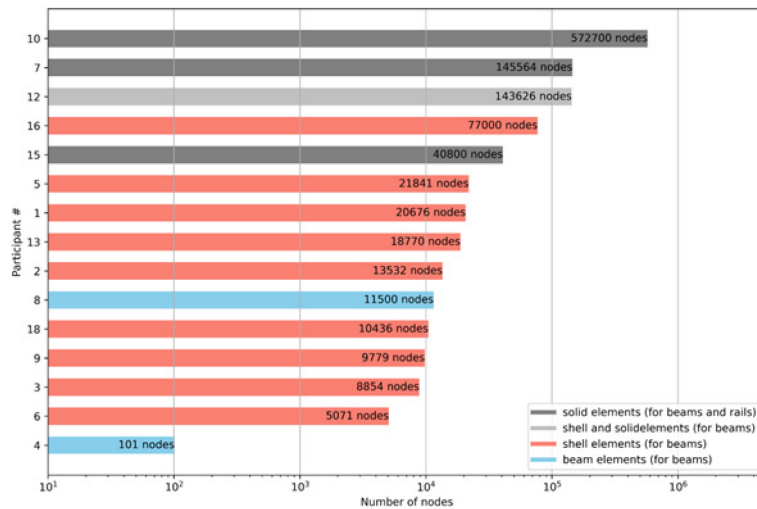
Models with beam elements (for the beams) are among the lightest; they have between 100 and 11 500 nodes.

Models with solid elements (for beams and rails) are the heaviest and have 40 800 to 57 3000 nodes.

Models with shell elements (for the beams) have between 5 000 and 77 000 elements.

The figure below sums up the number of nodes by type of elements (for the beams) and by participants (for participants who provided the number of nodes).

Figure 3.4. Number of nodes by type of elements (for the runway and girder beams) and by participants



3.2.1. Damping

Table 3.5 lists the available information on the different damping models with the corresponding rates used by the participants.

Table 3.5. Damping models used by participants

N° Team	Software	Analyse type	Damping	Damping rate	Comment
1	ANSYS	-	-	-	
2	ABAQUS	Explicit	Rayleigh damping	1%	
3	SOFISTIK	Implicit	Rayleigh damping	1%	
4	MATLAB	-	-	-	
5	LS-DYNA	Explicit	Band width-limited damping	2%	It does not damp the rigid body's modes
6	ANSYS	-	-	-	-
7	LS-DYNA	Explicit	Definition of a mass weighted nodal damping by a constant damping factor that is determined by analysis of experimental output data	-	-
8	ABAQUS	Implicit	Rayleigh damping	-	-
9	ANSYS	-	-	-	-

Table 3.5. Damping models used by participant (Continued)

N° Team	Software	Analyse type	Damping	Damping rate	Comment
10	CODE ASTER	-	Use of modal damping within the Craig-Bampton method	5% (modes < 100 Hz)	No damping added on rigid body modes Controlled damping on higher frequencies
11		-	-	-	-
12	RADIOSS + OptiStruct	-	-	-	No damping
13	LS-DYNA	-	-	-	-
14	ANSYS	Implicit	Rayleigh damping	4%	Additional viscous damping provided by the nonlinear contact modelling is activated
15	Cast3m + MATLAB	Implicit/Explicit	Rayleigh damping (implicit)	5%	No damping for the explicit domain
16	ABAQUS	-	-	-	-
17	-	-	-	-	-
18	-	-	-	-	-

One particular reason for using Rayleigh's damping was that it damps rigid body modes relative to the nonlinear phenomena of sliding. Indeed, the guide of the French Nuclear Safety Authority (ASN Guide 2/01) requires removing the coefficient proportional to the mass matrix as soon as the system is allowed to slide so as not to overdamp the rigid body modes.

On the one hand, some practices consist in optimising the calculation methodology by integrating the modal damping ratio with the modal synthesis method of the components. It consists in identifying the different sub-assemblies of the cranes, and in determining a super-element for each sub-assembly with an associated modal base and a damping ratio by mode; then in rebuilding a complete model with these super-elements and the interfaces made up of contacts, and couplings, and in performing a classical time history computation.

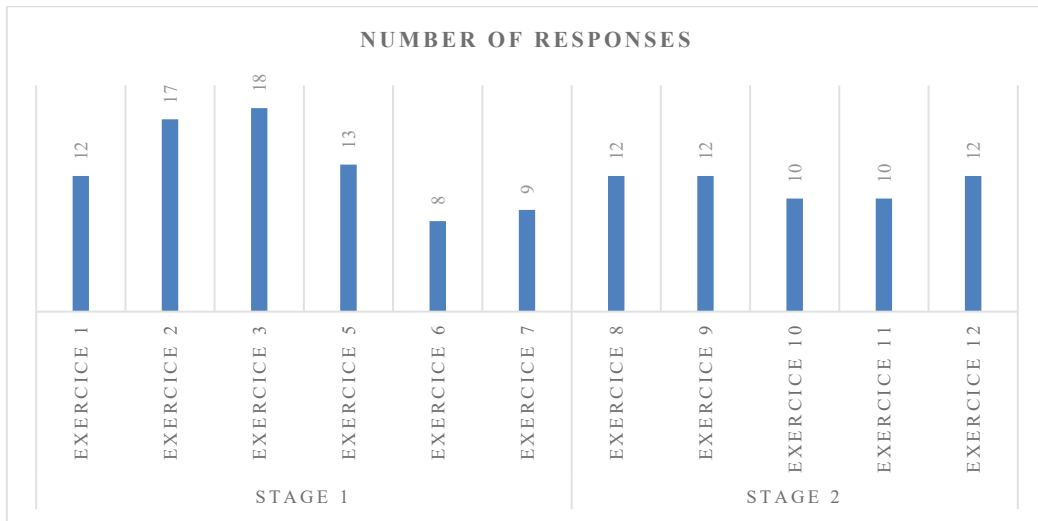
On the other hand, when using an explicit integration scheme, the application of Rayleigh damping requires the reduction of the computational time step, which can be already small. Therefore, a modelling practice in this case is to divide the computation into explicit and implicit domains and apply damping only on the domain that will be solved implicitly, while the other domain to be solved explicitly includes the contacts where nonlinear models will be added containing inherent damping mechanisms.

3.2.2. Overview of participants' results

The participants' results remain anonymous to ensure loyalty in processing the synthesis of the results.

Figure 3.5 shows the response rate and the results received for each exercise. Exercises 2 and 3 (modal analyses of the runway beams and the crane, calibration of the properties using eigen modes of the mock-up, *cf.* 4.1) received the most responses. Then there are approximately 10 to 11 results on average per exercise from 5 to 12.

Figure 3.5. Number of responses per exercise



4. Stage 1: Modelling assumptions and initial structural calibration

4.1. Main contents

The Stage 1 includes the six following exercises¹:

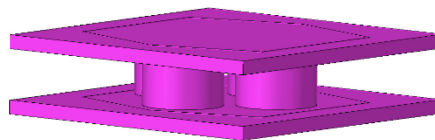
- Exercise 1 - Modal calibration: Load cell block A.
- Exercise 2 - Modal calibration: Runway beam 1.
- Exercise 3 - Modal calibration: Bridge crane mock-up.
- Exercise 5 - Friction coefficient and damping ratio.
- Exercise 6 - Local shocks parameters.
- Exercise 7 - High level calibration.

This report presents the above-mentioned exercises as well as the results provided by the participants.

4.2. Exercise 1: Modal calibration of the load cell block

Participants were invited to carry out a modal analysis of the load cell block A composed of its inferior plate, four load cells, and its superior plate. Modal analyses were asked in free-free conditions, with the inferior plate anchored to the table, with and without a one-tonne mass fixed at the top of the superior plate.

Figure 4.1. Load cell block with its two plates and four cells



Moreover, participants were invited to provide the results of transient analyses, considering input hammer shock test results, in the X direction (RUN 4), Y direction (RUN 1) and in the Z direction (RUN 8). For these transient analyses, the load cell block with a one-tonne mass fixed on the upper plate is considered (see Figure 4.2).

Acceleration time evolutions were asked:

- On the lower face of the upper plate, at the place of the sensor AxyzBlocsup1 (X direction only for RUN 4, Y for RUN 1 and Z for RUN 8).
- On the upper face of the lower plate, at the place of the sensor AxyzBlocinf1 (X direction only for RUN 4, Y for RUN 1 and Z for RUN 8).

4.2.1. Input data

For RUN 1, transient analysis of the {load cell block + mass of one tonne} is performed taking as input the impact force in the middle of the upper plate according to Y.

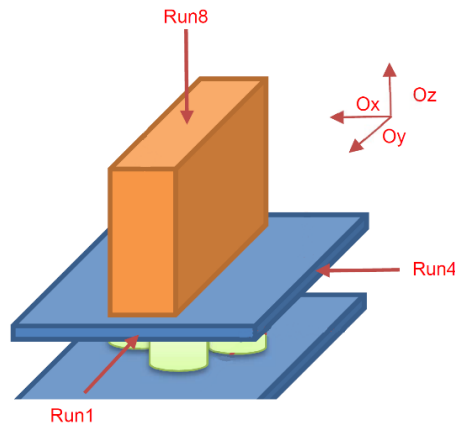
¹ After launching the benchmark, the steering committee decided to delete exercise 4, therefore it is not shown in the description above.

For RUN 4, transient analysis is carried out taking as input the impact force in the middle of the upper plate according to X.

For RUN 8, transient analysis is carried out taking as input the impact force in the middle of the upper mass according to Z.

The Figure 4.2 shows the load cell block with its mass of one tonne, and the location of impact forces for the 3 RUNs.

Figure 4.2. RUN 1-4-8 impact force



The natural frequencies of the load cells are not provided; only the “constructor” stiffnesses of the latter are given. Participants are free to choose how to model these load cell blocks consisting of a bottom plate, four load cells and a top plate. These stiffnesses are identified as parameters that influence the modal content of the rolling beam and the complete bridge; they are, therefore, possible calibration parameters.

After discussion with the expert committee, it was decided that the request of accelerations calculating from hammer shock simulations is not very relevant. Concerning the hammer tests, many uncertainties remain on the intensity of the signal, the energy transferred to the structure, the direction of the impact, etc. Therefore, the analysis of the numerically calculated signal, expressed in terms of acceleration and compared to the one measured during the tests, is not relevant (in shape and in amplitude). It would be preferable to focus on the modal characterisation of a load cell block (with the mass of a tonne, which is approximatively a quarter of the crane mass), and to ask the participants for the natural frequencies of this system. This recommendation was followed by the benchmark organisers. To do this, participants were free to perform modal analyses and/or transient hammer simulations (and for this, they were provided with the input and output signals of the tests). It was then up to them to perform the necessary processing (FFT, transfer function), to give the fundamental frequencies of the load cell block.

4.2.2. Results of participants

Modal analyses

Results of modal analyses carried out by the participants are tabulated below. These results highlight a rather high variability; the first frequencies for the load cell block without the one-tonne mass are around 400 Hz and around 120 Hz with the mass, but standard deviations associated with these results remain quite high.

Table 4.1. Modal analysis – Load cell block A fixed – Without one-tonne mass. Exercise 1

Participant \ Mode	1	2	3	4
2	221.1	258.8	258.8	454.8
3	413.2	415.8	415.8	423.0
4	446.4	664.0	664.0	932.0
5	389.0	419.0	419.0	
6	417.2	424.2	424.2	449.1
7	359.0	369.0	371.0	394.0
8	475.6	483.4	505.9	
10	385.5	395.1		
11	204.6	270.9	359.2	469.5
12	454.0	472.0	488.0	
16	348.0	348.0	362.0	436.0
17	285.0	334.0	334.0	357.0
18	62.0	243.0	473.0	700.0
Median	386	395	417	449
Stand. Dev.	120	112	103	185

Table 4.2. Modal analysis – Load cell block A fixed – With one-tonne mass. Exercise 1

Participant \ Mode	1	2	3	4
1	110.2	125.9	129.3	-
4	148.7	160.5	186.1	332.9
5	114.5	122.4	184.7	448.5
9	72.5	113.8	113.8	-
10	126.0	132.0	180.0	349.0
14	111.7	131.7	316.3	355.4
16	55.9	57.7	143.1	166.5
Median	112	126	180	349
Stand. Dev.	32	31	67	102

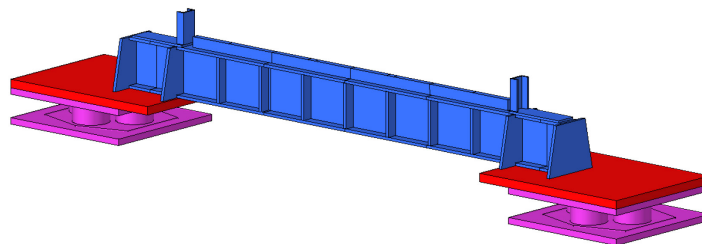
Transient analysis – Hammer shocks

Few participants carried out the transient analysis (hammer shocks) and the results obtained are difficult to interpret (in the case where the signal provided is very short) and scattered.

4.3. Exercise 2: Modal calibration of runway beam 1

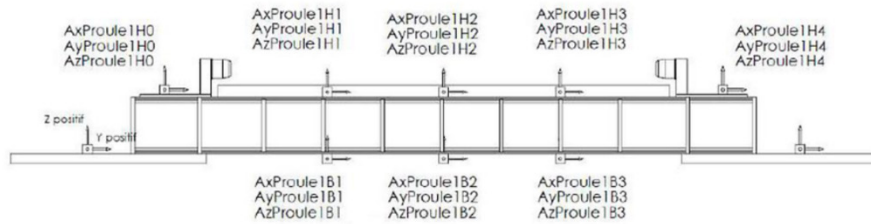
4.3.1. Statement of the exercise

Participants were invited to carry out a modal analysis of the runway beam 1 and its two plates plus two load cell blocks, in free-free conditions, and considering the two load cell blocks anchored to the table.

Figure 4.3. Runway beam

They were asked for pictures of the modal shapes they obtained, as well as the first four eigen frequencies. Moreover, participants were invited to provide the results of transient analyses, considering as input a white noise in acceleration, in the X direction (RUN 17), Y direction (RUN 18) and in the Z direction (RUN 19). Accelerations (time evolutions) were asked at the top centre of the Runway beam (AProule1H2 sensor, see Figure 4.3) in the X direction (RUN 17), Y direction (RUN 18) and in the Z direction (RUN 19). Figure 4.4 shows the position of the acceleration sensors.

Figure 4.4. The different acceleration sensors on the runway beam



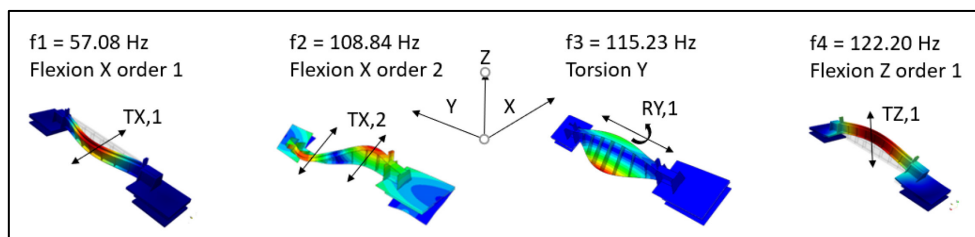
4.3.2. Input data

The four first experimental modes of the runway beam (+ two load cell blocks) anchored to the shaking table, calculated by the CEA, were provided to the participants. Eigen frequencies and modal shapes were given:

- $f_1 = f_{x,1} = 57.1$ Hz;
- $f_2 = f_{x,2} = 108.8$ Hz;
- $f_3 = f_y = 115.2$ Hz;
- $f_4 = f_z = 122.2$ Hz.

Modal shapes of these modes are given in Figure 4.5.

Figure 4.5. Experimental modal shapes of the runway beam



4.3.3. Results of participants

The results of participants regarding exercise 2 are provided in Table 4.3. Eighteen participants provided values. Red values indicate that modes are inverted; its means for instance that mode n°3 (Rotation Y – 115 Hz) comes at a lower frequency than mode n°2 (Translation X order 2 – 108.8 Hz) for participant one.

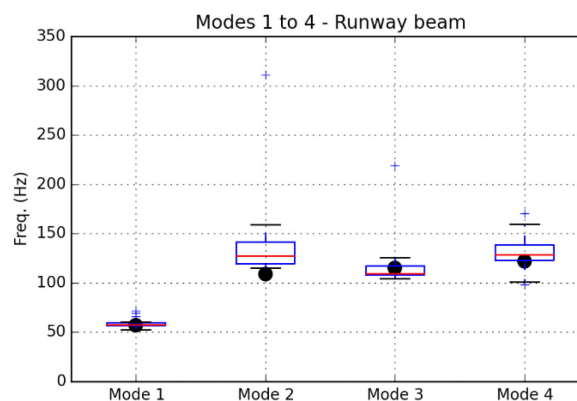
Table 4.3. Runway beam frequencies provided by the participants for exercise 2

Team	Mode 1 X1	Mode 2 X2	Mode 3 RY	Mode 4 Z
Mock-up	57.1	108.8	115.2	122.2
1	57.1	115.4	108.9	151.8
2	59.2	120.3	106.4	126.9
3	56.7	124.4	108.7	123.3
4	58.0	150.5		141.0
5	57.7	119.1		98.4
6	52.6	126.4	107.0	128.9
7	66.2	159.2	123.3	160.0
8	56.9	116.5	108.6	122.2
9	59.1	119.1	116.8	106.6
10	71.5	148.9	125.9	137.9
11	60.0		116.0	101.2
12	57.1	127.5	104.6	123.3
13	60.4			170.7
14	69.7	134.8	118.0	132.5
15				
16	57.3	129.3	108.9	133.6
17	57.6	132.8	110.1	128.5
18	53.3	311.0	219.0	
Median	57.70	127.51	109.52	128.70
Stand. Dev.	5.12	48.49	29.18	19.62

For each mode, the following percentiles of the sample values provided by the participants are also presented:

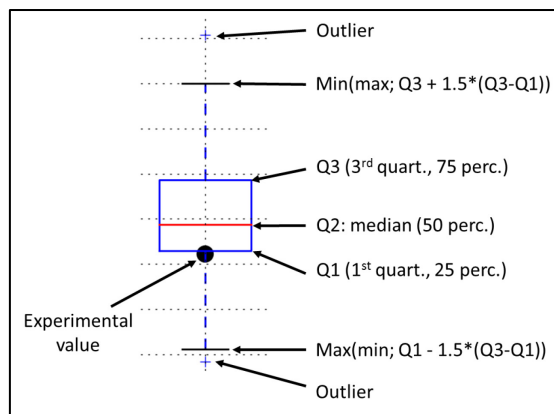
- Q₀: min
- Q₁: 25% percentile = first quartile
- Q₂: 50% percentile = median of second quartile
- Q₃: 75% percentile = third quartile
- Q₄: max

The boxplot Figure 4.6 contains statistical information about the sample of values provided by the participants.

Figure 4.6. Boxplots of the frequency values provided by the participants for the runway beam

The red line in Figure 4.6 is the median. The blue box is between the quartiles 1 and 3, that is between the 25 and 75 percentiles, which means that half of the participants' values are in the blue boxes. A quarter of the participants' values are below the blue box, and a quarter above. The black lines show the limit between the considered values (for computing the fractiles Q_1 , Q_2 , Q_3) and the outliers, when outliers are considered. When it is the case, a great value is considered as an outlier if it is greater than $Q_3 + 1.5 \cdot (Q_3 - Q_1)$, which is $Q_3 - Q_1$. In the same way a small value is an outlier if it is lower than $Q_1 - 1.5 \cdot (Q_3 - Q_1)$, which is $Q_3 - Q_1$. The following sketch can help with reading the provided boxplots:

Figure 4.7. Reading of a box plot

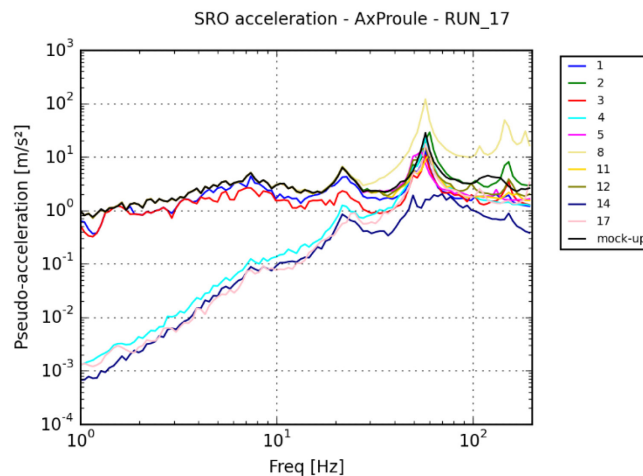


If outliers are not considered, the black lines from above and below are respectively the max and the min (Q_4 and Q_0) from the full sample.

Transient analyses – RUN 17 - White noise X

Spectra calculated from accelerations AxProule (see Figure 4.4 for the location of the sensor) provided by participants are plotted for 2% of damping in Figure 4.8. These spectra are plotted between 1 Hz and 200 Hz in logarithmic scale.

Figure 4.8. Response spectra calculated from accelerations [g] given by participants at the AxProule location with a damping of 2%, RUN 17



Response spectra provided by three participants are much lower, suggesting that these accelerations are relative and not absolute accelerations. Likewise, one or the other make it possible to appreciate the proper frequencies of the system by visualising the peaks of the spectra.

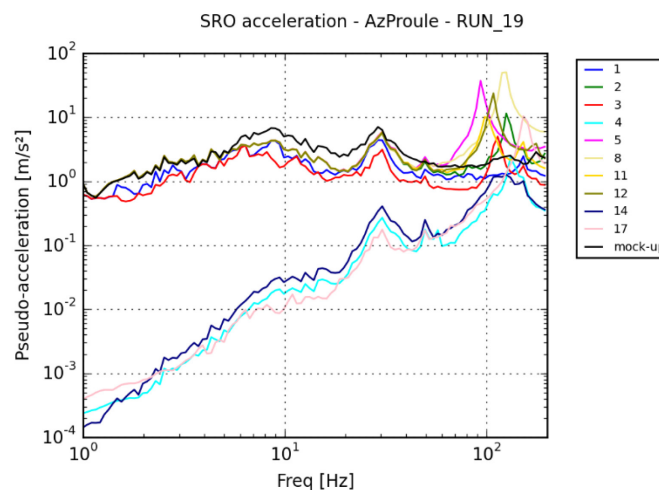
Transient analyses – RUN 18 - White noise Y

Results of the transient computations in the Y direction are judged to be irrelevant and difficult to interpret. Natural frequencies obtained by these calculations are not obvious, and some results are abnormal and therefore are considered outliers. Since direction Y is the axis of the runway beam, the fundamental mode along Y is less important for the overall behaviour of the bridge than the two bending modes in X and Z directions.

Transient analyses – RUN 19 - White noise Z

Spectra were calculated from accelerations at AzProule and provided by each participant (see Figure 4.4 for the location of the sensor) are plotted for 2% of damping in Figure 4.9). These spectra are plotted between 1 Hz and 200 Hz in logarithmic scale.

Figure 4.9. Response spectra calculated from accelerations given by participants at the AZProule location with a damping of 2%, RUN 19



4.3.4. Comments on the results

RUN 17 – X direction:

Each spectrum (calculated from participant's results and from the mock-up) highlights a strong peak around 60 Hz, which corresponds to fundamental modes along X.

Another peak can be noticed at lower frequencies, around 20 Hz, for each spectrum, and another one at higher frequencies, which could correspond to a coupling between horizontal and vertical directions.

It should be noted that modes n°2 and n°3 are often inverted in order of appearance in the modal basis, assuming that the modes are ordered according to their associated frequency.

RUN 19 – Z direction:

Firstly, spectrum highlights a strong peak between 98 Hz and 130 Hz, which correspond to fundamental vertical modes calculated by the participants. It can be noticed that the mock-

up spectrum (black line) does not show a strong peak around 122 Hz (vertical experimental mode), but a rather smooth one, and another one around 150 or 170 Hz.

Secondly, each spectrum (calculated from participant's results and from the mock-up) highlights another peak at 30 Hz.

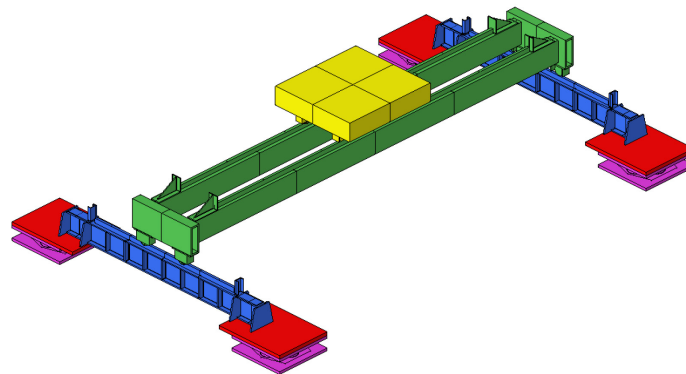
For the values of the principal modes, the values given by the performers of the experimental campaign, which is the CEA, following their experimental modal analysis, are taken as reference.

4.4. Exercise 3: Modal calibration of the crane

4.4.1. Statement of the exercise

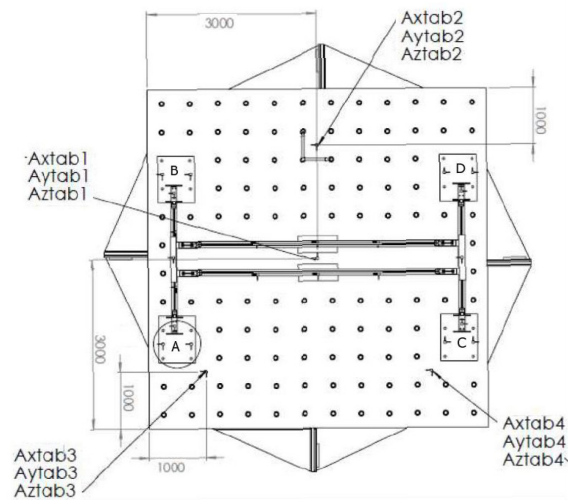
Participants were invited to carry out a modal analysis of the whole crane, with its four load cell blocks, in the centred position, in free-free conditions, and considering the four load cell blocks anchored to the table. In this exercise, only the centred configuration of the bridge (centred trolley and centred girder beams, *cf.* picture below) was considered.

Figure 4.10. Bridge crane – Centred configuration



Participants were also asked to perform a transient analysis assuming that the bridge crane and its load cell blocks are fixed on the table and taking as input a given white noise signal, RUN 33. Figure 4.10 shows the position of the tri-axial accelerometer (Axtab1, Aytab1, Aztab1 on the centre of the table) on the shaking tabletop.

Figure 4.11. Distribution of the tri-axial accelerometers on the shaking tabletop



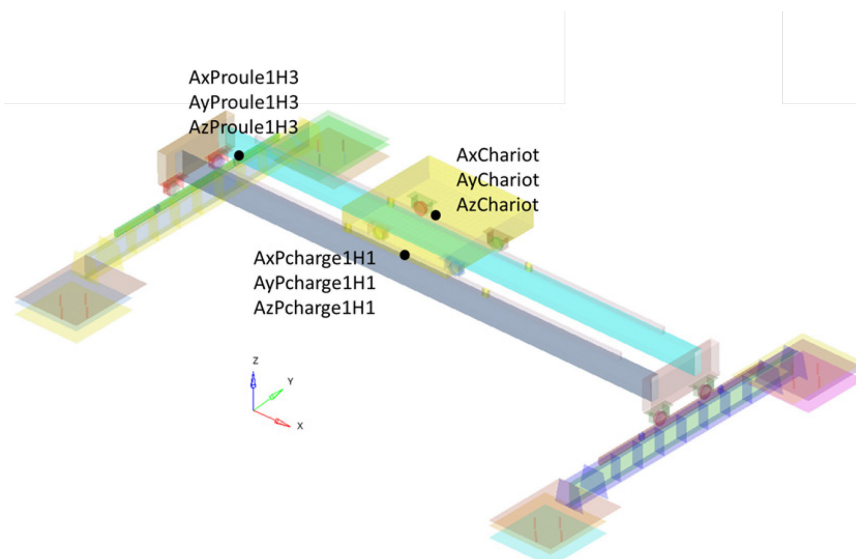
Wheels cannot slide or roll in this RUN since they are considered fixed to the rails.

Participants were asked for the following accelerations:

- acceleration time histories at points AxChariot, AyChariot, AzChariot on the trolley;
- acceleration time histories at points AxPcharge1H1, AyPcharge1H1, AzPcharge1H1 on the girder beams;
- acceleration time histories at points AxProule1H3, AyProule1H3, AzProule1H3 on the runway beam.

These different sensors are represented on Figure 4.12.

Figure 4.12. Sensors AxyzChariot, AxyzProule1H3, AxyzPcharge1H1



Moreover, participants were invited to perform a modal analysis of the crane without the four load cell blocks (optional exercise 3b).

For exercise 3, wheels had to be fixed to the rails, so that modal analyses could be performed. During the experimental campaign, wheels were fixed to the rails by using clamps.

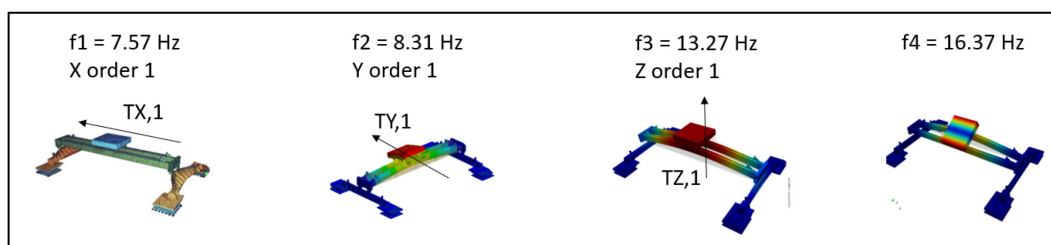
4.4.2. Input data

The first four experimental modes obtained by the CEA were given so participants could calibrate their models:

- $f_1 = f_x = 7.57$ Hz;
- $f_2 = f_y = 8.31$ Hz;
- $f_3 = f_z = 13.27$ Hz;
- $f_4 = 16.37$ Hz.

Associated mode-shapes to these modes are given in Figure 4.13.

Figure 4.13. Experimental mode-shapes of the crane



4.4.3. Results of participants

The results of participants for exercise 3 are provided in Table 4.4.

Table 4.4. Crane frequencies provided by the participants for exercise 3

Team	Mode 1 X	Mode 2 Y	Mode 3 Z	Mode 4
Mock-up	7.6	8.3	13.3	16.24
1	8.37	8.29	13.66	15.88
2	7.90	8.61	13.91	15.64
3	7.76	7.71	13.11	15.88
4	7.67	8.28	13.88	16.40
5	7.50	8.70	11.80	18.70
6	7.73	8.21	14.10	19.85
7	10.92	9.51	14.52	21.13
8	7.60	8.30	13.28	17.98
9	7.55	8.46	12.87	16.52
10	9.45	8.86	14.06	17.33
11	7.52	8.32	12.54	19.20
12	8.21	8.58	13.17	17.91
13	11.62	8.77	14.80	22.66
14	8.27	8.42	12.83	23.46
15	8.30	10.00	13.30	
16	8.30	7.90	13.70	16.30
17	7.67	8.86	12.94	18.67
18	5.45	7.12	13.62	14.72
Median	7.83	8.44	13.46	17.91
Stand. Dev.	1.35	0.63	0.73	2.50

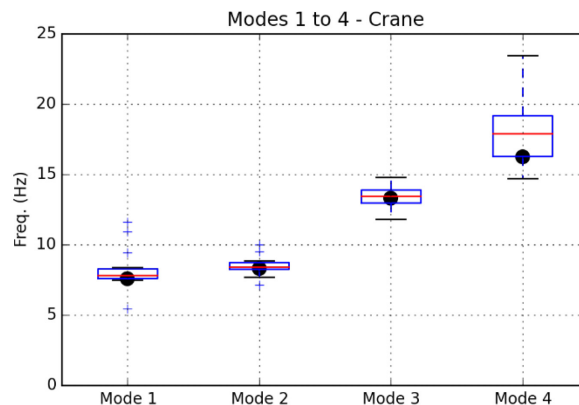
Modal analysis anchored

For each mode, the following percentiles are also presented:

- Q₀: min
- Q₁: 25% percentile = first quartile
- Q₂: 50% percentile = median of second quartile
- Q₃: 75% percentile = third quartile
- Q₄: max

The boxplot Figure 4.14 contains statistical information about the sample of values provided by the participants.

Figure 4.14. Boxplots of the frequency values provided by the participants for the crane



The red line in Figure 4.14 is the median. The blue box is between the quartiles 1 and 3, which is between the 25 and 75 percentiles, which means that half of the participants' values are in the blue boxes. A quarter of the participants' values are below the blue box, and a quarter above. The black lines show the limit between the considered values (for computing the fractiles Q₁, Q₂, Q₃) and the outliers, when outliers are considered.

4.4.4. Comments on the results

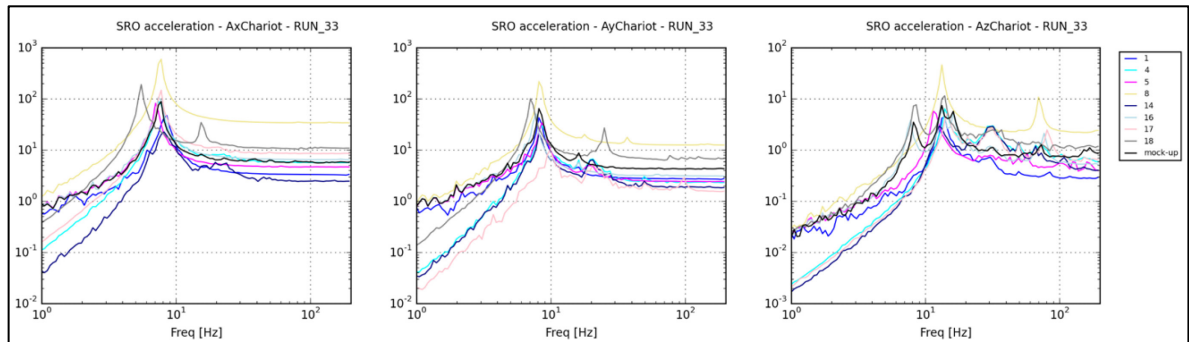
Results are globally satisfying since experimental values (black dots) are not so far from the median value, and inside (almost) the blue box. There are still some outliers for modes n°1 and n°2.

Trolley

The response spectra of the measurements as well as the few results received from the participants are shown in Figure 4.15. Spectra calculated from signals from AChariot in the X and Y directions highlight a strong peak around 8 Hz, which correspond to the natural horizontal frequencies of the crane.

In the vertical direction, spectra highlight a peak between 10 Hz and 20 Hz, with a higher variability, which corresponds to the vertical mode (13 Hz). Some spectra also present another peak at higher frequencies. The mock-up spectra (black line) present a peak at 8 Hz, which can denote a coupling between vertical and horizontal directions. None of the participants' spectra show this peak.

Figure 4.15. Response spectra [m/s²] of the Trolley – Run 33

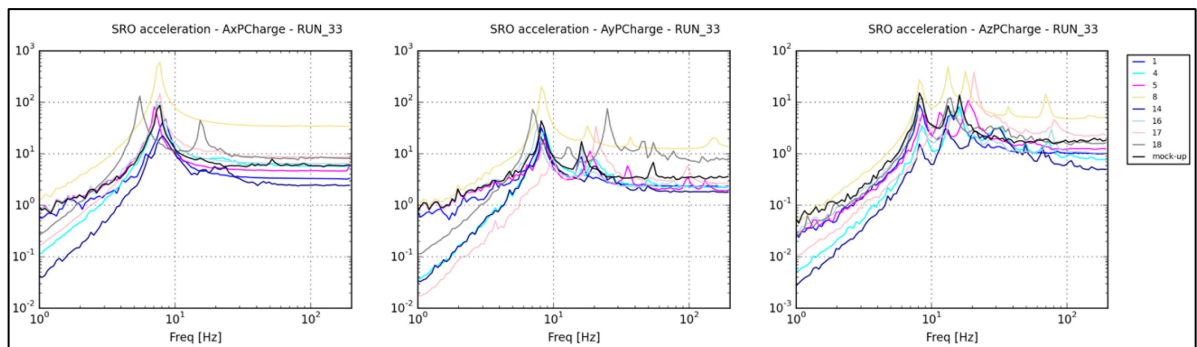


Girder beam

Spectra in horizontal directions calculated on the girder beam present the same peaks at 8 Hz, which correspond to the horizontal modes. Spectra in Y present several peaks at higher frequencies, around 15-20 Hz (possibly a coupling with Z-direction), and higher, see Figure 4.16.

In the vertical direction, peaks are visible between 10 Hz and 20 Hz (vertical mode), and at 8 Hz (coupling H-V).

Figure 4.16. Response spectra of the Girder beam [m/s²] - RUN 33



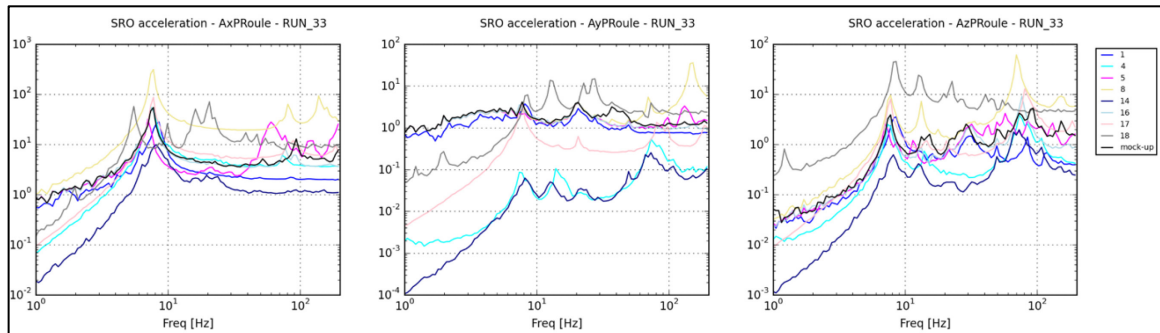
Runway beam

Spectra in the X direction calculated on the runway beam present a peak at 8 Hz, which corresponds to the mode along X, see Figure 4.17.

Spectra in the Y direction do not present a peak corresponding to the Y mode (or a very small peak) since the global mode of the crane along Y (at 8 Hz) corresponds above all the bending of the girder beams (above the runway beams), and not to a deformation of the runway beams (as a reminder, these beams are along Y).

In the vertical direction, peaks are visible at 8 Hz, which corresponds to a coupling with the X mode, around 13 Hz, which corresponds to the Z mode, and at higher frequencies with a high variability among participants, which corresponds to higher order modes of the beam.

Figure 4.17. Response spectrum on the Runway beam [m/s²] - RUN 33



4.5. Exercise 5: Calibration of friction coefficients

4.5.1. Statement of the exercise

The objective of this exercise is to calibrate friction coefficients between the wheels and the rails. It means wheels are no longer fixed to the rails, they can slide or roll.

Participants were asked to perform three transient analyses with unidirectional pulses as inputs:

- RUN 64: Pulse in X
- RUN 62 and 82: Pulses in Y

RUN 64 is meant to calibrate friction coefficient between wheels of the trolley and rails of the girder beams and RUN 62-82 are meant to calibrate friction coefficients between wheels of the end-truck beam and rails of runway beams.

Required results are the following:

- RUN 64 (X): Displacements according to X of the trolley (Chariot)
- RUN 62-82 (Y): Displacements according to Y of the end-truck beams (Sommiers)

RUN 64 and 62 are carried out with all the wheels fixed to their support, which means that they can only slide and not roll. This wheel configuration is called “Sliding configuration”.

RUN 82 is carried out with half of the wheels that can only slide (fixed to their support), and half of the wheels that can roll. This configuration is called “Mixed configuration”.

These two wheels configurations are presented in Figure 4.18 and Figure 4.19.

Figure 4.18. Sliding configuration

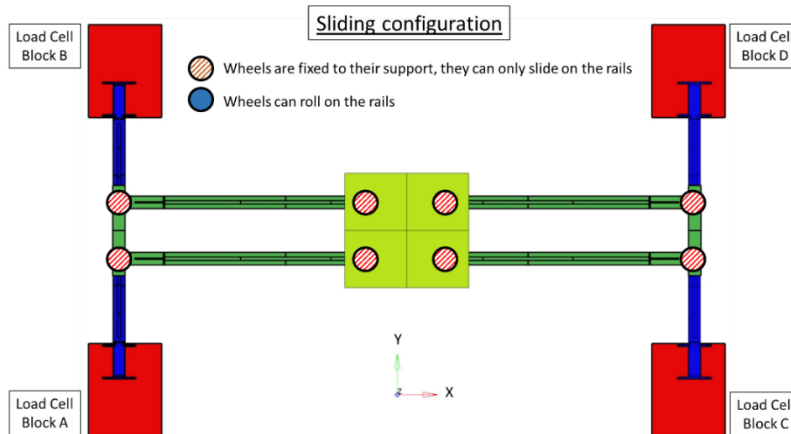
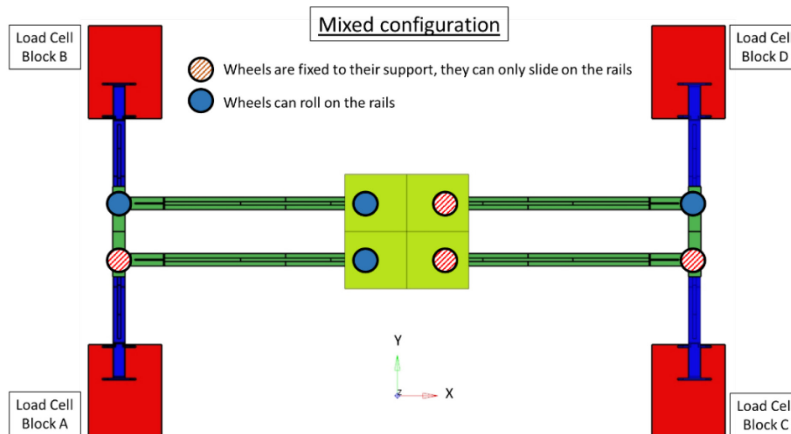


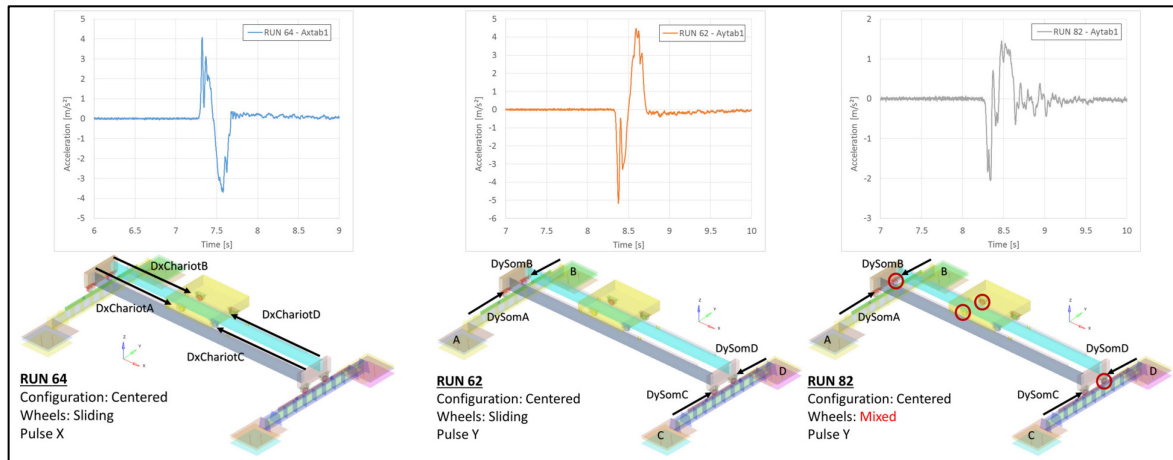
Figure 4.19. Mixed wheels configuration



4.5.2. Input data

Input signals (pulses) given to the participants are accelerations measured by Atab1 (Axtab1 for RUN 64 and Aytab1 for RUN 62 and 82). These signals are plotted in Figure 4.20.

Figure 4.20. Input pulses for Exercise 5



4.5.3. Results of participants

For RUN 64 in the X direction, displacements calculated by the participants are compared to the one measured by sensors of the mock-up called DxChariotA, DxChariotB, DxChariotC and DxChariotD.

Displacements in Y direction for RUN 62 and 82 are compared to the one from sensors DySomA, DySomB, DySomC and DySomD of the mock-up.

4.5.4. Comments on the results

RUN 64 in X direction

The median X displacements of the trolley, among the participant's results, are around 8.0 mm for the maximal value (in the X+ direction), for the four wheels. The standard deviation associated with this set of values is around 3.2 mm. This median displacement is in great accordance with the one measured on the mock-up, also around 8.0 mm for the four wheels.

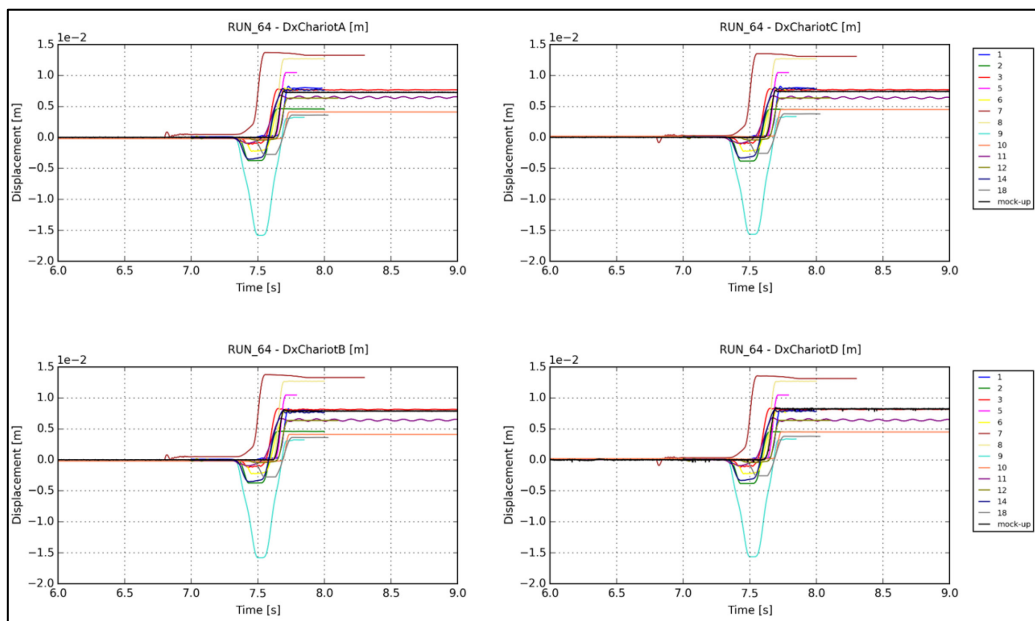
Table 4.5. X displacements of the trolley in cm- RUN 64

Team	DxChariotA min	DxChariotB min	DxChariotC min	DxChariotD min	DxChariotA max	DxChariotB max	DxChariotC max	DxChariotD max
mock-up	-0.01	-0.01	-0.01	-0.05	0.75	0.81	0.76	0.84
1	0.00	0.00	0.00	0.00	0.82	0.82	0.82	0.82
2	-0.38	-0.38	-0.38	-0.38	0.46	0.46	0.45	0.45
3	-0.11	-0.12	-0.11	-0.12	0.78	0.83	0.79	0.83
5	0.00	0.00	0.00	0.00	1.05	1.05	1.05	1.05
6	-0.23	-0.23	-0.23	-0.23	0.80	0.80	0.80	0.80
7	0.00	0.00	-0.08	-0.09	1.37	1.38	1.35	1.36
8	-0.02	-0.02	-0.02	-0.02	1.27	1.27	1.27	1.27
9	-1.58	-1.58	-1.57	-1.57	0.32	0.32	0.34	0.34
10	-0.03	-0.03	0.00	0.00	0.41	0.41	0.45	0.45
11	-0.10	-0.10	-0.09	-0.10	0.68	0.67	0.67	0.68
12	-0.05	-0.05	-0.04	-0.04	0.63	0.64	0.64	0.64
14	-0.35	-0.35	-0.33	-0.33	0.79	0.79	0.81	0.81
18	-0.28	-0.28	-0.26	-0.26	0.36	0.36	0.38	0.38
median	-0.10	-0.10	-0.09	-0.10	0.78	0.79	0.79	0.80
std dev	0.42	0.42	0.42	0.42	0.33	0.33	0.32	0.32

This maximal displacement corresponds to the displacement obtained at the end of the RUN since the shape of the signal in the X+ direction is a step; once the maximal displacement is obtained, the trolley stops.

Graphs in Figure 4.21 show the evolutions of these displacements. It can be observed that most of the participants wanted to obtain the same maximal displacement in the mock-up, around 8.0 mm (which is the objective of this model calibration exercise).

Figure 4.21. Displacement of the four wheels of the trolley, RUN 64

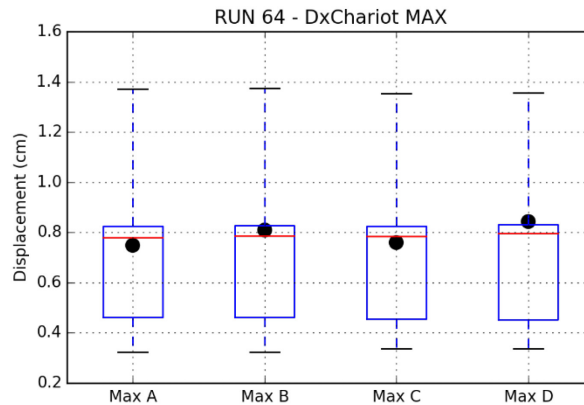


Nevertheless, some participants have maximum displacements far enough from the model, with an error factor between x0.5 (Team 9) and x1.7 (Team 7).

Although trolley displacement of the mock-up is only along the X+ direction (step shape curve), many participants obtained a displacement of the trolley in the opposite X- direction before the step in X+ direction.

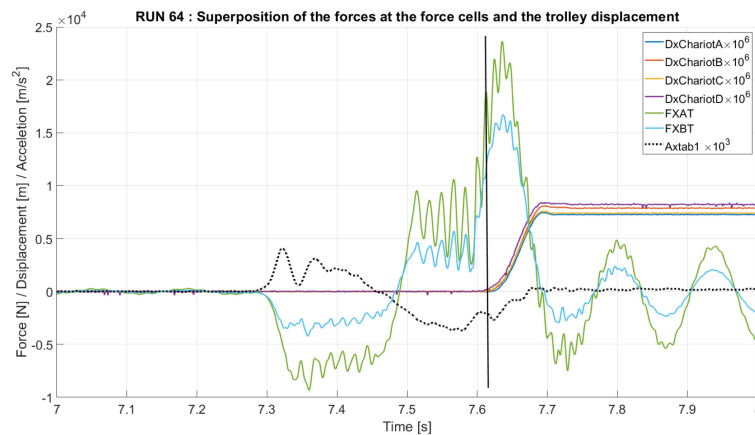
In the figure below, boxplots of the maximal values of these displacements are presented. The median is close to the experimental value. For these boxplots, outliers are not considered: the horizontal black lines are the min and the max of the participants' values.

Figure 4.22. Boxplots of maximum values of wheel displacements of the trolley obtained by the participants



The experimental observation, i.e. the movement of the trolley in one direction only, can be explained by the occurrence of lateral contact between the flanges of the end tuck wheels and the rails of the runway beams in a first step, and then by a slip in a second step at the level of the trolley wheels on the rails of the load beams. Indeed, in Figure 4.22, an increase in force can be observed at the load cells (FXAT and FXBT) located at the level of the vertical straight line, which may indicate that a shock/impact has taken place. This can be corroborated by the fact that the movement of the trolley starts at the same time as the force increase.

Figure 4.23. Analysis of the experimental results of RUN 64



RUN 62 in Y direction

Y displacement over the time is a curve that starts from zero, increases to a maximum (positive), then decreases to a minimum (negative, except for a participant).

The median Y displacements of the end trucks, among the participant's results, are around:

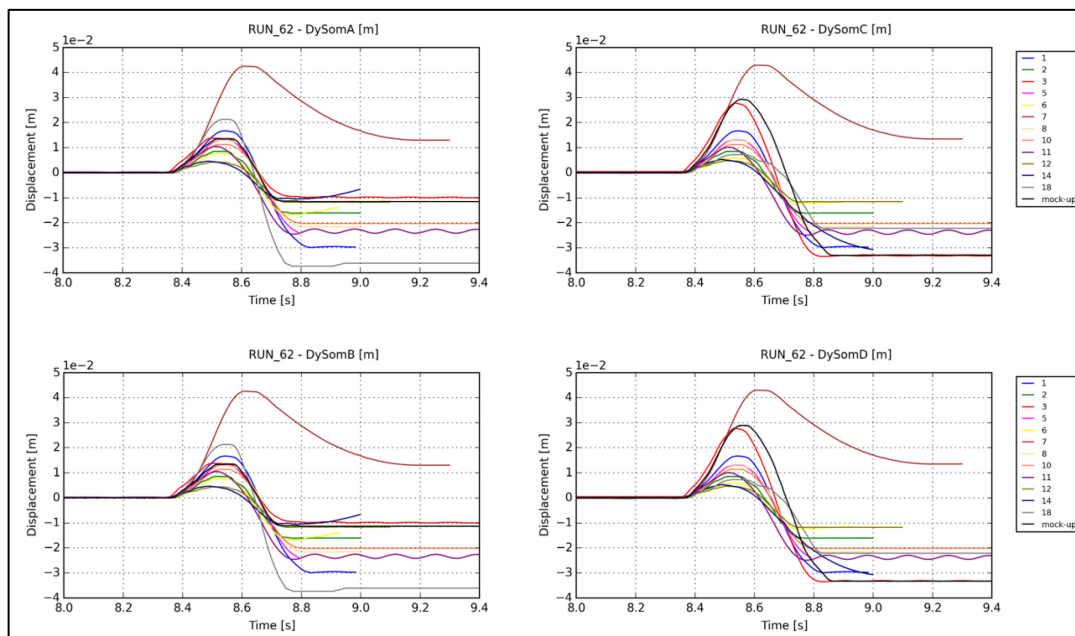
- End-truck A-B:
 - +1.2 cm for the max value;
 - -1.8 cm for the min value.
- End-truck C-D:
 - +1.1 cm for the max value;
 - -2.2 cm for the min value.

The mock-up displacement has the following maximum values:

- End-truck A-B:
 - +1.4 cm for the max value;
 - -1.2 cm for the min value.
- End-truck C-D:
 - +2.9 cm for the max value;
 - -3.3 cm for the min value.

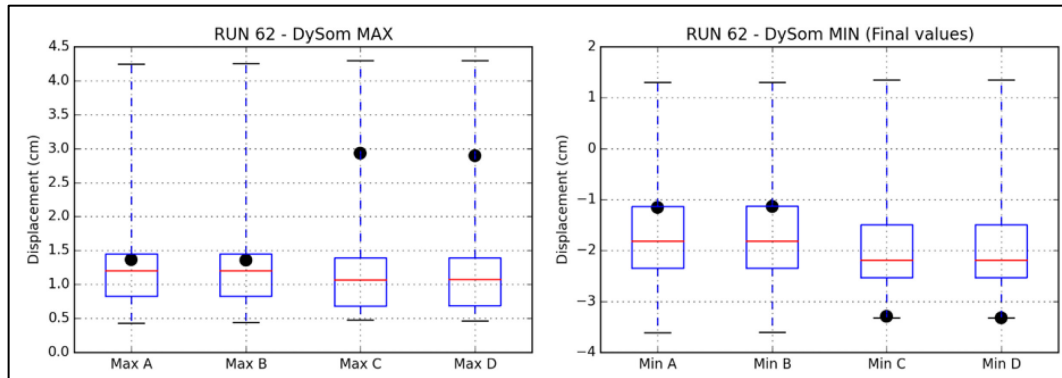
Max value (positives) calculated on the A-B end-truck are in great accordance with the one measured on the mock-up, 1.4 cm. For the min values of the A-B end-truck, the median result is a little farther from the measured displacement (-1.8 cm (results) versus -1.2 cm (mock-up)).

Figure 4.24. Y displacement of the four wheels of the end-truck beams, RUN 62



Accordance between results from participants and the one measured on the mock-up are less satisfactory for the C-D end-truck beam than for the A-B end-truck beam, which leads to believe that the participants calibrated their model on the A-B beam only, without considering the asymmetrical behaviour of the mock-up.

Figure 4.25. Boxplots of maximum and minimum (final values) values of wheel displacements of the end-truck beams obtained by the participants, RUN 62



It must be noted that the right box plot contains percentiles calculated on the final values (at the end of the RUN) of the participants results, which is not always a MIN value (for instance for participant 2).

To conclude, participants calibrated the friction coefficients by looking at results rather from the A-B end-truck, and rather by trying to fit to the maximum value. Few participants put different friction coefficients on the A-B side and the C-D side, even if the results of the mock-up show a non-symmetrical behaviour.

RUN 82 in Y direction

Input signal has a lower amplitude than for RUN 62, and the wheels configuration is the mixed one (half of the wheels can roll).

The results appear overall less satisfactory than for the RUN 62 (same direction), which tends to show that the participants did not readjust the friction coefficients for this new RUN but rather used the same values as those of the previous RUN.

Figure 4.26. Y displacement of the four wheels of the end-truck beams, RUN 82

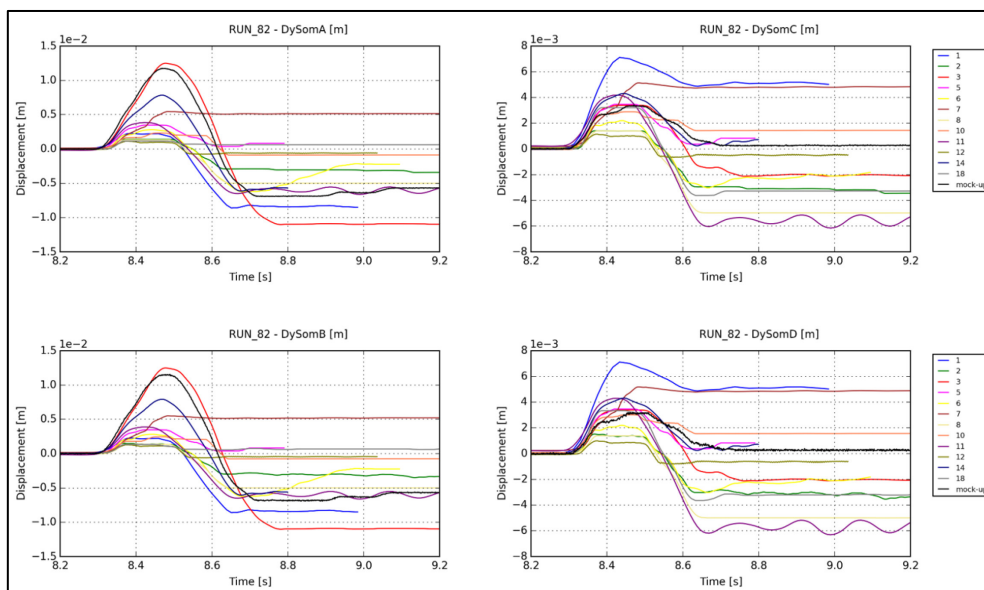
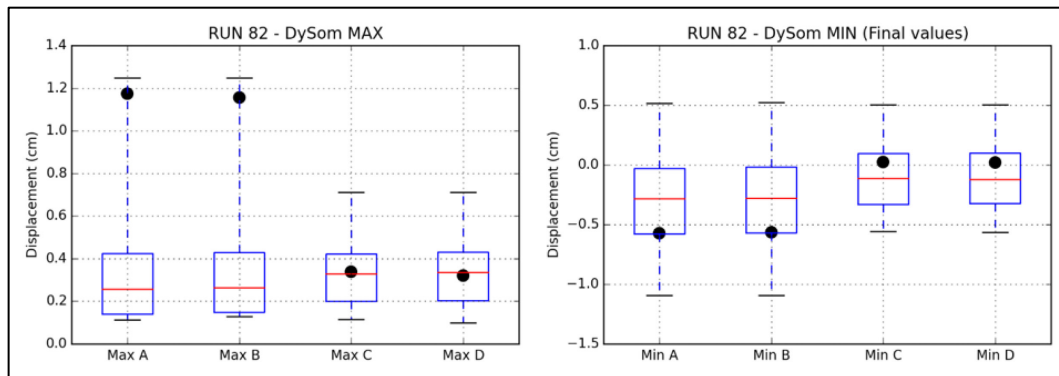


Figure 4.27. Boxplots of maximum and minimum values (final values) of wheel displacements of the end-truck beams obtained by the participants, RUN 82



Friction coefficients

Friction coefficients were requested and provided by 13 participants. One participant considered a dynamic coefficient (different from the static coefficient), and three participants considered different friction coefficients for AB and CD end-truck beams (RUN 62 and 82).

Table 4.6. Friction coefficients

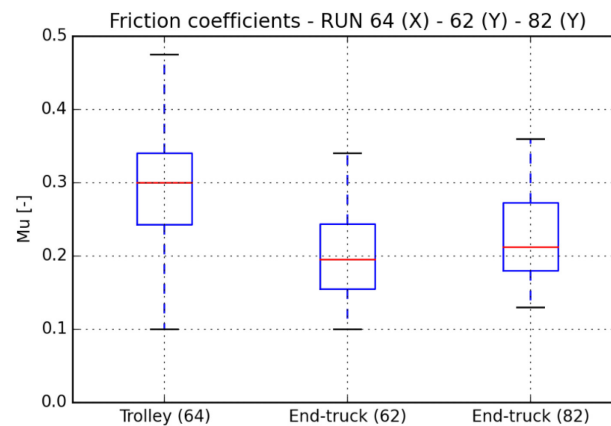
N° Team	Exercise 5						Exercise 6		Exercise 7	
	RUN 64		RUN 62		RUN 82		RUN 117		RUN 53	
	Trolley-girder	Girder-runway								
1	0.31	0.19	0.31	0.19	0.31	0.19				
2	0.30	0.25	0.30	0.25	0.30	0.25	0.30	0.25	0.30	0.25
3	0.29	0.14	0.29	0.14	0.31	0.31	0.31	0.14	0.31	0.14
4										
5	0.30	0.20	0.30	0.20	0.30	0.20	0.30	0.20	0.30	0.20
6	0.34	0.34	0.34	0.34	0.28	0.28			0.15-0.05	0.15-0.05
7	0.45-0.1	0.3-0.15	0.45-0.1	0.3-0.15	0.45-0.1	0.3-0.15	0.45-0.1	0.3-0.15	0.45-0.1	0.3-0.15
8	0.25	0.20	0.25	0.20	0.25	0.20	0.25	0.20		
9	0.15	0.17	0.15	0.17						
10	0.21-0.15	0.20	0.21	0.20	0.21	0.20	0.21	0.20	0.21	0.20
11										
12	0.27	0.27	0.27	0.27	0.27	0.27				
13										
14	0.24	0.30	0.24	0.294/0.291	0.24	0.13/0.15	0.28	0.10	0.28	0.05/0.01
15			0.10	0.10					0.10	0.10
16	0.48	0.20	0.48	0.15/0.175	0.48	0.13/0.175	0.35	0.40/0.20	0.33	0.40/0.50
17										
18	0.35	1.00	0.35	0.23/0.17	0.35	0.23/0.17				

When two values separated by a hyphen are given for a friction coefficient, it means the participant considered a static and a dynamic friction coefficient. The first value is the static one, and the second the dynamic.

When two values separated by a slash are given and the case is coloured in blue for the friction coefficient between the runway’s rails and the girder’s wheels, it means the participant affected two different values for the runway beams AB and CD. Otherwise, both beams have the same friction coefficient.

Participant 18 took a friction coefficient equal to 1.0 (red value) between the runway beams and the girder rails; this value should not have an important effect on the result since RUN 64 is a pulse along the X-axis. The participant may have thought that given the fact that the friction coefficient along Y of the trolley had not been calibrated yet (since it was done in the next RUN, RUN 62), a “real” value could not be used.

Figure 4.28. Friction coefficients for RUNs 64-62-82



For the trolley (so for the girder’s rails), **the median coefficient is 0.3**. The friction coefficients are between 0.1 and 0.5.

For the end-truck beams (so for the runway’s rails), **the median coefficient is around 0.2**. And the friction coefficients are between 0.1 and 0.35.

The median of the coefficients used for RUN 82 is slightly higher than that for RUN 62.

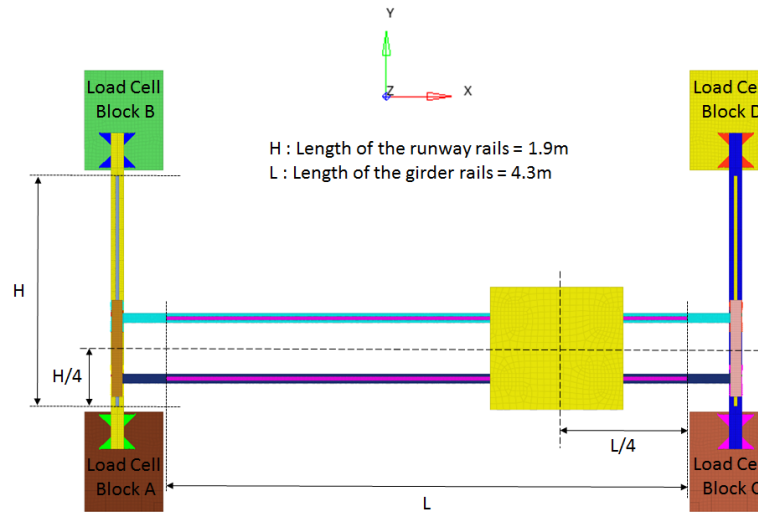
4.6. Exercise 6: Seismic analysis – RUN 117

4.6.1. Statement of the exercise

Like for exercise 5, the whole model, with the four load cell blocks, and the sliding configuration, is considered: wheels are not fixed on the rails; they can slide, jump, but not roll (it means they are blocked on their support, but not on the rails).

The decentred configuration is considered; “decentred” means that the girder beams and the trolley are positioned at a quarter of the length of the rails that support them (instead of the middle for the centred configuration):

Figure 4.29. Decentred configuration



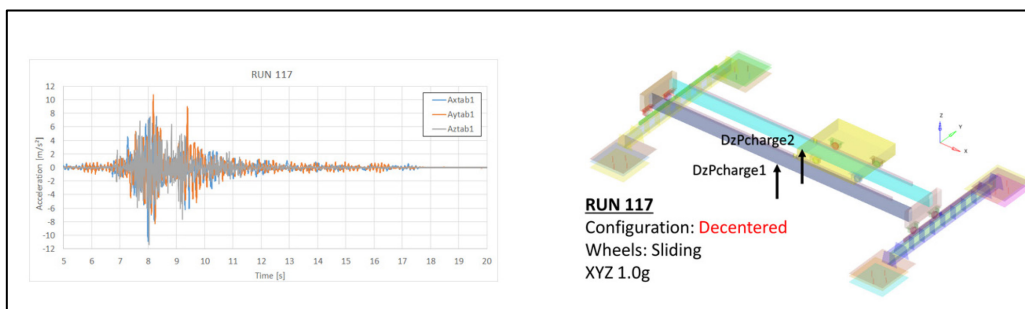
Participants were invited to compare the vertical displacement of the girder beams (sensors DzPCharge1 and DzPCharge2 of the mock-up) to the experimental results of the RUN 117. The crane configuration and the DzPCharge vertical displacement sensors are presented in Figure 4.30.

Moreover, the Y displacements of the End-truck beams and the X displacements of the trolley (DySom(A-B-C-D) and DxChariot(A-B-C-D)) are also provided to the participants.

4.6.2. Input data

The signal used is a three-directional seismic signal (PGA = 1 g). It is given in term of accelerations imposed by the shaking table (Axtab1, Aytab1 and Aztab1: sensor at the centre of the shaking table). It has a duration of 30 s. This signal is plotted in Figure 4.30.

Figure 4.30. Input signal and crane configuration for RUN 117



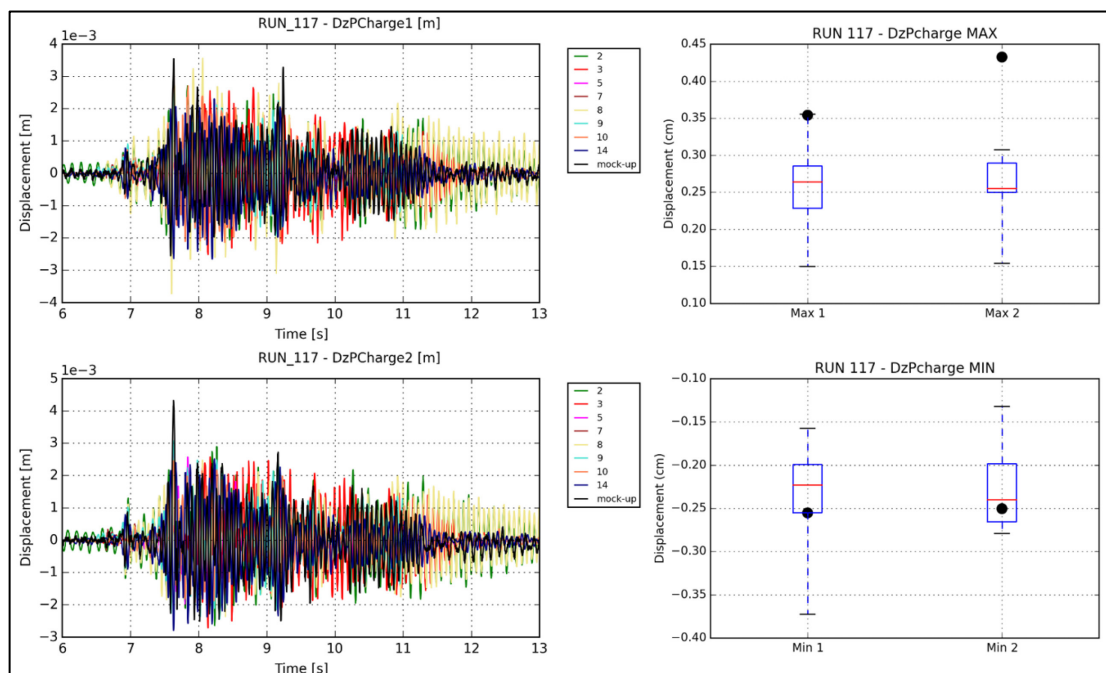
4.6.3. Results of participants

The following table sums up the max and min vertical displacements calculated by the participants.

Table 4.7. Z displacements of Girder beams in cm- RUN 117

Team	DzPCharge1_min [cm]	DzPCharge2_min [cm]	DzPCharge1_max [cm]	DzPCharge2_max [cm]
mock-up	-0.26	-0.25	0.35	0.43
2	-0.21	-0.26	0.27	0.29
3	-0.25	-0.27	0.27	0.26
5	-0.18	-0.20	0.22	0.29
7	-0.16	-0.13	0.15	0.15
8	-0.37	-0.24	0.36	0.25
9	-0.21	-0.24	0.26	0.31
10	-0.24	-0.20	0.33	0.25
14	-0.27	-0.28	0.23	0.25
median	-0.21	-0.24	0.27	0.26
std dev	0.07	0.05	0.07	0.05

The median vertical displacements of the girder beams, among the participant's results, are around 2.5 mm for both girder beams and both minimal and maximal values. The standard deviation associated with this set of values is around 0.5 mm. This median vertical displacement is in great accordance with the one from the mock-up for both girder beams for the minimal value (around 2.5 mm). For the maximal value, the mock-up shows a greater value of about 4.0 mm.

Figure 4.31. Vertical displacement of the girder beams and boxplots of the max and min values, RUN 117

For girder beam n°2 (DzPCharge2), the maximal vertical displacement (4.3 mm at 7.6 s) is quite far from the values calculated by the participants (see the box plot of max values), but this gap seems to concern only this value (which is the max) and the amplitude of the rest of the participants' signals is in better accordance with the mock-up displacements.

4.7. Exercise 7: Seismic analysis – RUN 53

4.7.1. Statement of the exercise

This exercise consists in a seismic simulation with the centred configuration, and the sliding configuration of the wheels.

Participants were invited to provide:

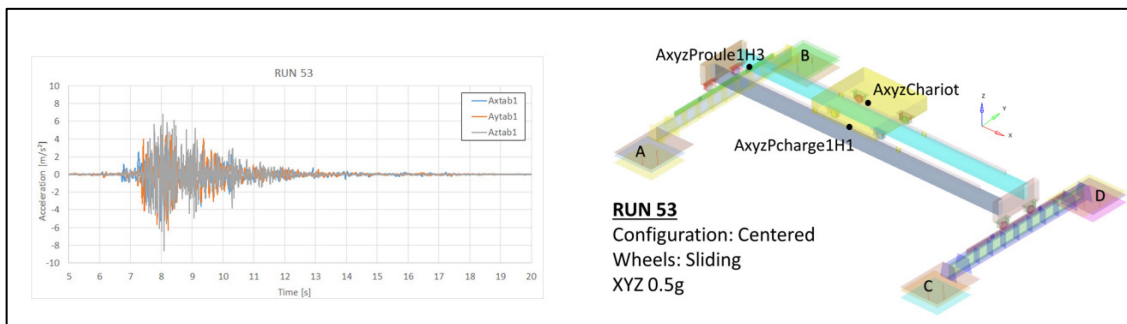
- acceleration time histories at points AxChariot, AyChariot, AzChariot on the trolley;
- acceleration time histories at points AxPcharge1H1, AyPcharge1H1, AzPcharge1H1 on the girder beams;
- acceleration time histories at points AxProule1H3, AyProule1H3, AzProule1H3 on the runway beam.

The crane configuration and the requested accelerations are presented in Figure 4.32.

4.7.2. Input data

The signal used is a three-directional seismic signal (PGA = 0.5 g). It is given in terms of accelerations imposed by the shaking table (Axtab1, Aytab1 and Aztab1). It has a duration of 30 s. This signal is plotted in Figure 4.32.

Figure 4.32. Input signal and crane configuration for RUN 53



4.7.3. Results of participants

Spectra calculated from accelerations provided by participants are plotted for 2% of damping, for the three sensors AChariot, APCharge and APRoule, in the three directions X-Y-Z in Figure 4.33, Figure 4.34 and Figure 4.35.

These spectra are plotted between 0 Hz and 30 Hz in a linear scale. Also plotted are:

- the median spectrum in blue, which contains for each frequency the median pseudo-acceleration among the participants' values;
- the spectra of first quartile values (or 25th percentile) and of the third quartile values (or 75th percentile), and the area between these two spectra coloured in dark grey;
- the min and max spectra among participants' spectra, with the area between these two spectra coloured in light grey.

Figure 4.33. Response spectra of tri-axial accelerations calculated by the participants at the trolley for RUN 53

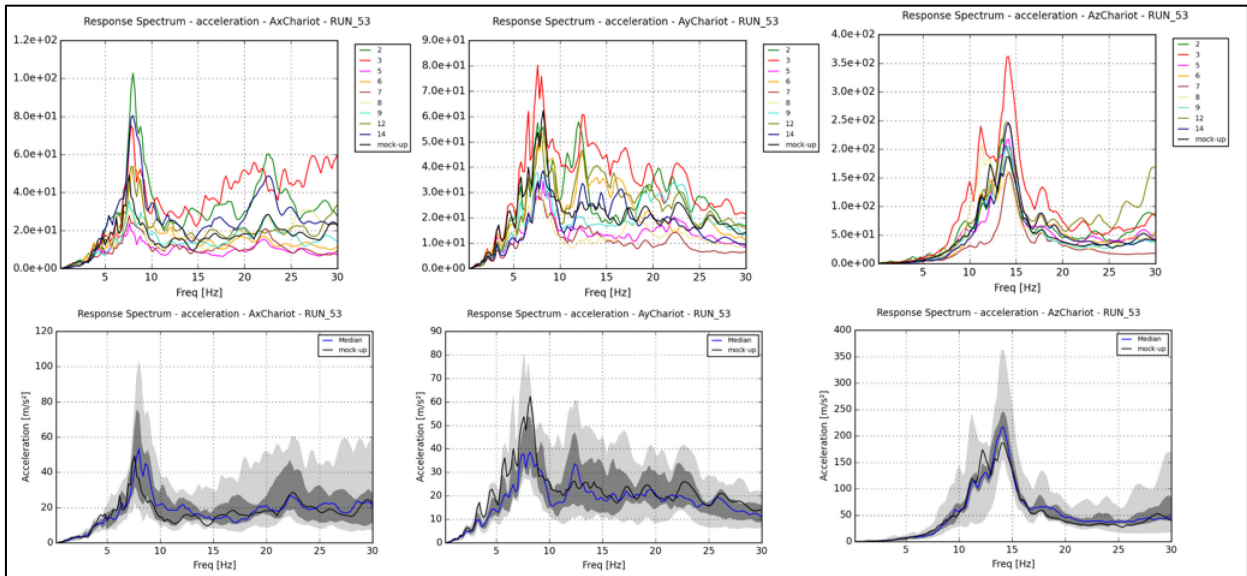


Figure 4.34. Response spectra of tri-axial accelerations calculated by the participants on the girder beam for RUN 53

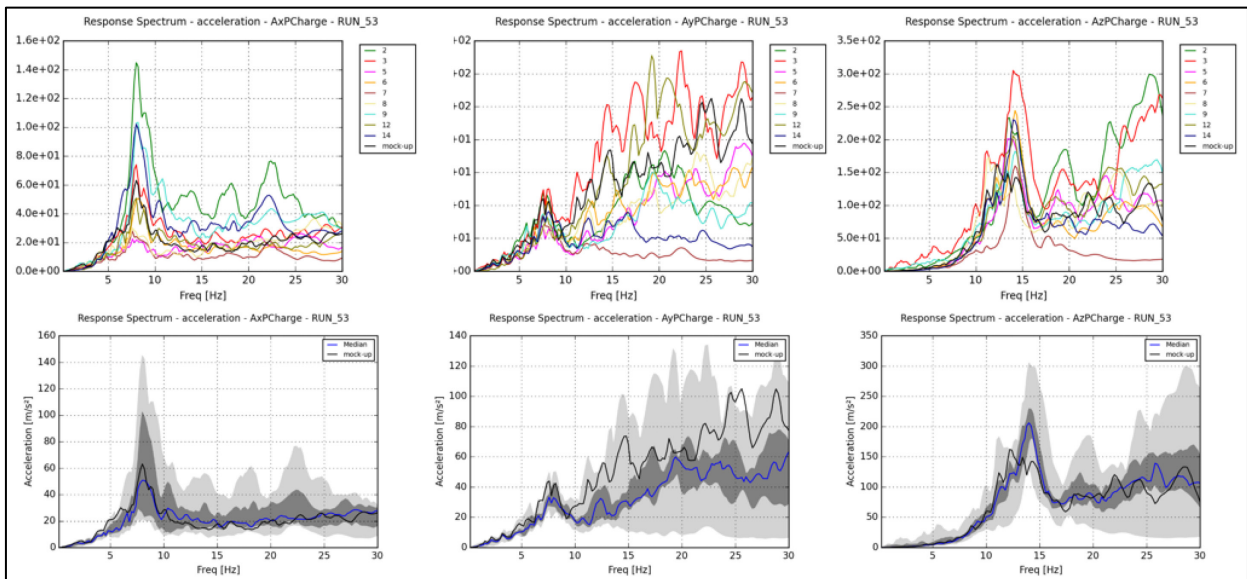
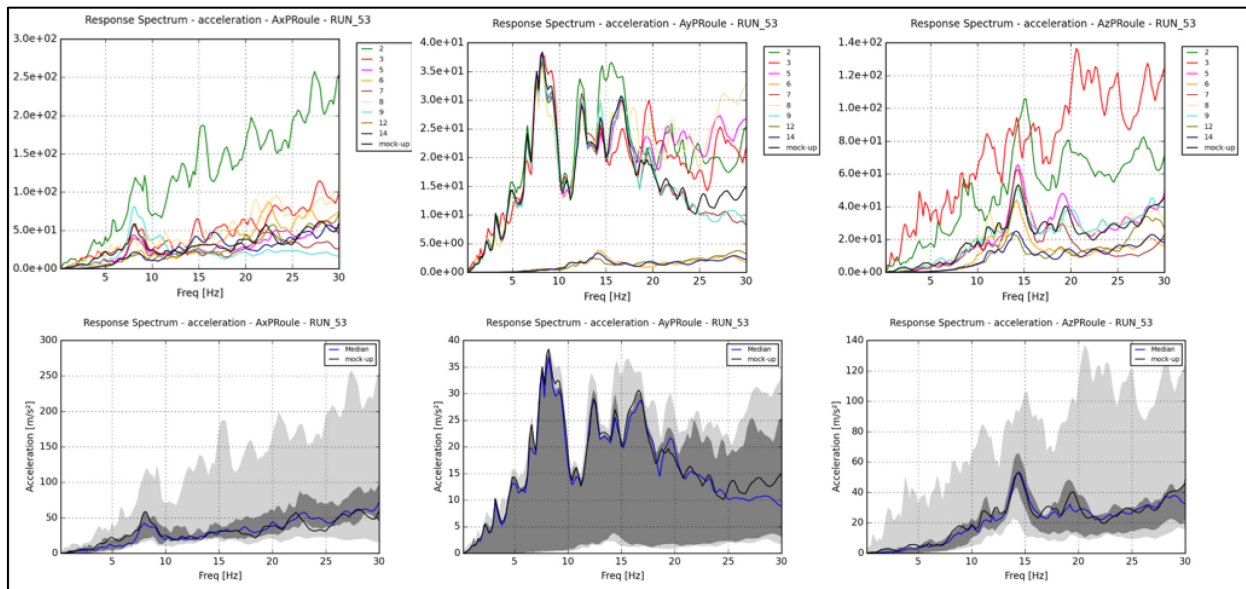


Figure 4.35. Response spectra of tri-axial accelerations calculated by the participants on the runway beam for RUN 53



4.7.4. Comments on the results

Spectra calculated with AxChariot and AyChariot accelerations show a main peak around 8 Hz, which corresponds to the natural frequency of the whole crane along X and Y.

Frequency content of participants' spectra show an overall distribution around the mock-up's spectrum that is quite satisfactory up to about 30 Hz. At higher frequencies, results deviate further from the mock-up spectrum. It can be noticed that even the mock-up spectrum has a high frequency content that is quite high (higher than around 30 Hz).

This analysis remains true in the Z direction, except that the main peak is at 13 Hz, corresponding to the natural frequency of the crane along Z.

Comparing X and Y spectra after 8 Hz (between 10 Hz and 20 Hz), it can be noticed that the Y spectra show greater pseudo-accelerations (comparing to the main peak) than the X spectra for some participants. This can be explained by a coupling between Y and Z (the Z mode is at 13 Hz): this coupling is possible since girder beams are along X, so when these beams bend along Y, the trolley can move along Z. Moreover, mode N°4 around 16 Hz is a coupled mode between Y and Z, both girder beams bend vertically in opposite direction (see Exercise 3), which results in a rotation around X. This rotation of the trolley can lead to displacements along Z (except if the measurement point is placed at the exact centre of the trolley, on the axis of rotation).

At the bottom graphs of Figure 4.33, Figure 4.34 and Figure 4.35, the spectrum of the mock-up is in black, while the median spectrum (that of the participants) is in blue.

The dark grey area is the area between the first and third quartile (or the 25 and 75 percentiles). This is the same idea as the blue box in the boxplots in the previous paragraphs. This dark grey area contains, for each frequency, half of the participants' spectral values.

The light grey area contains all the values, which means that the upper edge of this area is the spectrum composed of the maximums of the participants' spectral values, and this area's lower edge is composed of the minimums of the participants' spectral values.

In the Y direction for the acceleration at the trolley level, Figure 4.33, the fundamental peak at 7 Hz is underestimated.

For the girder beams, Figure 4.34, spectra are higher than for the trolley around 20 or 30 Hz, in the Y direction, and a little bit in the Z direction. They are satisfactory in the X direction and underestimated in the Y direction.

For the runway beams, Figure 4.35, results are satisfactory in the X and Z directions. Accelerations in the X directions are higher than on the girder beams or the trolley and this is because they occur below the friction zones/rails. In the Y direction, the second graph of Figure 4.43 looks strange, but the results are very good for most participants; the median is very close to the measurement, but for three participants the spectra are very low, which had an effect on the widening of the grey area.

Thus, in general, the results can be considered satisfactory if the median is close to the model, and if the dark grey area is not too wide. Among all the results provided by the participants, there are no results that seem to be inconsistent (great homogeneity).

5. Stage 2: Nonlinear blind simulations

5.1. Main content

After the calibration of the models retained by the participants, a prediction exercise was planned. Stage #2 aimed at evaluating the nonlinear response of the bridge crane mock up under high intensity seismic loadings. Only seismic signals at the centre of the table level were communicated for use as input data for the simulation. The following five exercises were defined for this stage:

Table 5.1. Exercises of Stage 2

Exercise	RUN	Direction	PGA [g]	Crane Config.	Wheels Config.
8	80	XY	1.5	Centred	Mixed
9	42	XY	1.5	Centred	Sliding
10	112	XY	1.5	Decentred	Sliding
11	128	XY	1.5	Decentred	Mixed
12	100	XYZ	1.0	Centred	Mixed

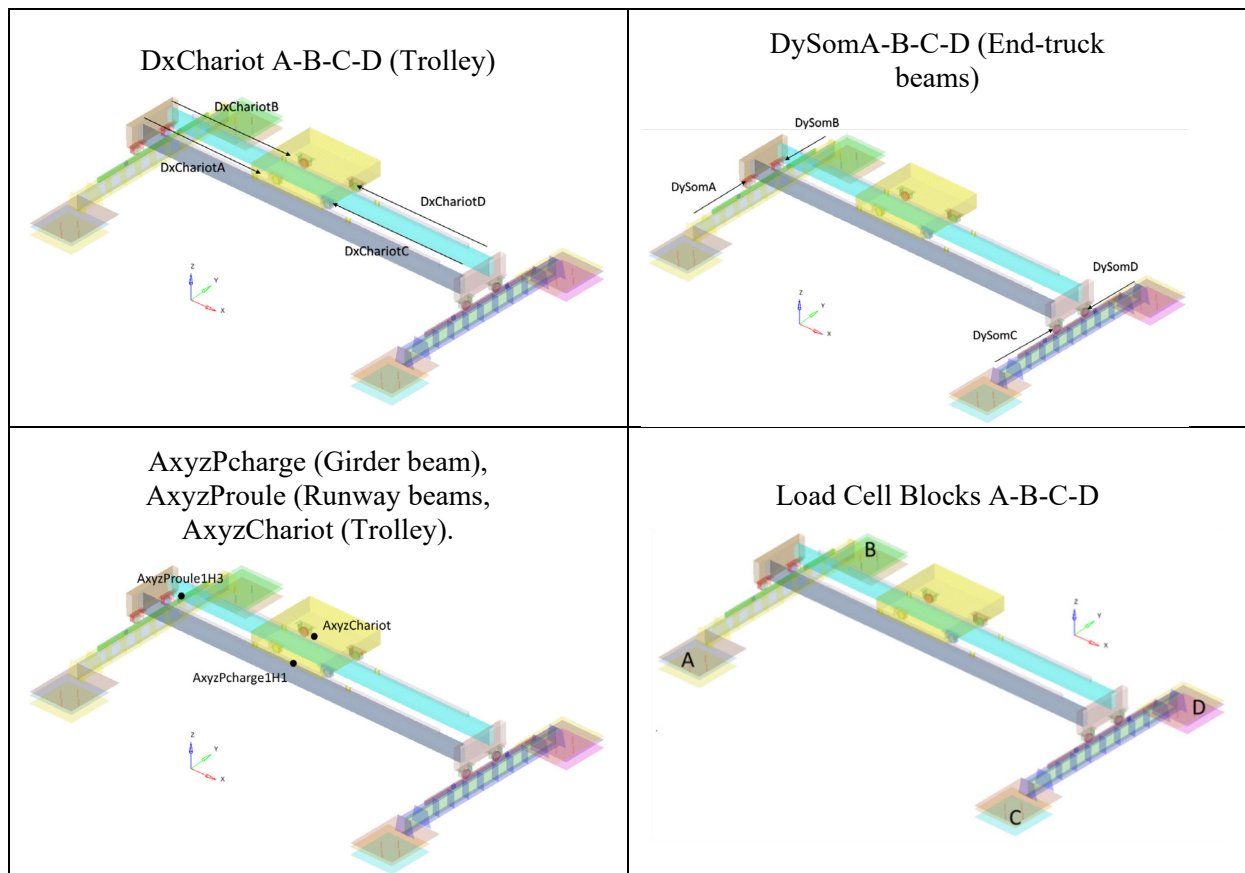
Given the two-directional or three-directional input signals (seismic excitation) for the five exercises of Stage 2, participants were invited to perform transient analyses, and then:

- provide acceleration time evolutions at different points:
 - on the trolley; at point AxyzChariot1;
 - on the girder beam; at point AxyzPcharge1H1;
 - on the runway beam; at point AxyzProule1H3.
- provide displacement time evolutions of different points:
 - of the trolley, in direction X: DxChariotA-B-C-D;
 - of the end-truck beams, in direction Y: DySomA-B-C-D;
 - of the girder beams, in direction Z: DzPcharge1-2.
- provide force time evolutions at supports:
 - in the four load cells of each load cell block (A, B, C, D).

The location of these sensors and of the four load cell blocks are given in the Figure 5.1.

The results of Stage 2 of the participants are presented below by post-processed EDP; displacements, accelerations, support reactions.

Figure 5.1. Location of the sensors and the four load cell blocks



5.2. Displacements

5.2.1. Post-processing description

Displacements calculated by the participants are presented below. Note that these displacements are relative displacements with respect to the initial position (so initial values are zero).

For each of the five RUNs, only the time evolution of DxChariotA and DxChariotB only are presented since they are almost equal to DxChariotC and DxChariotD respectively. The time evolution of DySomA and DySomC, and of DzPcharge1 and 2 are presented.

These displacements are compared to the one measured by the sensors of the mock-up, in black in the graphs.

The maximum values of these displacements in absolute value are provided in box plot graphs, which represent different percentiles of participants' values:

- Q_0 : min (black tick),
- Q_1 : 25th percentile = first quartile (bottom of the blue box),
- Q_2 : 50th percentile = median (red line),
- Q_3 : 75th percentile = third quartile (top of the blue box),
- Q_4 : max (black tick).

The mock-up value is represented on these boxplots with a black dot.

The trolley’s horizontal trajectory is represented. The X value is equal to the value of DxChariotA, so it means that rotations of the trolley are neglected. Y value is equal to

$$0.5 * DySomA + 0.5 * DySomC$$

for the centred configuration, and

$$0.25 * DySomA + 0.75 * DySomC$$

for the decentred configuration, which means that the displacement of the Trolley along the X-axis is neglected compared to the length of the girder beams ($DxChariot \ll Lx_girder$).

The following paragraphs present all the results for each RUN, and the last one an analysis of the results.

5.2.2. Results of RUN 42 (Exercise 9)

Figure 5.2. RUN 42 – Displacements of the trolley

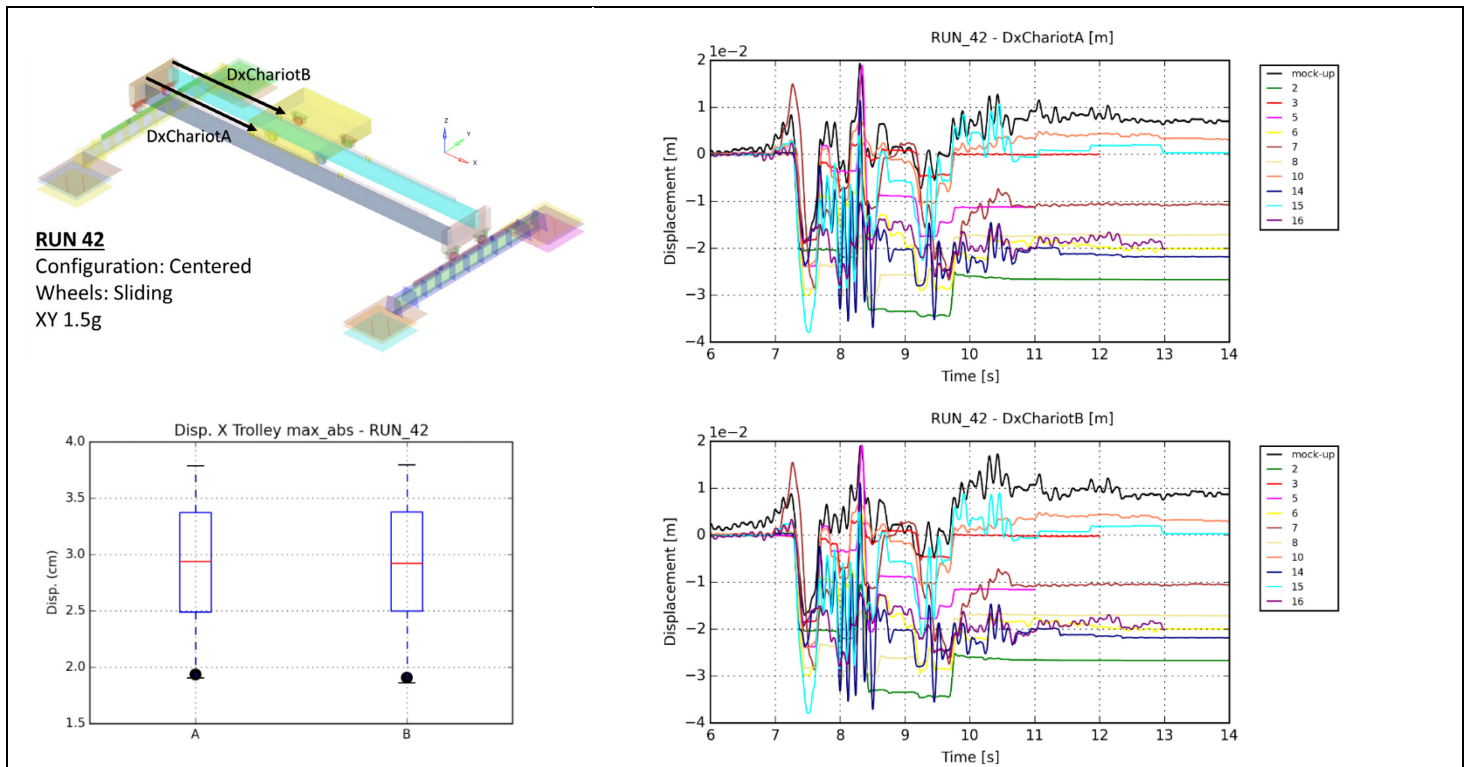


Figure 5.3. RUN 42 – Displacements of the end-truck beams

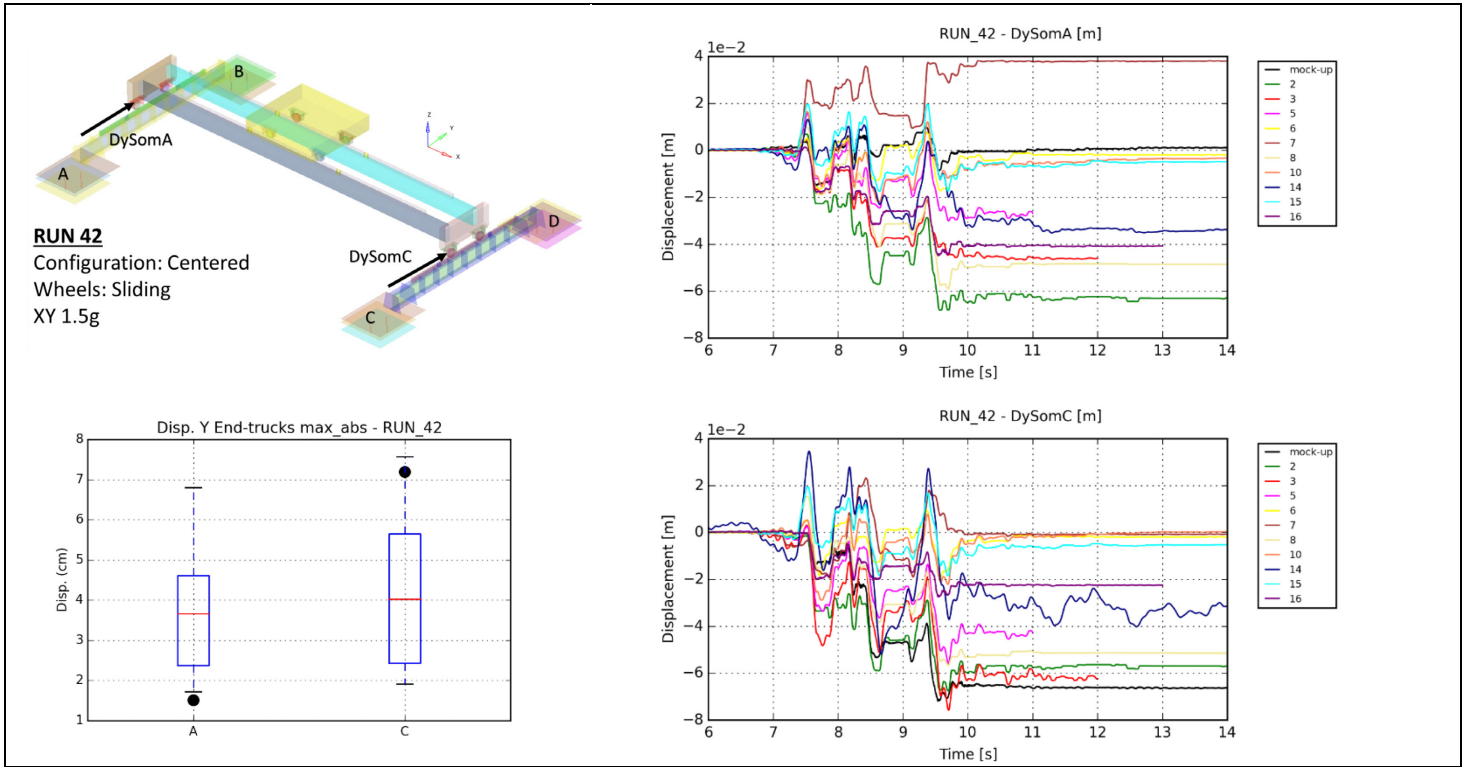


Figure 5.4. Trolley's trajectory - RUN 42

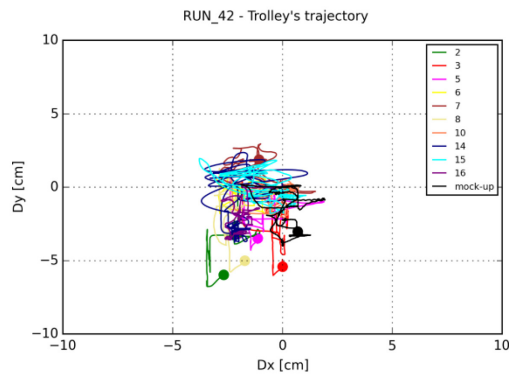
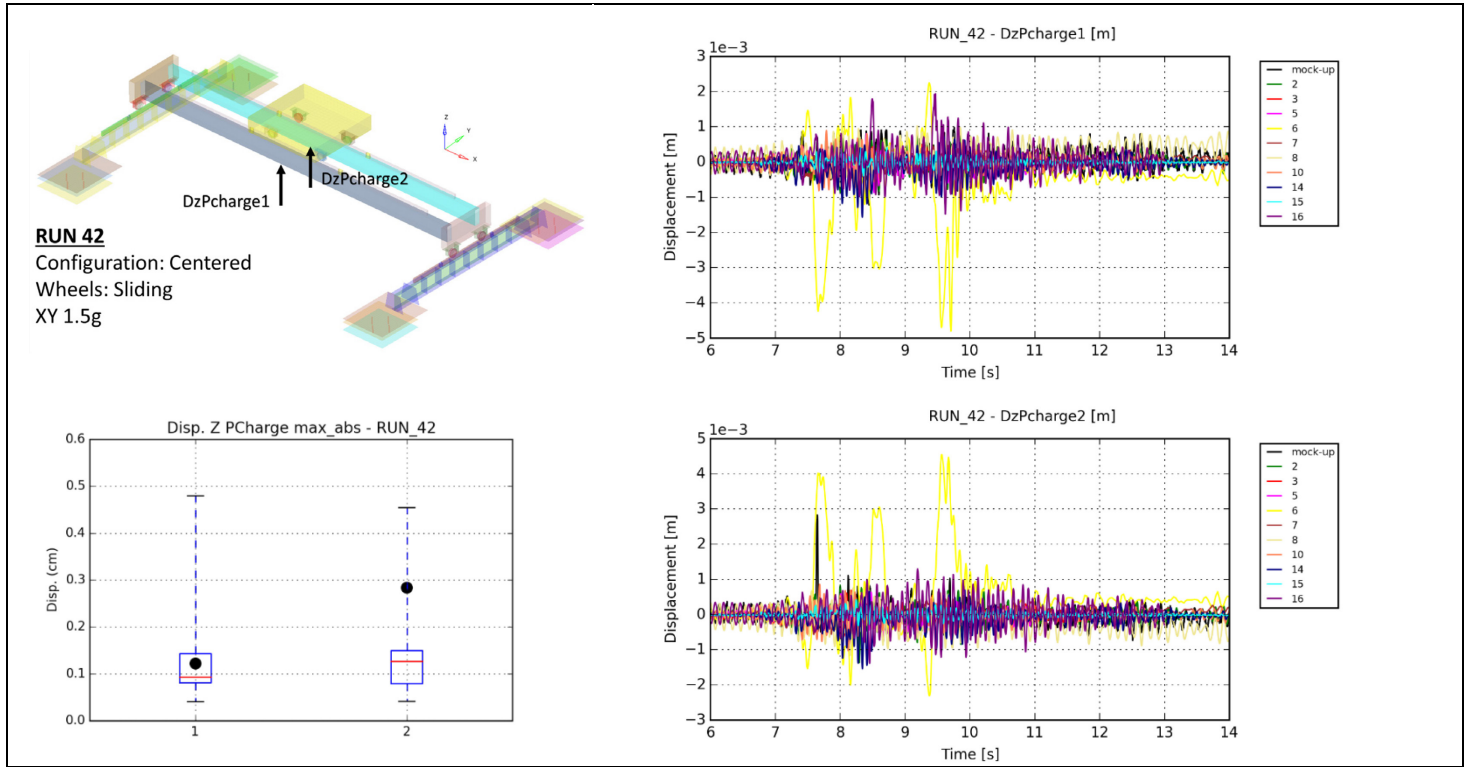


Figure 5.5. RUN 42 – Vertical displacements of the Girder beams



5.2.3. Results of RUN 80 (Exercise 8)

Figure 5.6. RUN 80 – Displacements of the trolley

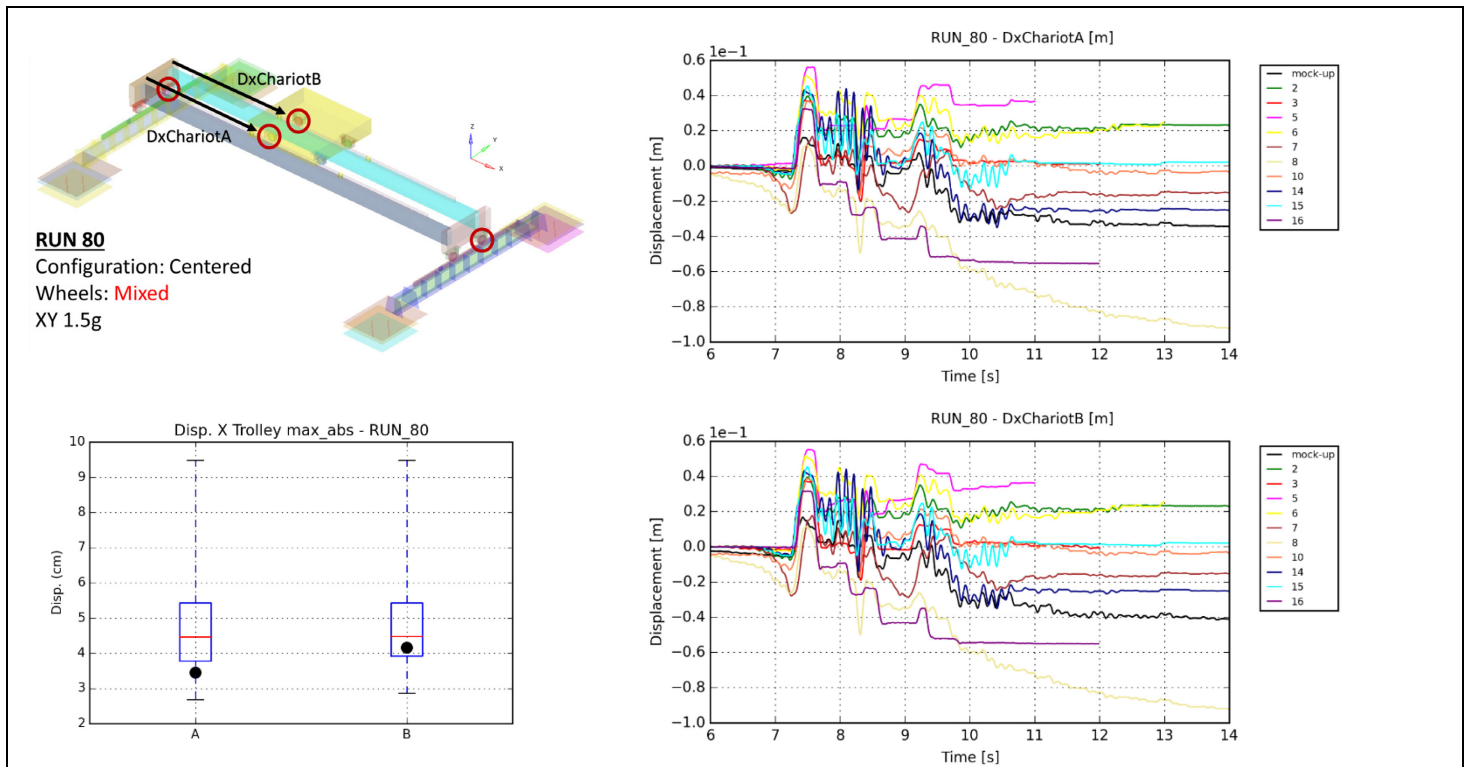


Figure 5.7. RUN 80 – Displacements of the end-truck beams

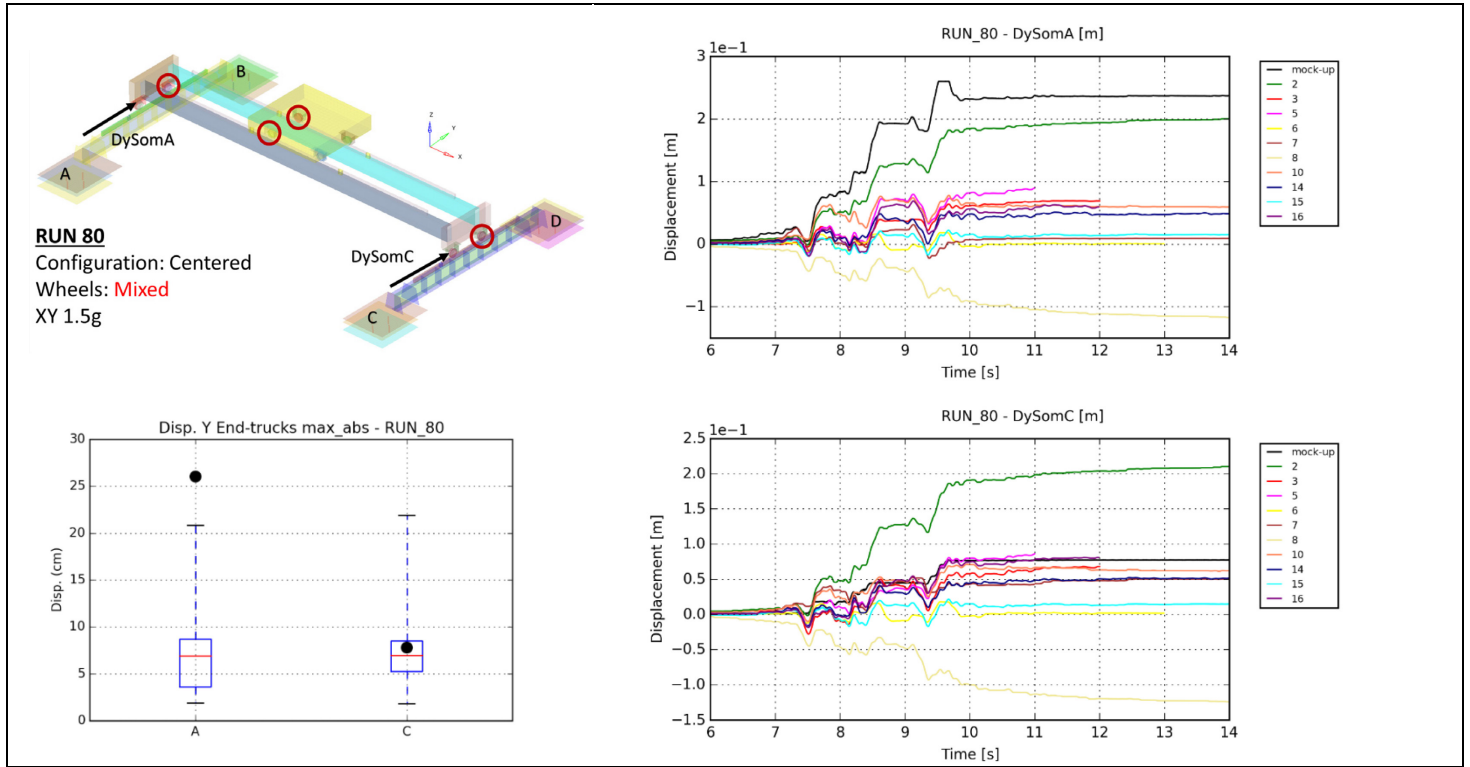


Figure 5.8. Trolley's trajectory - RUN 80

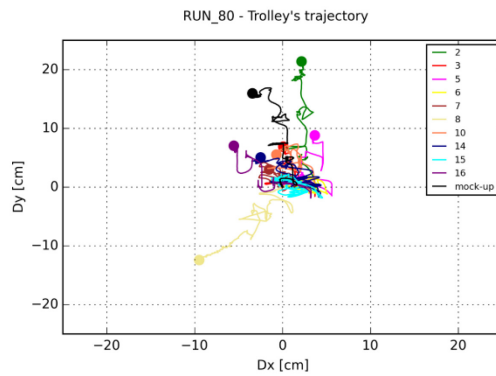
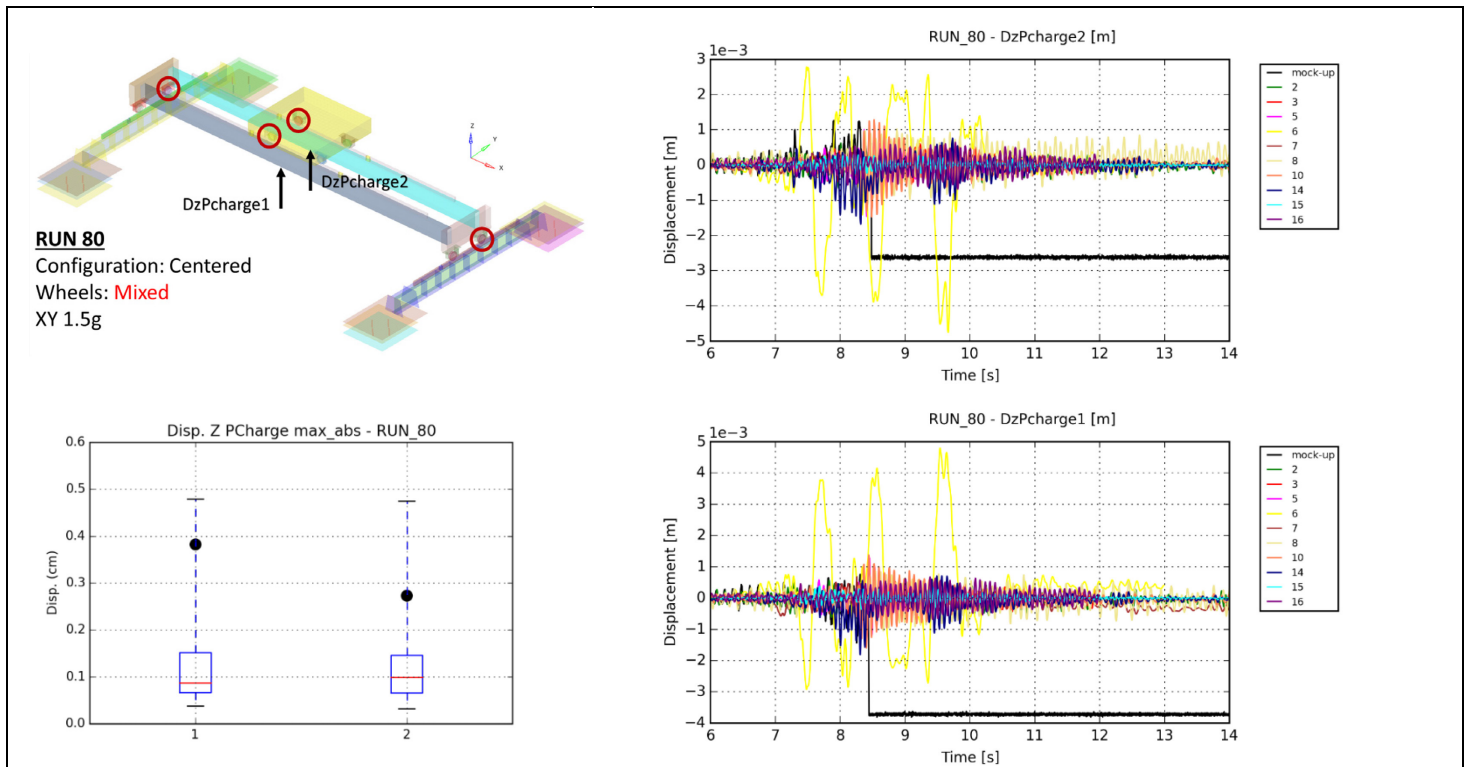


Figure 5.9. RUN 80 – Vertical displacements of the Girder beams



5.2.4. Results of RUN 112 (Exercise 10)

Figure 5.10. RUN 112 – Displacements of the trolley

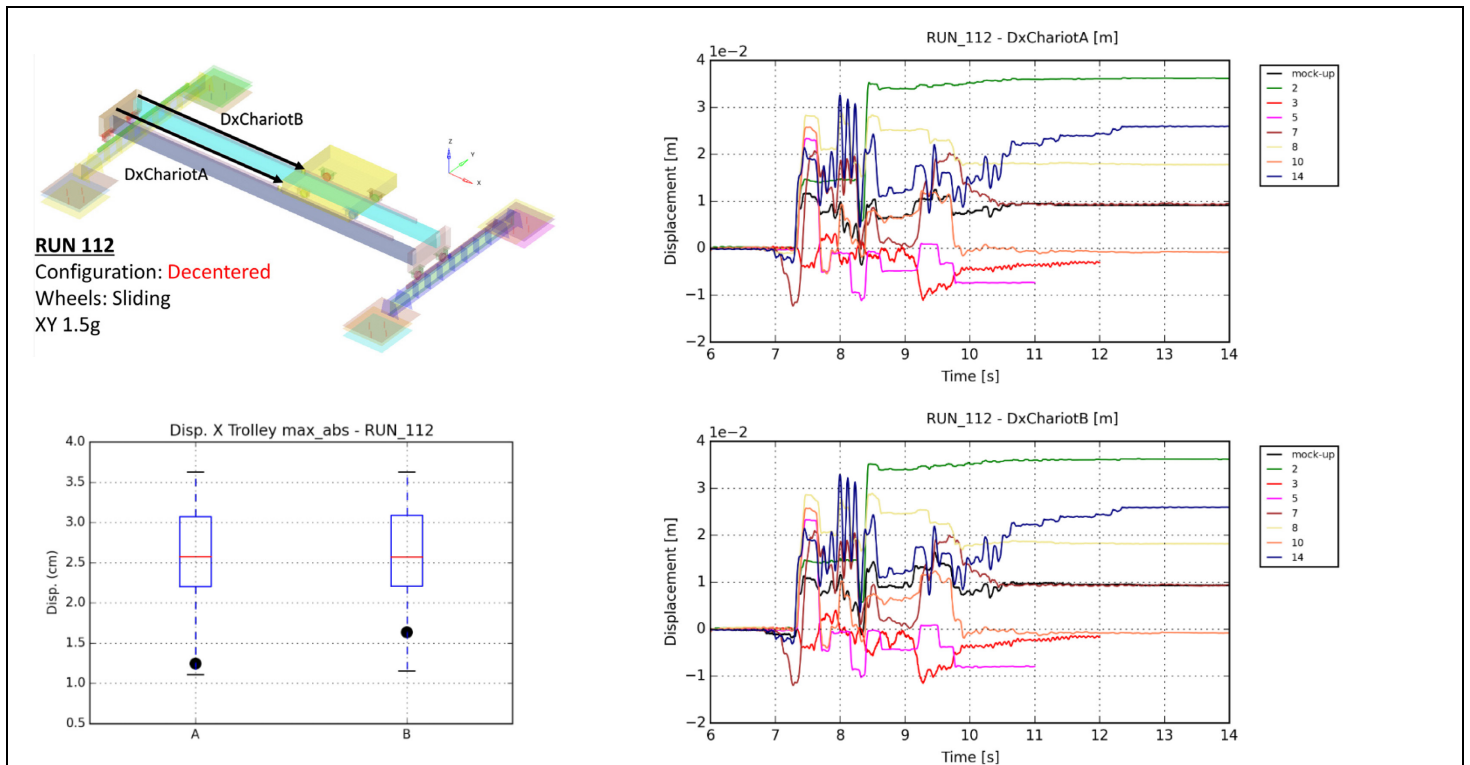


Figure 5.11. RUN 112 – Displacements of the end-truck beams

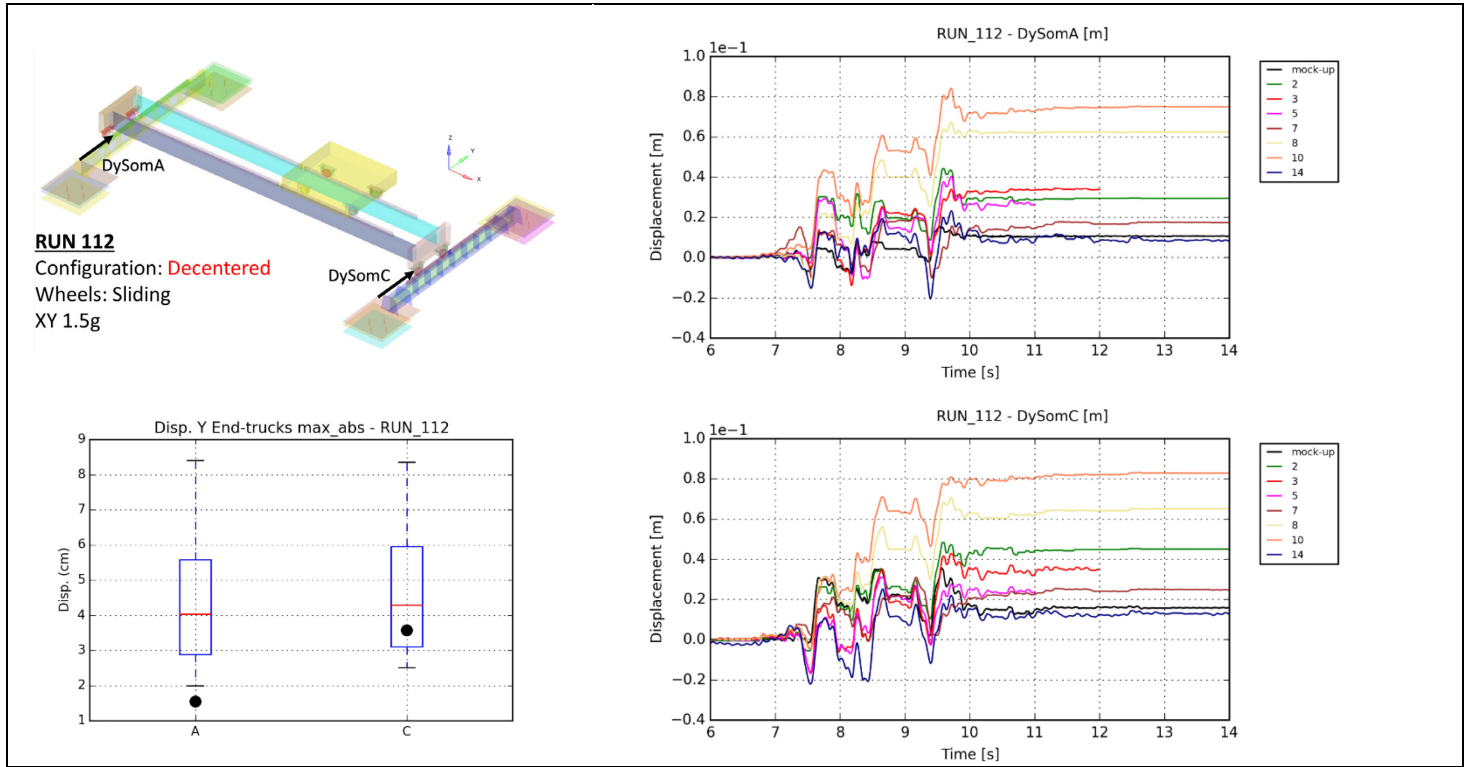


Figure 5.12. Trolley's trajectory - RUN 112

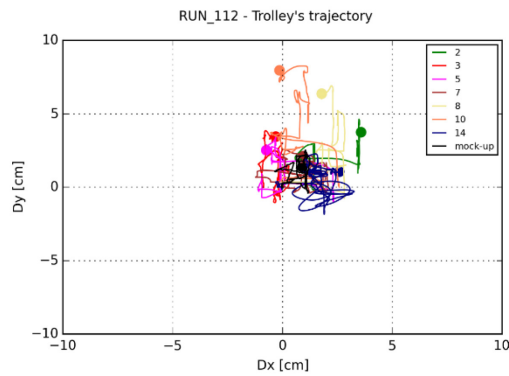
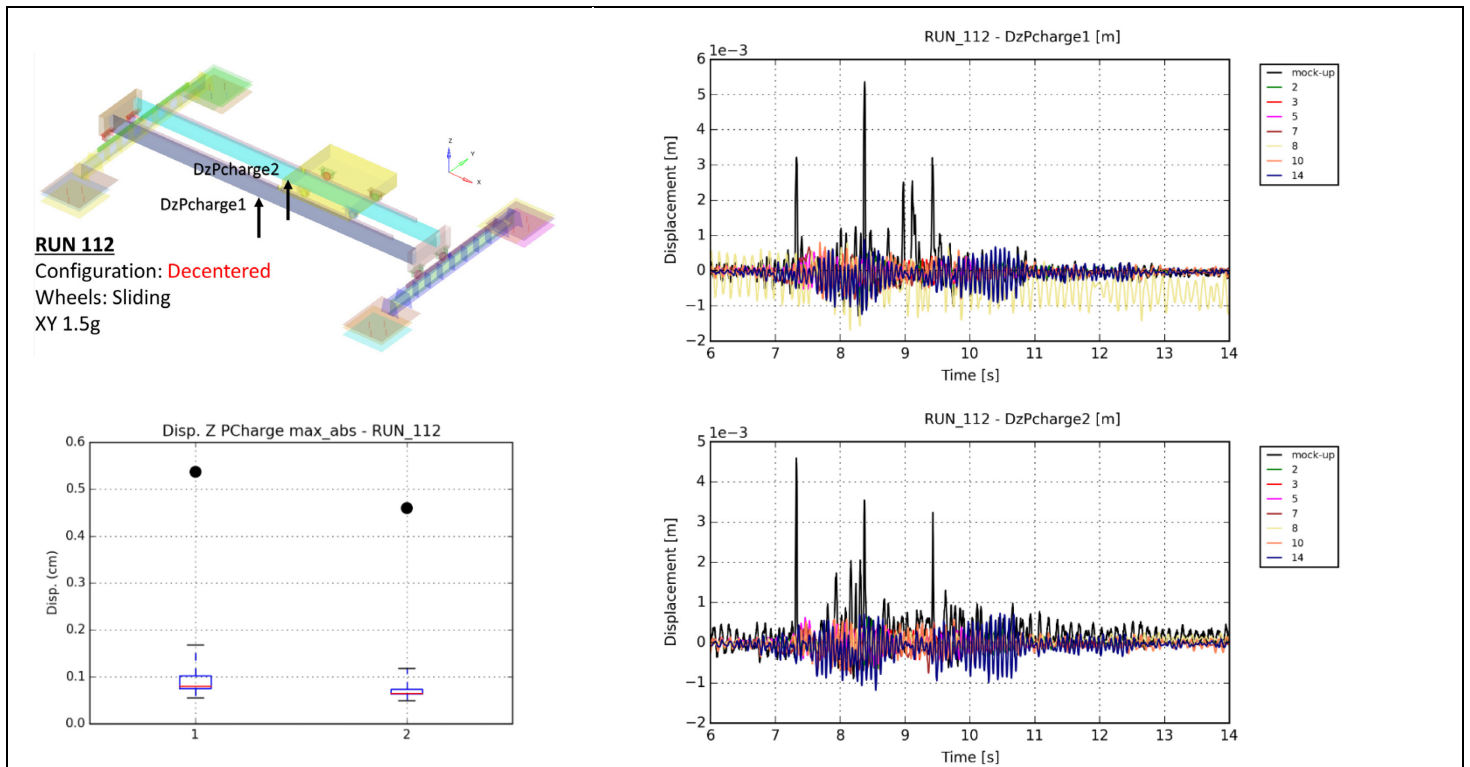


Figure 5.13. RUN 112 – Vertical displacements of the girder beams



5.2.5. Results of RUN 128 (Exercise 11)

Figure 5.14. RUN 128 – Displacements of the trolley

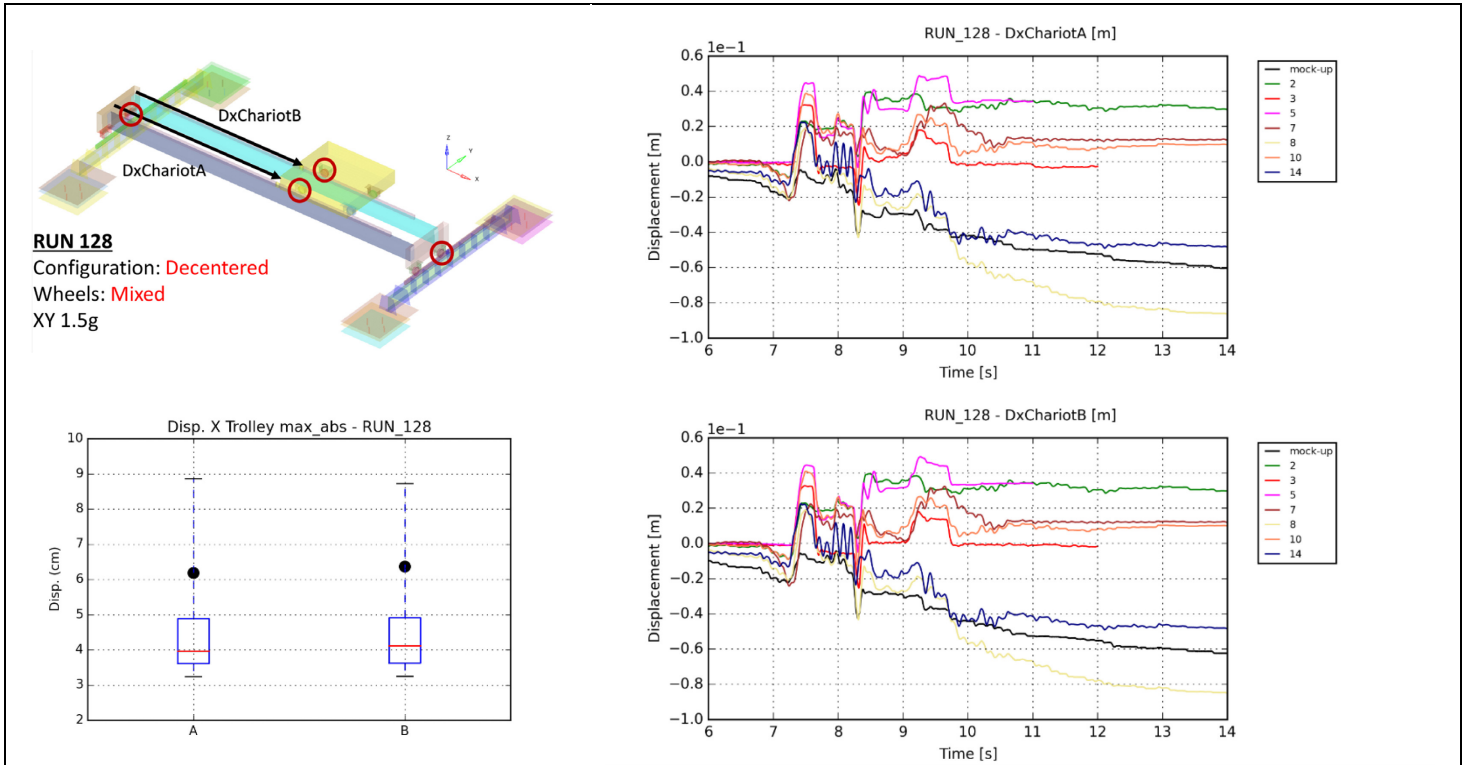


Figure 5.15. RUN 128 – Displacements of the end-truck beams

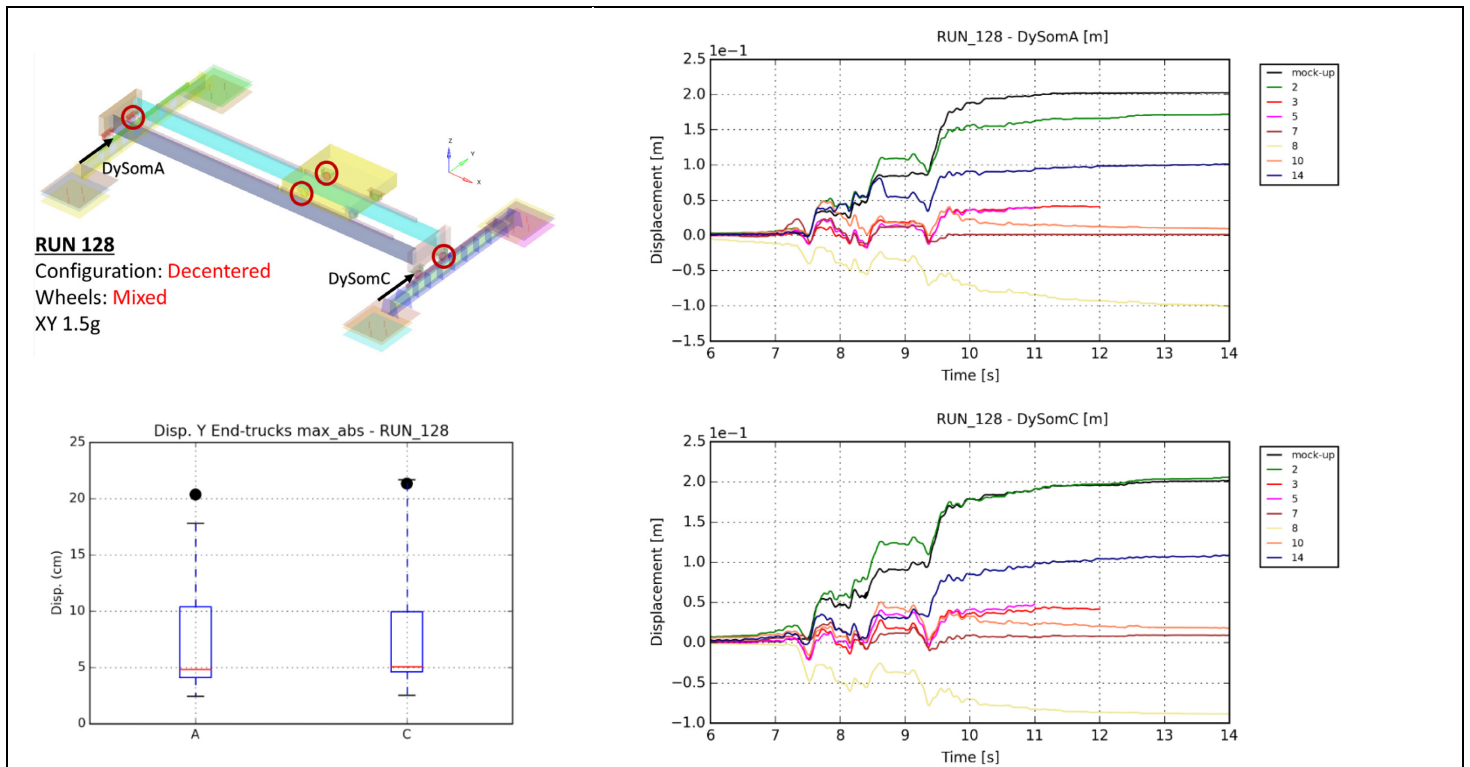


Figure 5.16. Trolley's trajectory - RUN 128

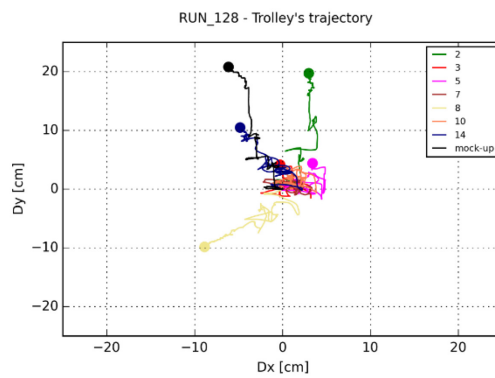
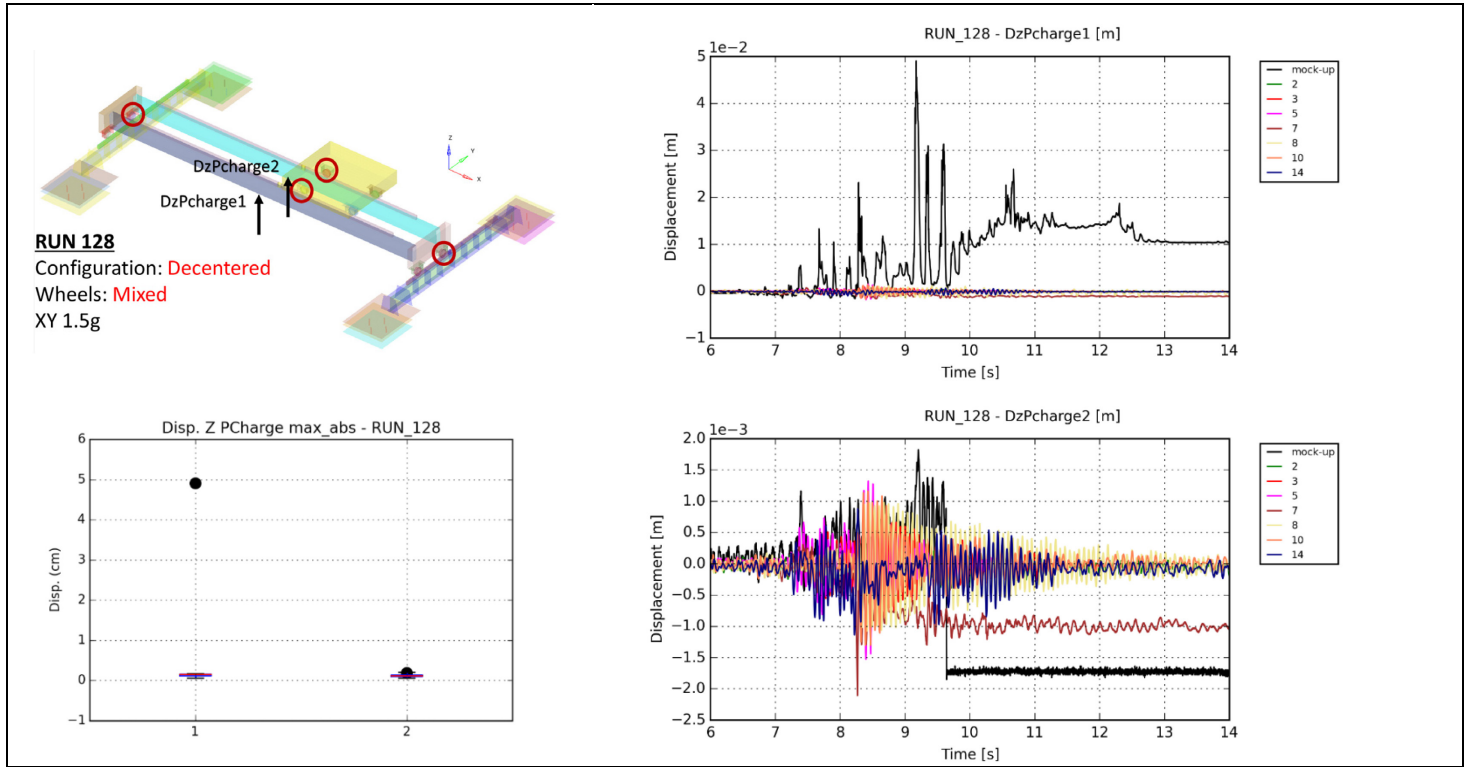


Figure 5.17. RUN 128 – Vertical displacements of the girder beams



5.2.6. Results of RUN 100 (Exercise 12)

Figure 5.18. RUN 100 – Displacements of the trolley

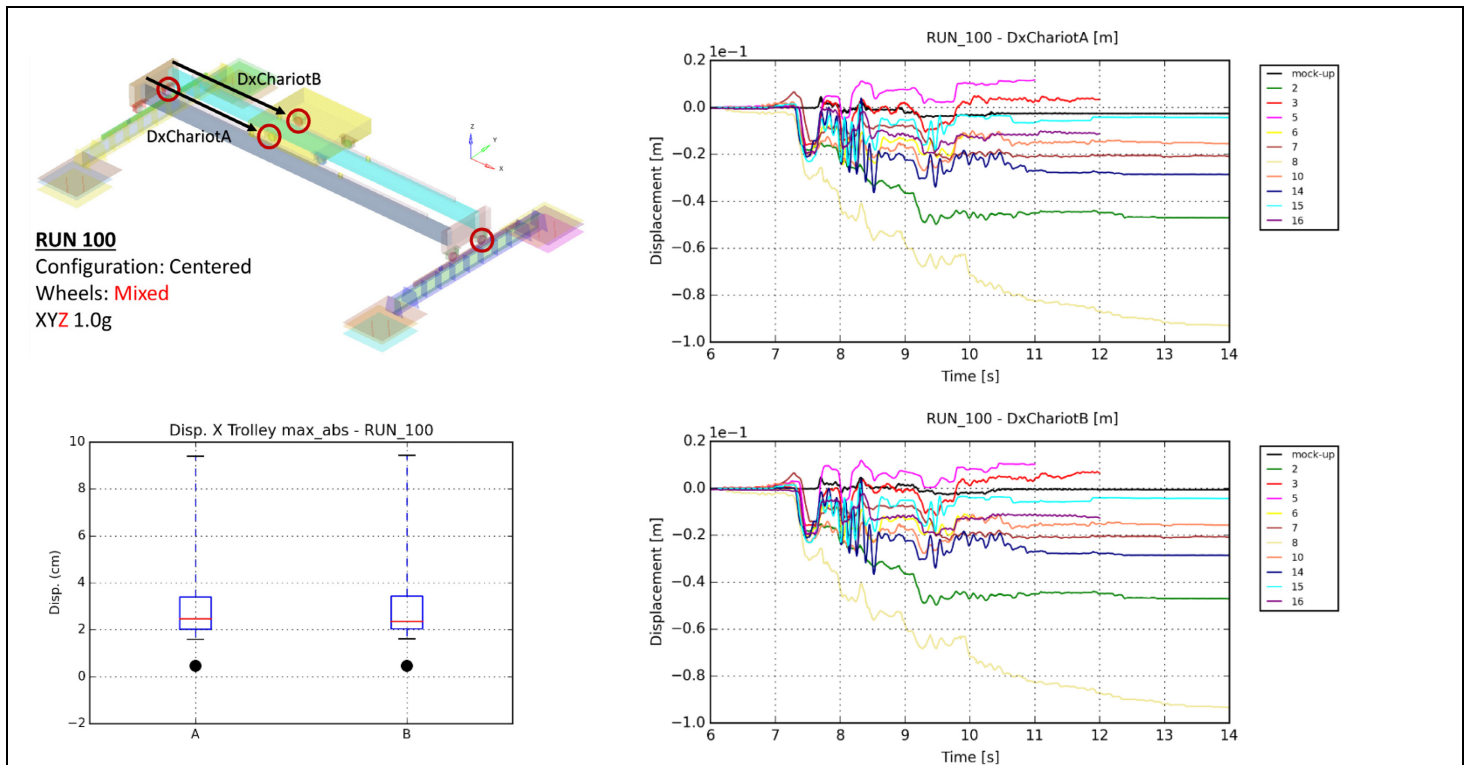


Figure 5.19. RUN 100 – Displacements of the end-truck beams

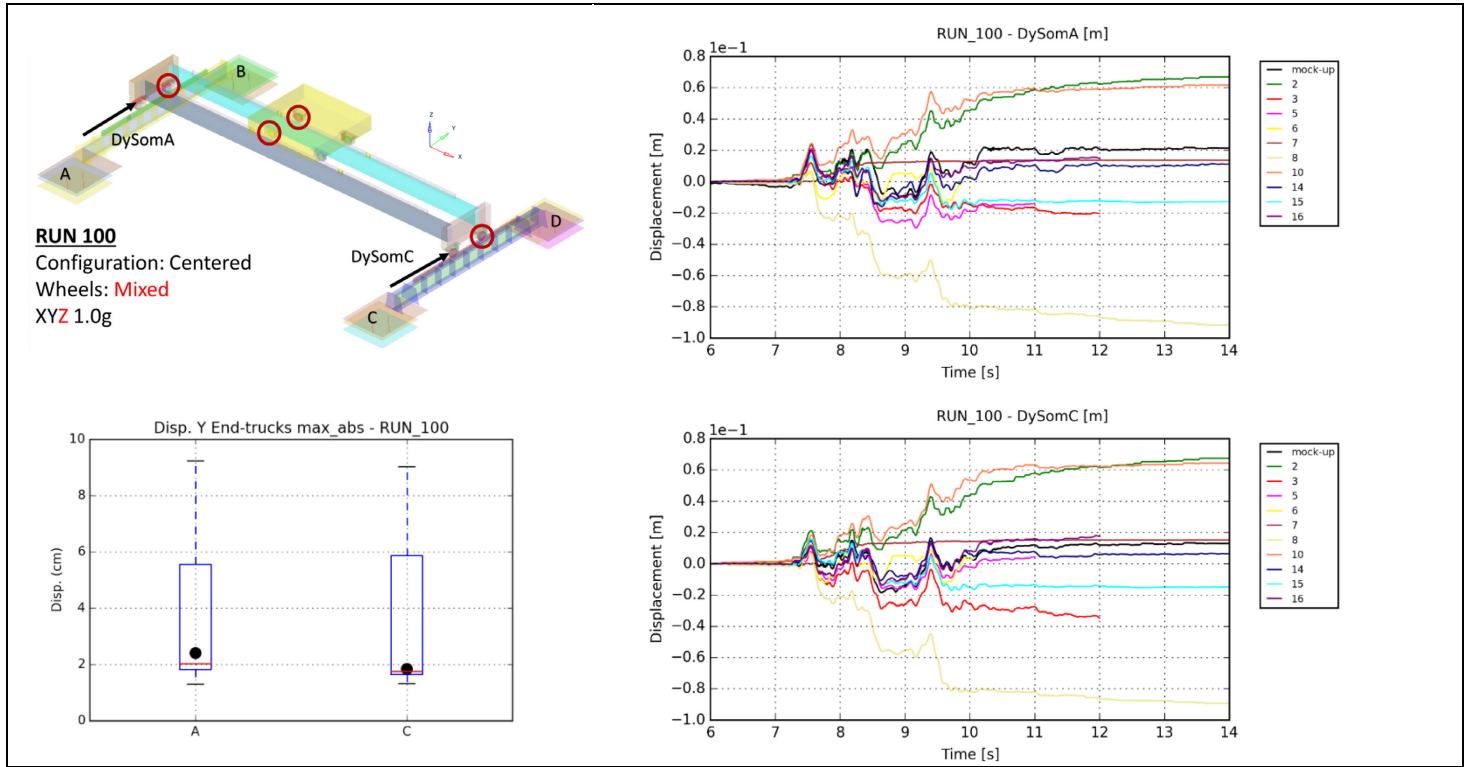


Figure 5.20. Trolley's trajectory - RUN 100

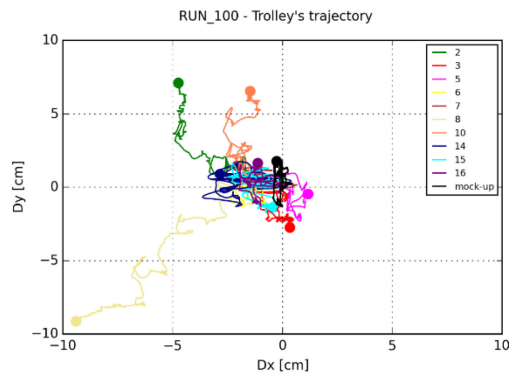
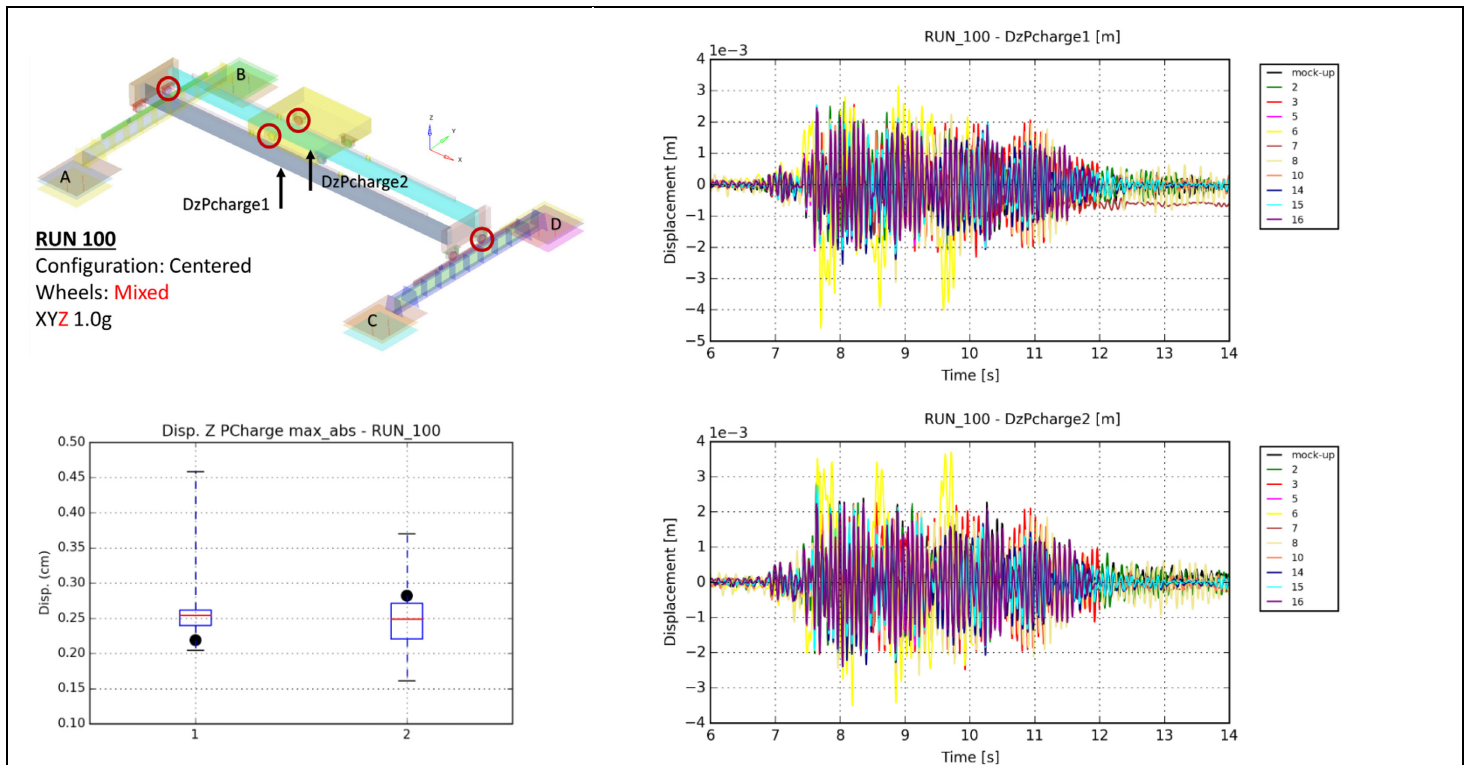


Figure 5.21. RUN 100 – Vertical displacements of the girder beams



5.2.7. Comments on the results

The maximal values of the calculated displacement are overall in great accordance with the ones from the mock-up, for the three directions. The maximal horizontal displacement is centimetric, from a few centimetres to 25 cm, while the maximal vertical displacements are millimetric. These comments can be made once vertical displacements from the mock-up for some RUNs have been corrected where measurement errors are detected, for instance for RUN 42 and 112, where some values are very high compared to the rest of the signal, or for RUN 80 and 128, where the whole signal is constant from a particular instant, meaning that the laser sensor has moved too far from its initial position. The only RUN that does not present measurement errors in DzPcharge is RUN 100, which is at a lower PGA, 1.0 g compared to 1.5 g for the others RUNs. This is consistent with the fact that girder beams may have moved less for RUN 100.

Time history displacements vary at higher frequency in the vertical direction than horizontally. This is consistent with the frequency of the vertical mode, around 13 Hz, whereas horizontal modes are around 7 Hz. Moreover, the frequency component of the signal around 7 Hz is less visible in horizontal displacements since these signals are relative to nonlinear phenomena: wheels slide and hit the rails, leading to displacement curves that contain steps.

If some portions of these displacement curves are the same for all participants and the mock-up, the final displacements can be very different since they are the result of several successive non-linearities.

For the given intensity of 1.5 g, it means considering every RUN except RUN 100; a mixed wheels configuration led to higher maximal displacements of the girder beams. This can be

seen in the time evolutions and in the trajectories of the trolley of each RUN, for the mock-up (black trajectories) and the participant's results.

During the tests, a different displacement can be observed between the AB end-truck beam and the CD end-truck beam (i.e. rotating girder beams). This is also the case in the results of the participants (looking at the median displacement), but this differential displacement is less important.

5.3. Accelerations – Response spectra

5.3.1. Post-processing description

For each exercise, accelerations are calculated by the participants at points AChariot, APcharge1H1 and AProule1H3, in the three directions. The response spectra of these accelerograms, calculated at 2% of damping, are provided for each participant and for the mock-up (in black).

These spectra are plotted between 0 Hz and 30 Hz in a linear scale. Also plotted are:

- The median spectrum in blue, which contain for each frequency the median pseudo-acceleration among the participants' values.
- The spectra of first quartile values (or 25th percentile) and of the third quartile values (or 75th percentile), with the area between these two spectra coloured in dark grey.
- The min and max spectra among participants' spectra, with the area between these two spectra coloured in light grey.

Thus, the results are presented in the form of a synthetic figure to make the reading easier. For each exercise there are three figures and each of these figures is based on the results obtained on a given acceleration factor according to the three directions.

The following sections present all the results for each RUN, and the last one provides an analysis of the results.

5.3.2. Results of RUN 42 (Exercise 9)

Figure 5.22. RUN 42 – Acceleration spectra - trolley

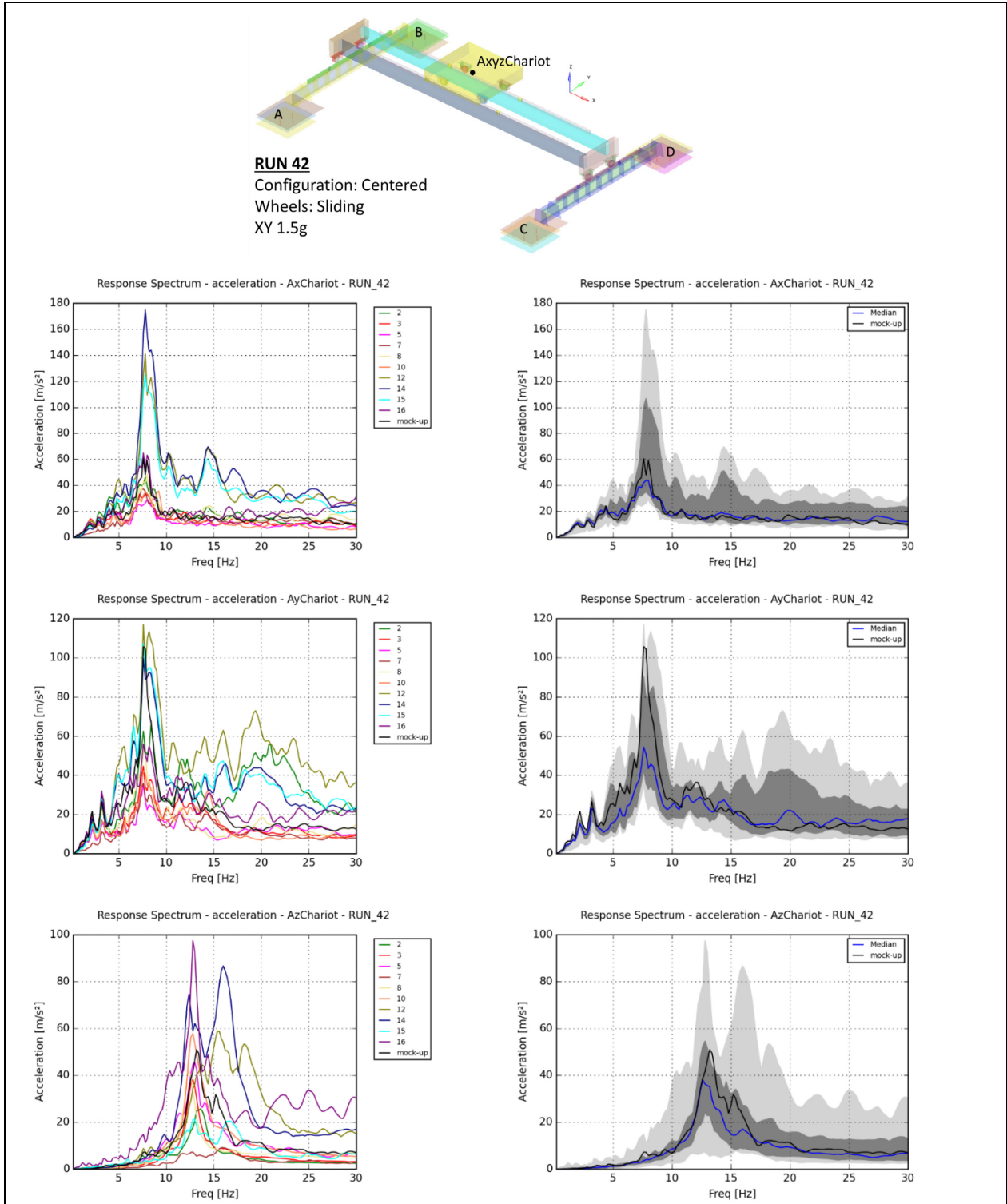


Figure 5.23. RUN 42 – Acceleration spectra – Girder beam

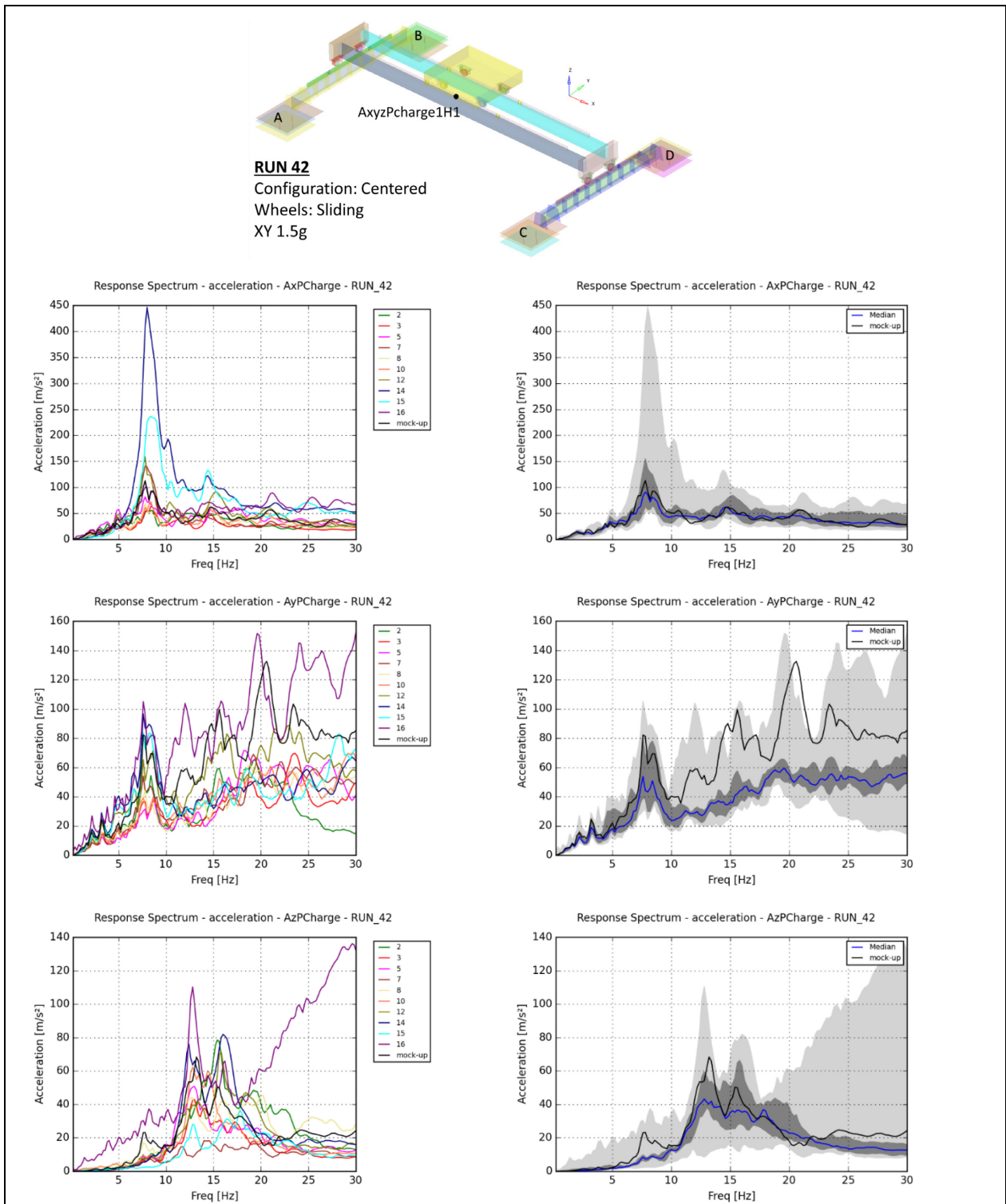
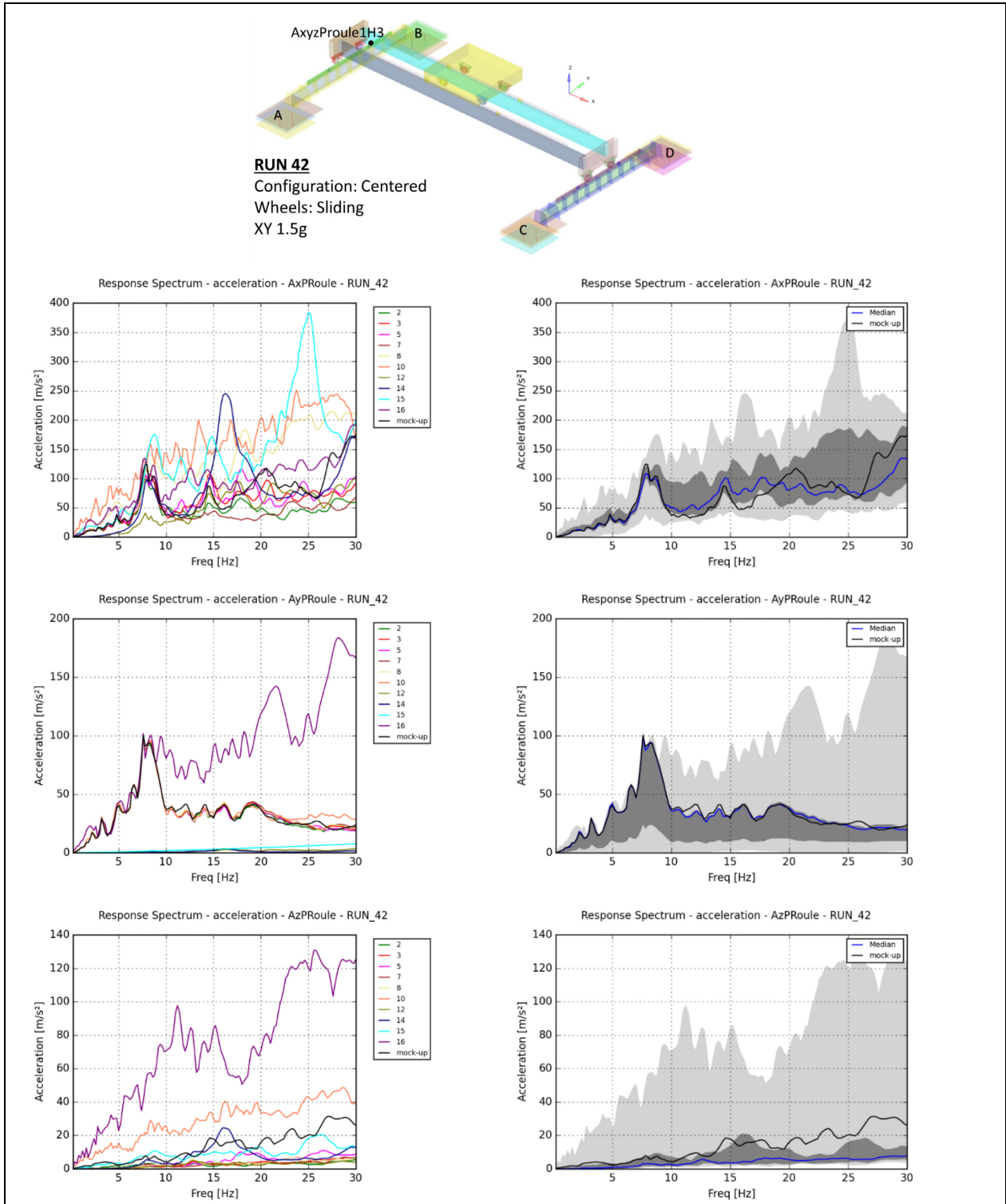


Figure 5.24. RUN 42 – Acceleration spectra – Runway beam



5.3.3. Results of RUN 80 (Exercise 8)

Figure 5.25. RUN 80 – Acceleration spectra - Trolley

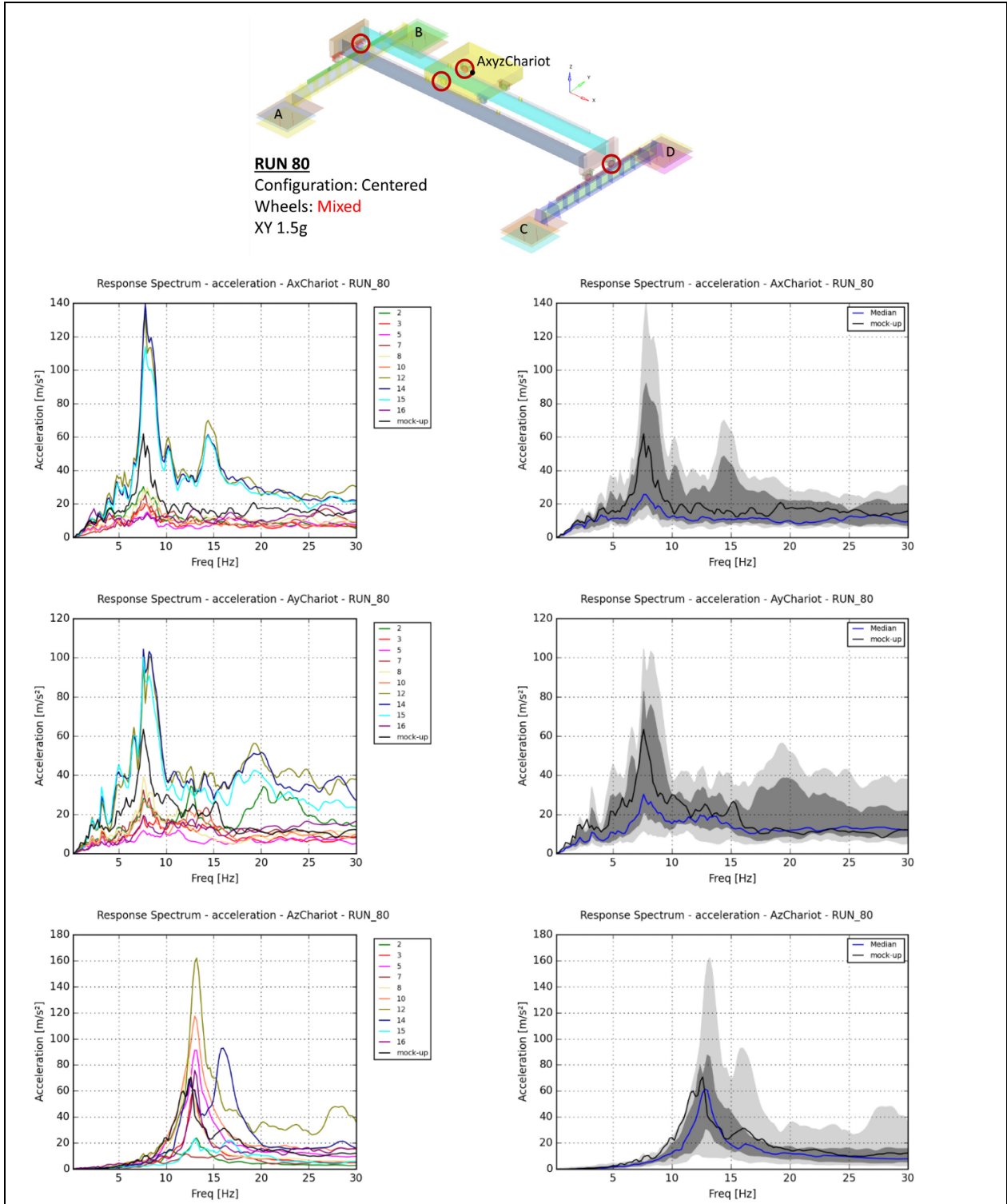


Figure 5.26. RUN 80 – Acceleration spectra – Girder beam

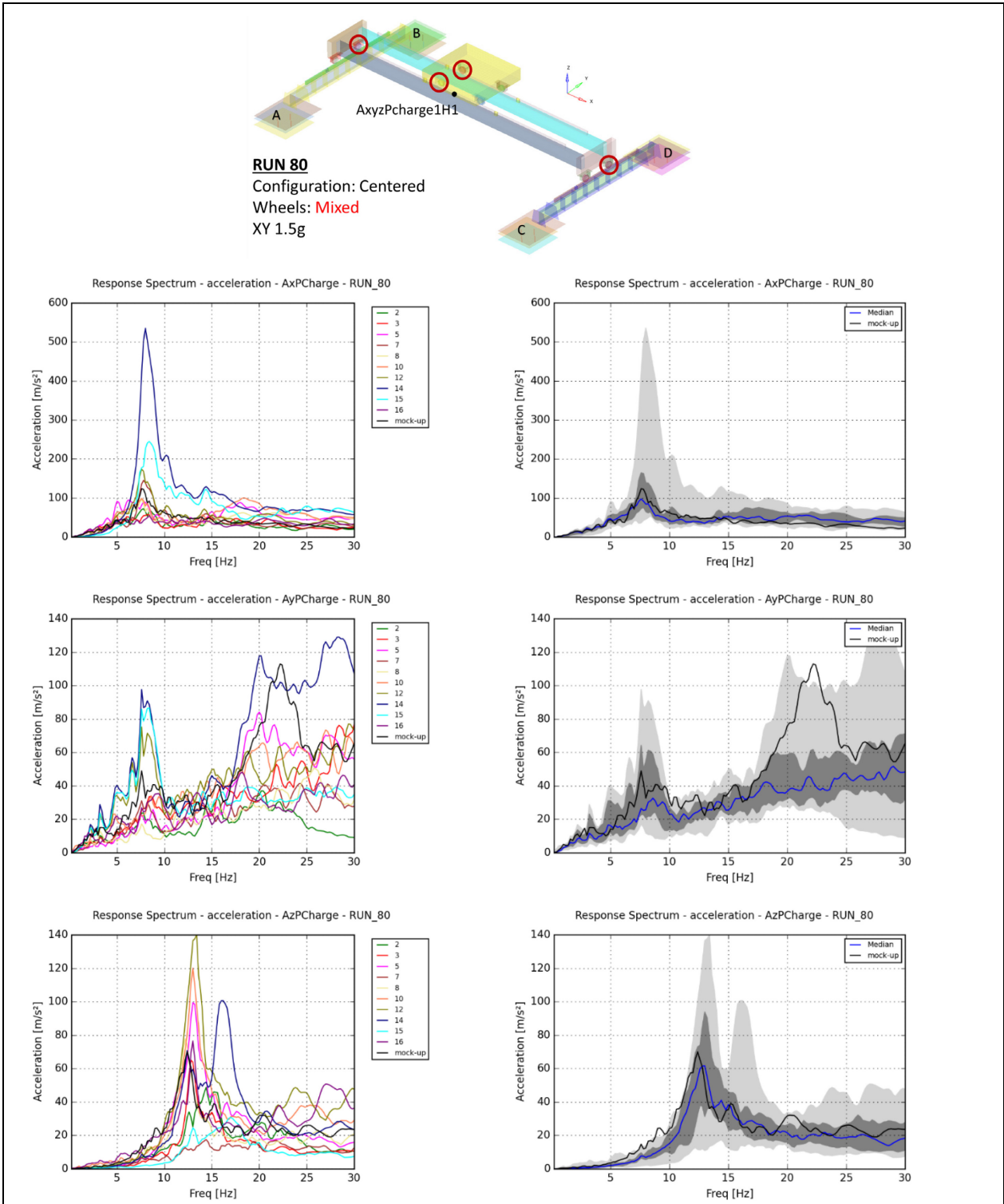
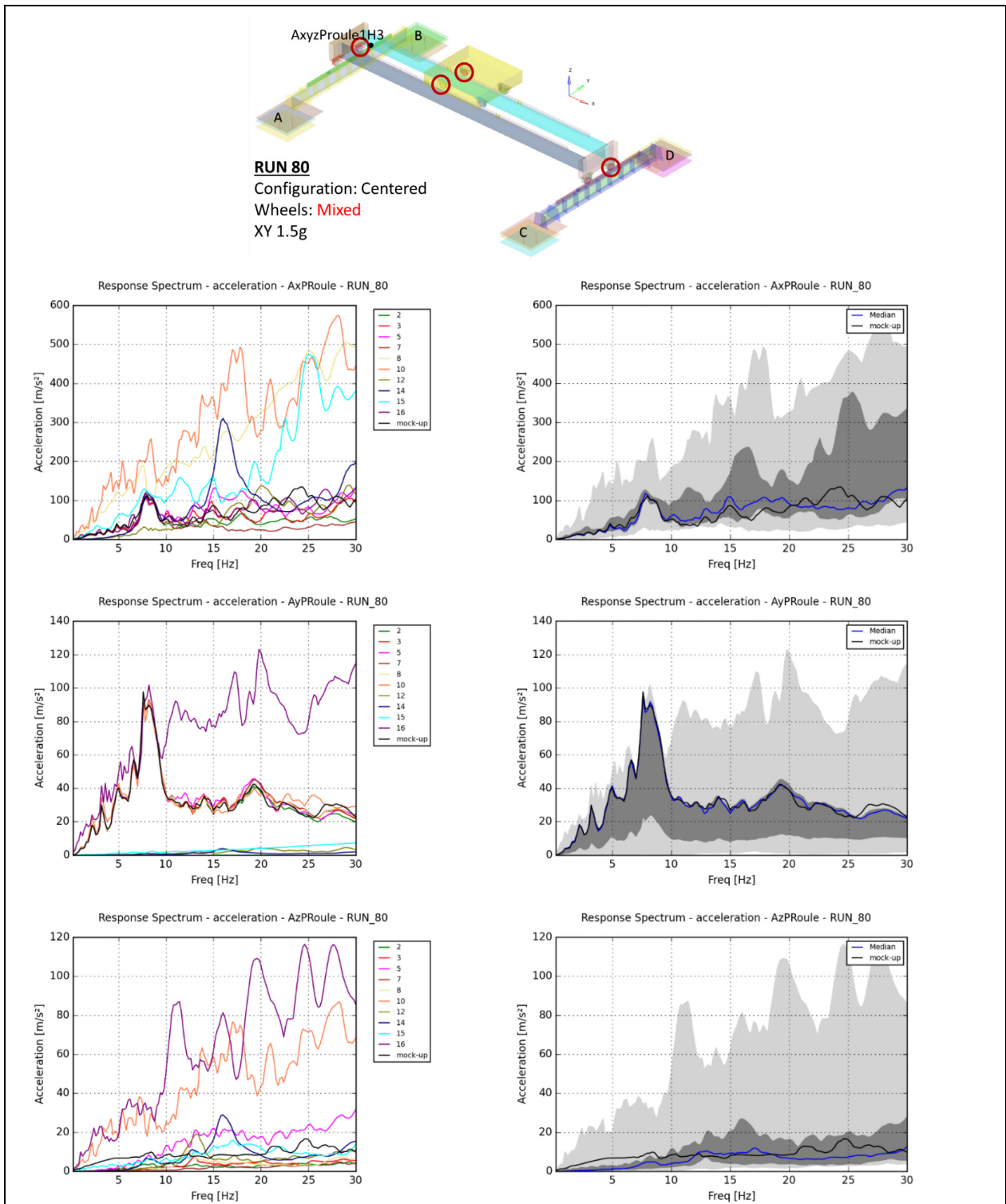


Figure 5.27. RUN 80 – Acceleration spectra – Runway beam



5.3.4. Results of RUN 112 (Exercise 10)

Figure 5.28. RUN 112 – Acceleration spectra – Girder beam

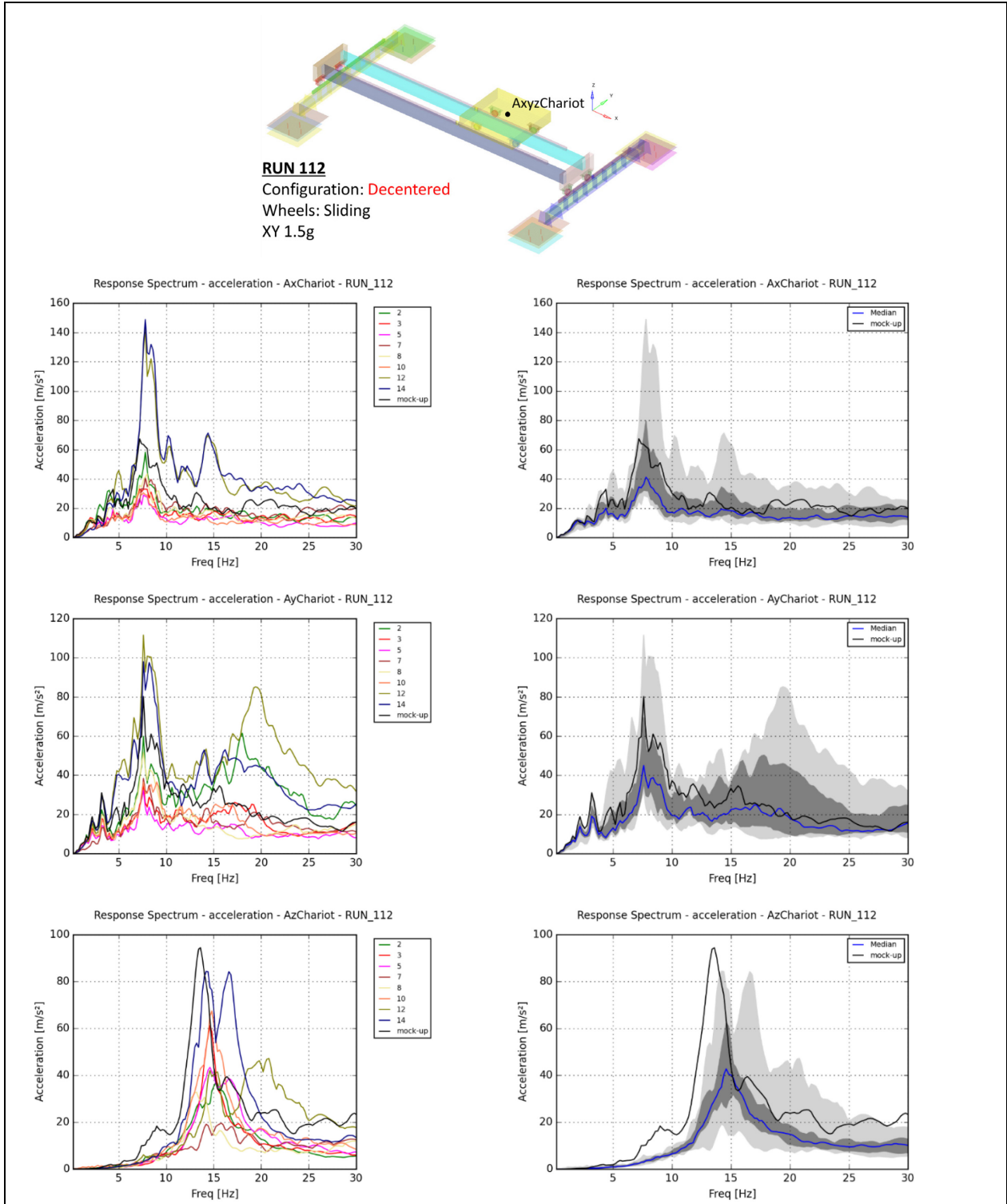
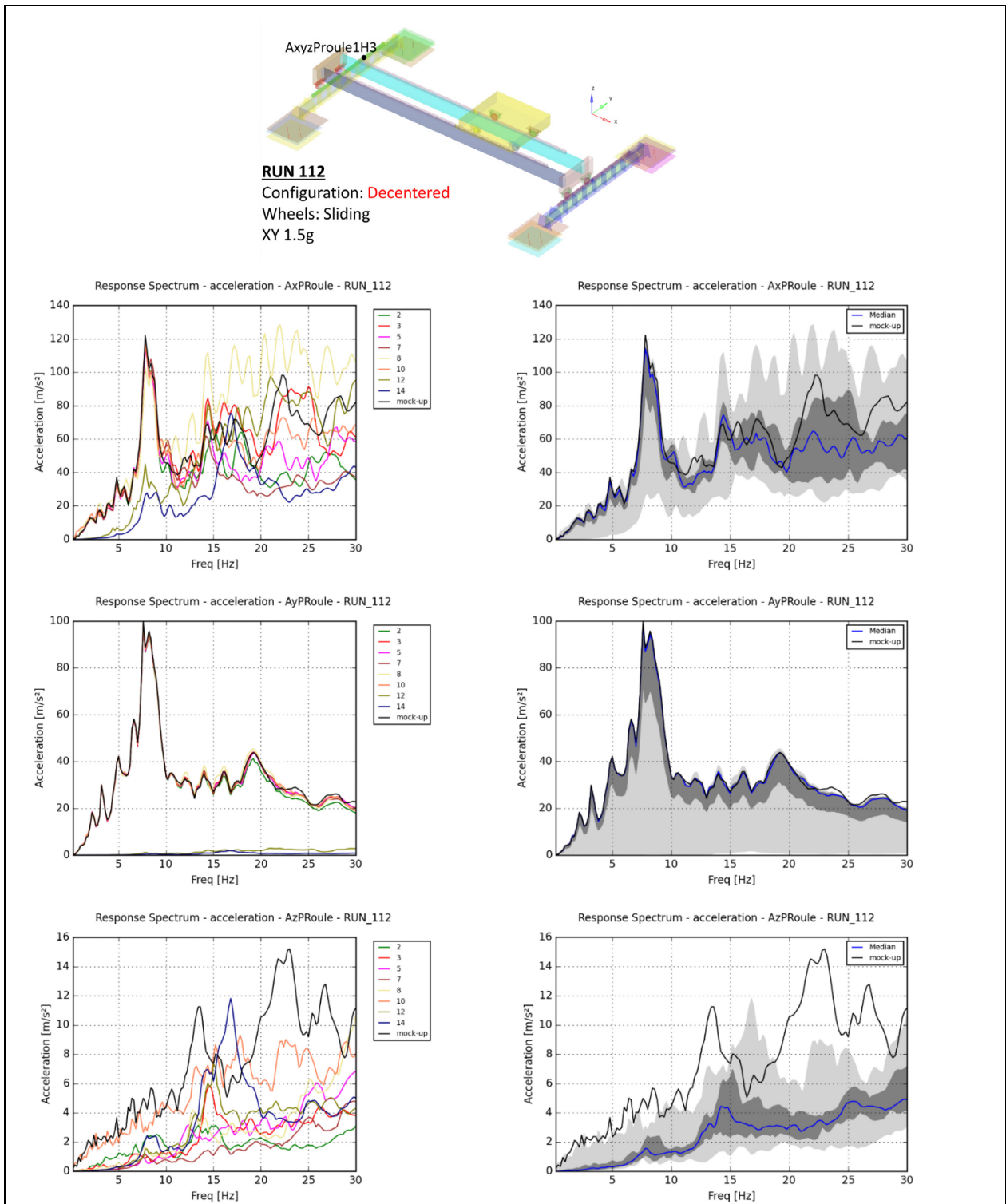


Figure 5.29. RUN 112 – Acceleration spectra – Runway beam



5.3.5. Results of RUN 128 (Exercise 11)

Figure 5.30. RUN 128 – Acceleration spectra - Trolley

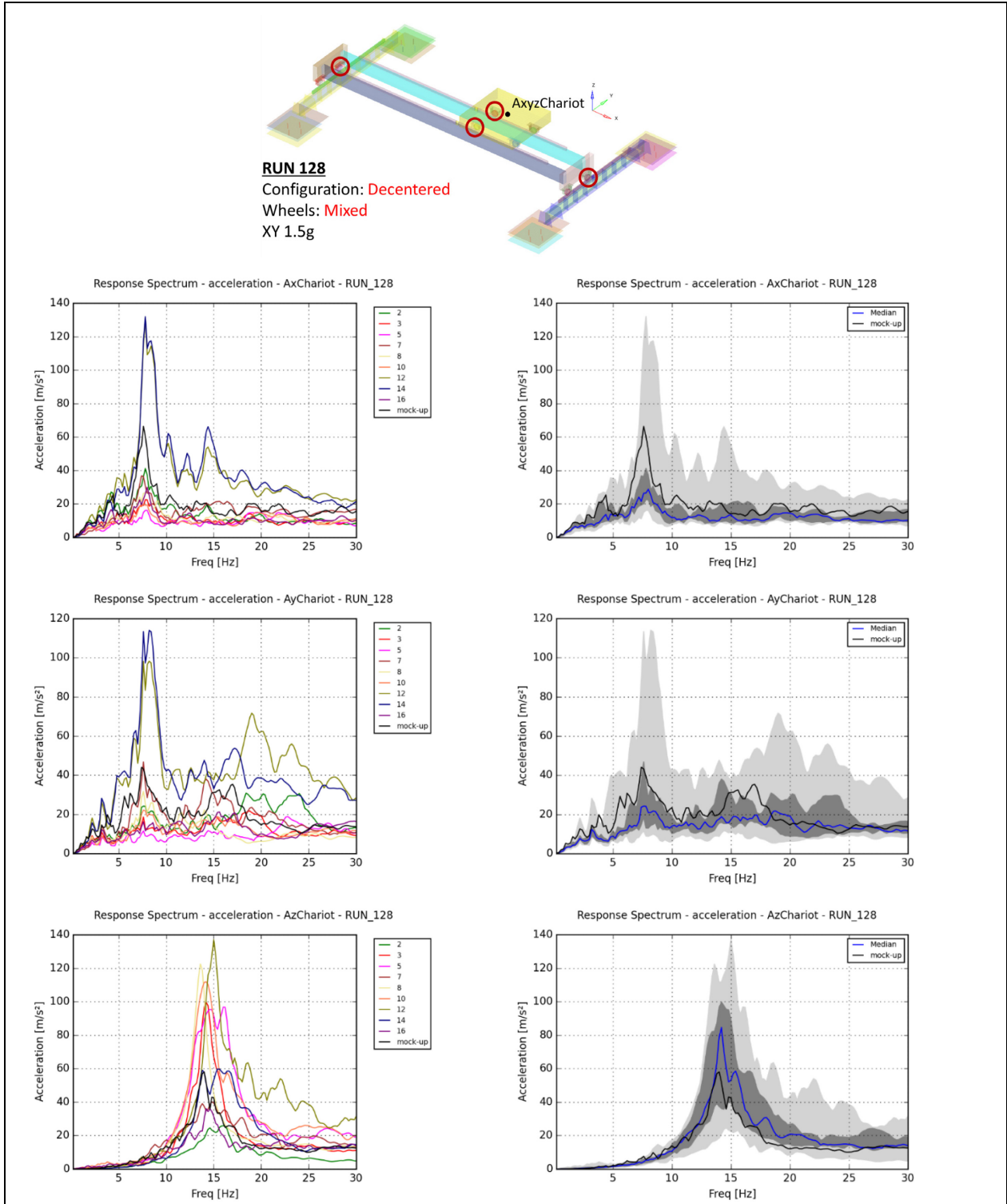


Figure 5.31. RUN 128 – Acceleration spectra – Girder beam

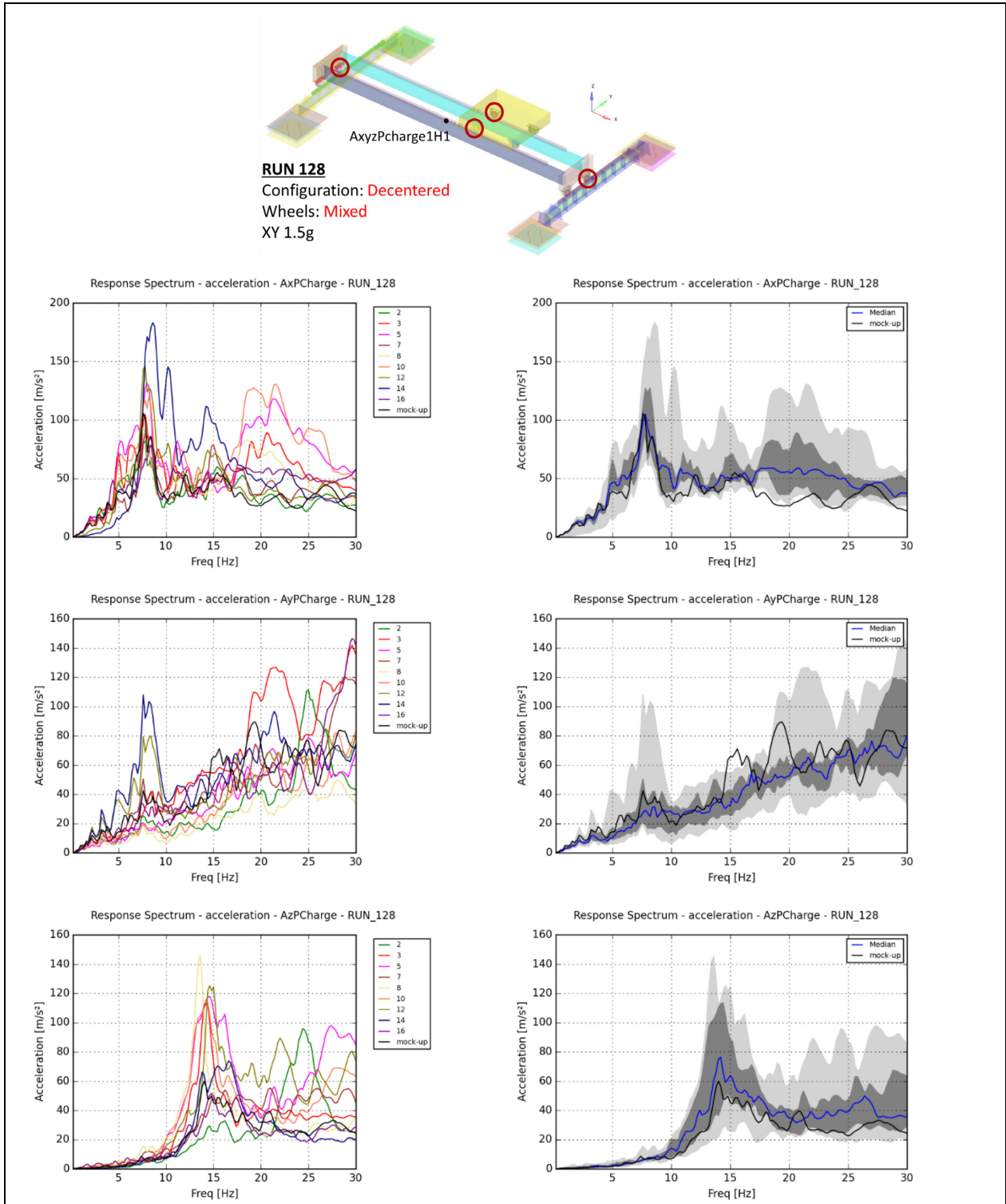
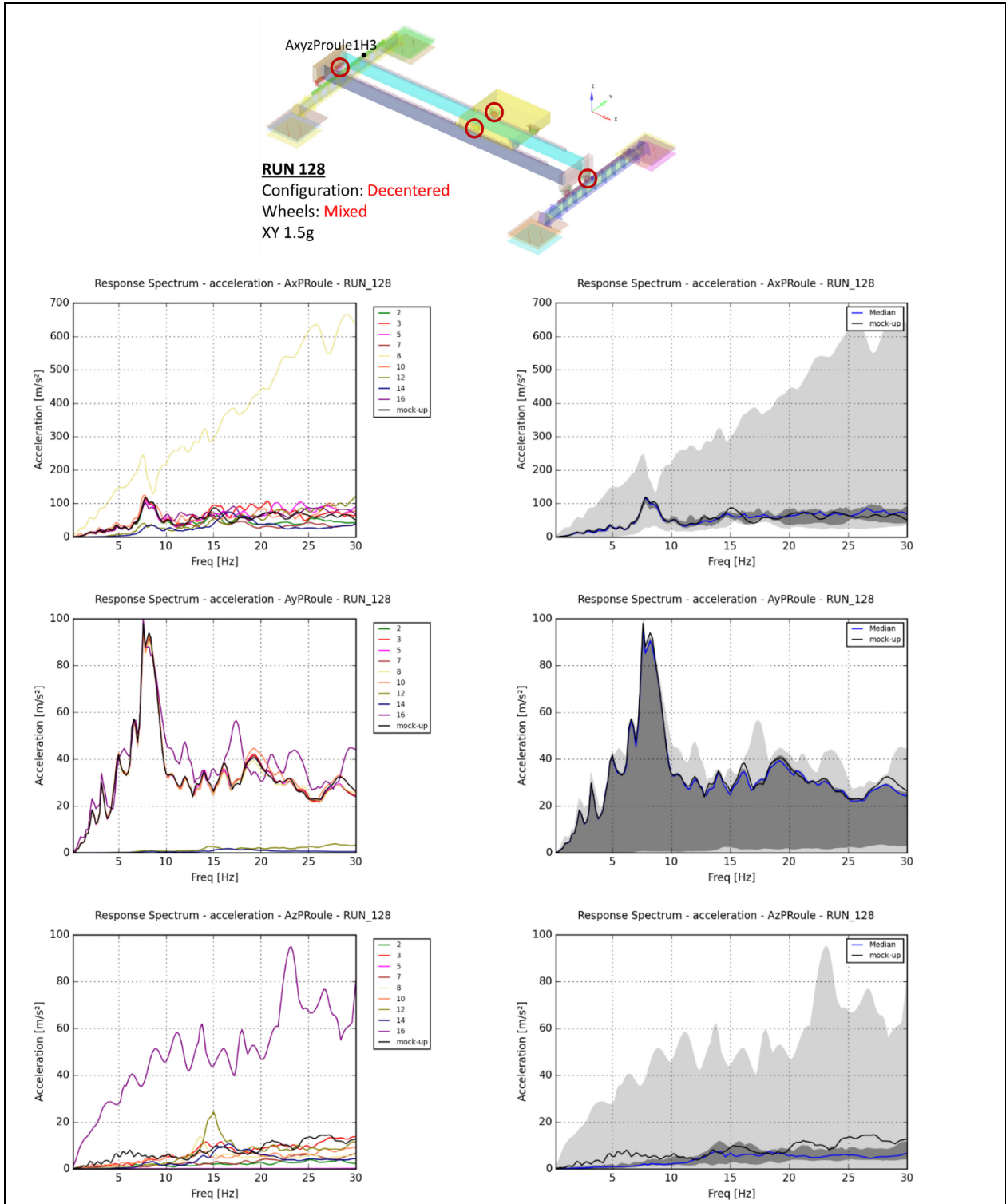


Figure 5.32. Acceleration spectra – Runway beam



5.3.6. Results of RUN 100 (Exercise 12)

Figure 5.33. RUN 100 – Acceleration spectra - Trolley

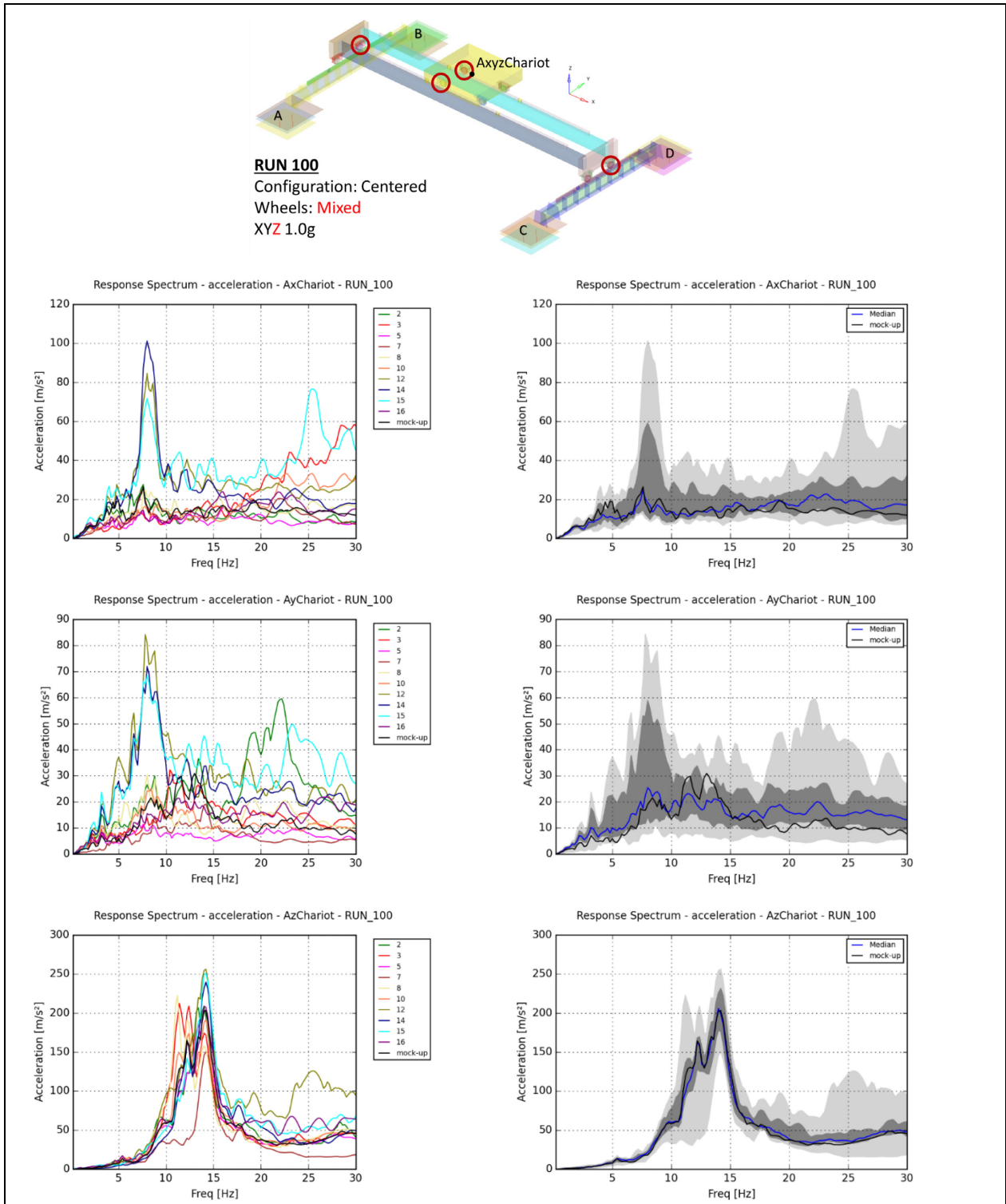


Figure 5.34. RUN 100 – Acceleration spectra – Girder beam

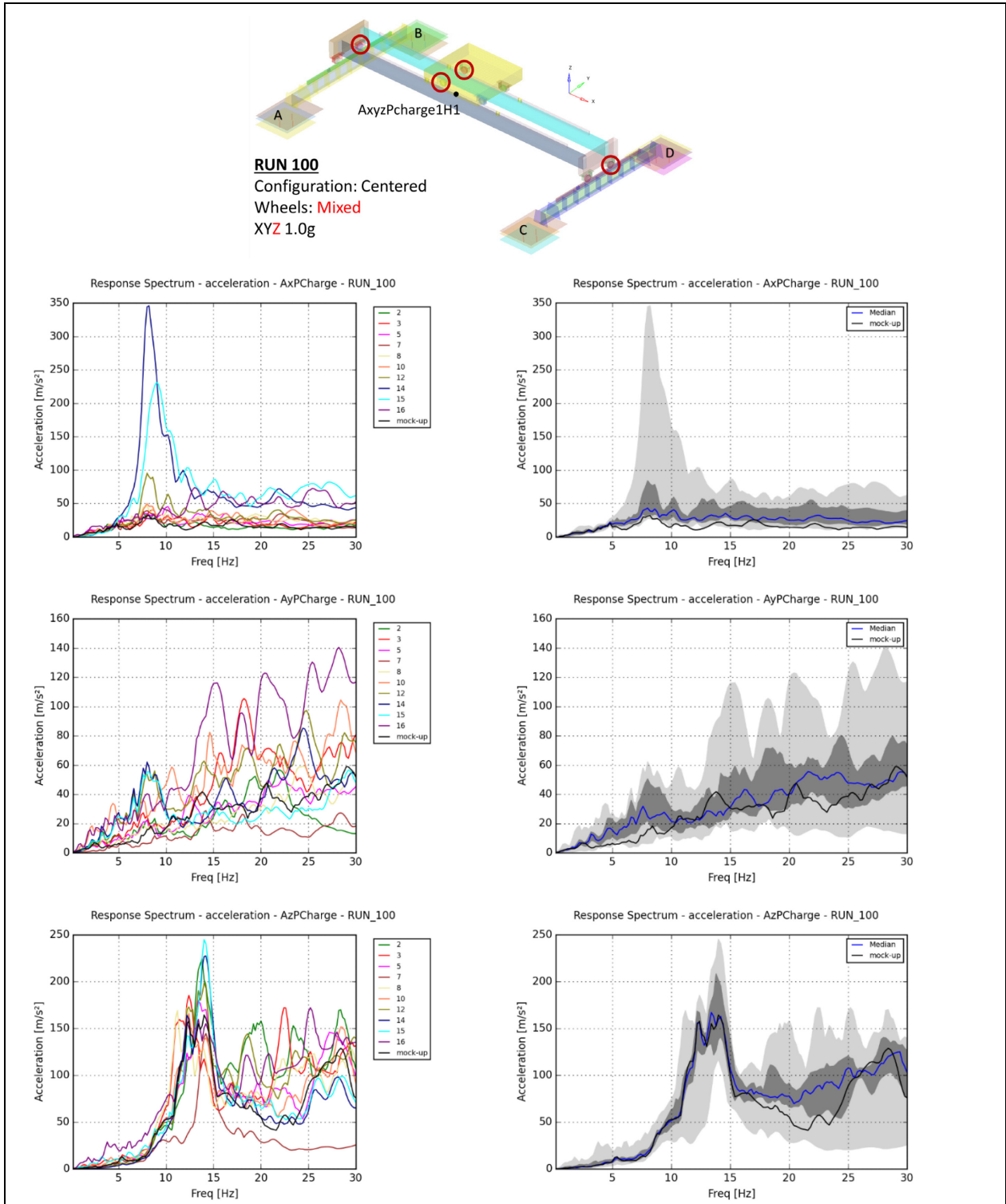
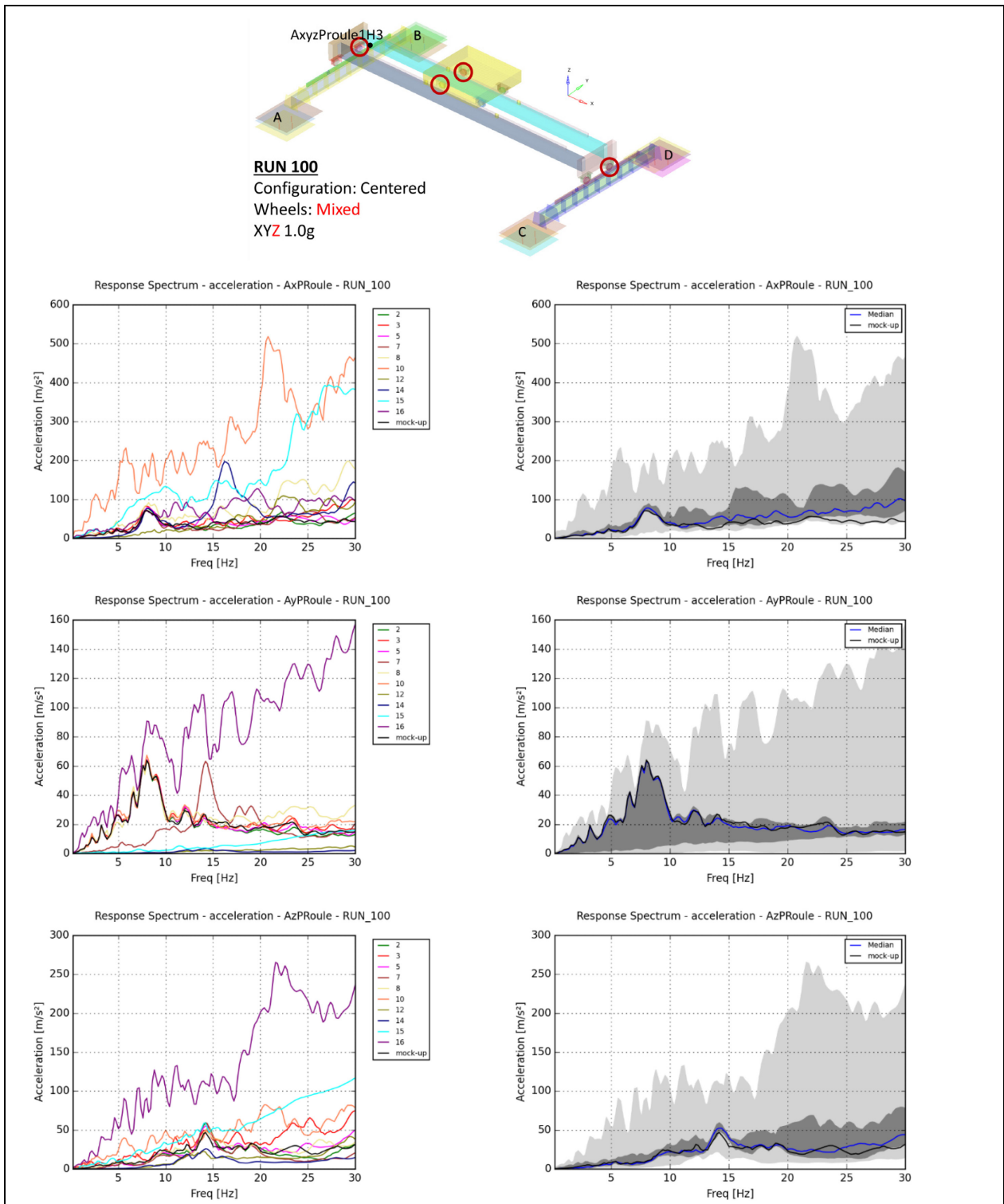


Figure 5.35. RUN 100 – Acceleration spectra – Runway beam



5.3.7. Comments on the results

Spectra calculated on the Trolley present a first peak at 7 Hz horizontally and at 13 Hz for vertically, which is consistent with the mock-up and the first modes of the Crane.

Spectral acceleration calculated on the trolley from the participants' results are overall in great accordance with the mock-up spectra, being rather well contained in the inter-quartile space Q_1 - Q_3 (dark grey area, between first quartile and third quartile), except for RUN 112 in the vertical direction, where the mock-up spectrum is clearly higher.

In the vertical direction, results are even better for the RUN 100 (three-dimensional excitation), where the median spectrum from participant's values and the mock-up spectrum match.

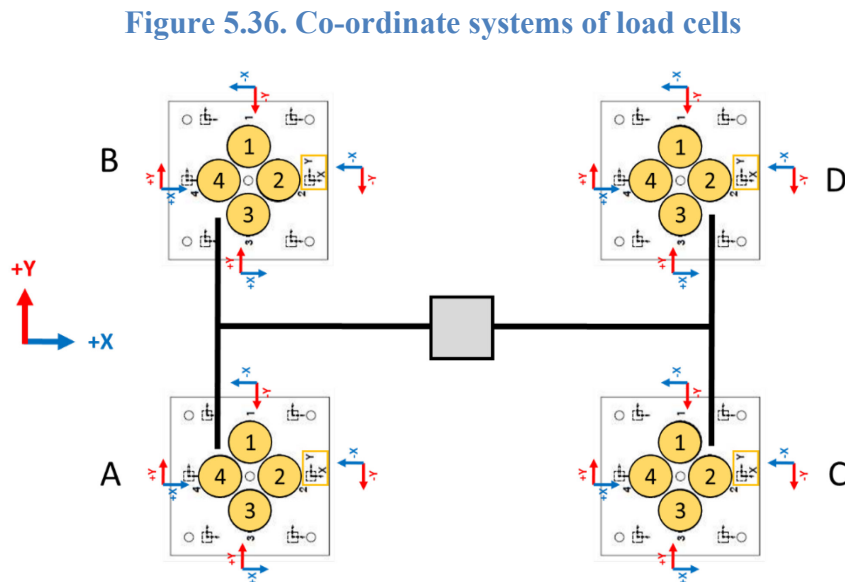
5.4. Support reactions

5.4.1. Post-processing description

For each RUN, support reactions at load cell blocks A, B, C and D were requested. Some participants provided the steering committee with resultants for each block, and others provided reactions in each of the 16 load cells. In this case, reactions per block were calculated.

Some participants provided reactions that include self-weight, whereas support reactions in the load cells of the mock-up are null before the seismic excitation. Moreover, units, the initial time of the simulation or sign convention may be different between participants. Signals were modified so they can be compared to the mock-up signals.

Figure 5.36 presents the local co-ordinate systems of the load cells of the mock-up compared to the global co-ordinate system.



The local co-ordinate systems of the load cells were confirmed analysing support reactions in these load cells for unidirectional RUNs from Stage 1 such as RUN 64 (pulse in X direction).

The time evolutions of these reactions per Blocks (A, B, C, D) are plotted below, in the three directions, with the one of the mock-ups in black. Also provided are box plot graphs

of the maximum value of the absolute value of the horizontal reactions, for each block, and of the minimum and maximum values of the vertical reactions, as well as for displacements:

- Q_0 : min (black tick)
- Q_1 : 25% percentile = first quartile (bottom of the blue box)
- Q_2 : 50% percentile = median (red line)
- Q_3 : 75% percentile = third quartile (top of the blue box)
- Q_4 : max (black tick)

Support reactions of the mock-up are represented by a black dot.

The following sections present the results for each RUN, and the last one an analysis of the results.

5.4.2. Results for RUN 42 (Exercise 9)

Figure 5.37. RUN 42 – Support reactions – min/max

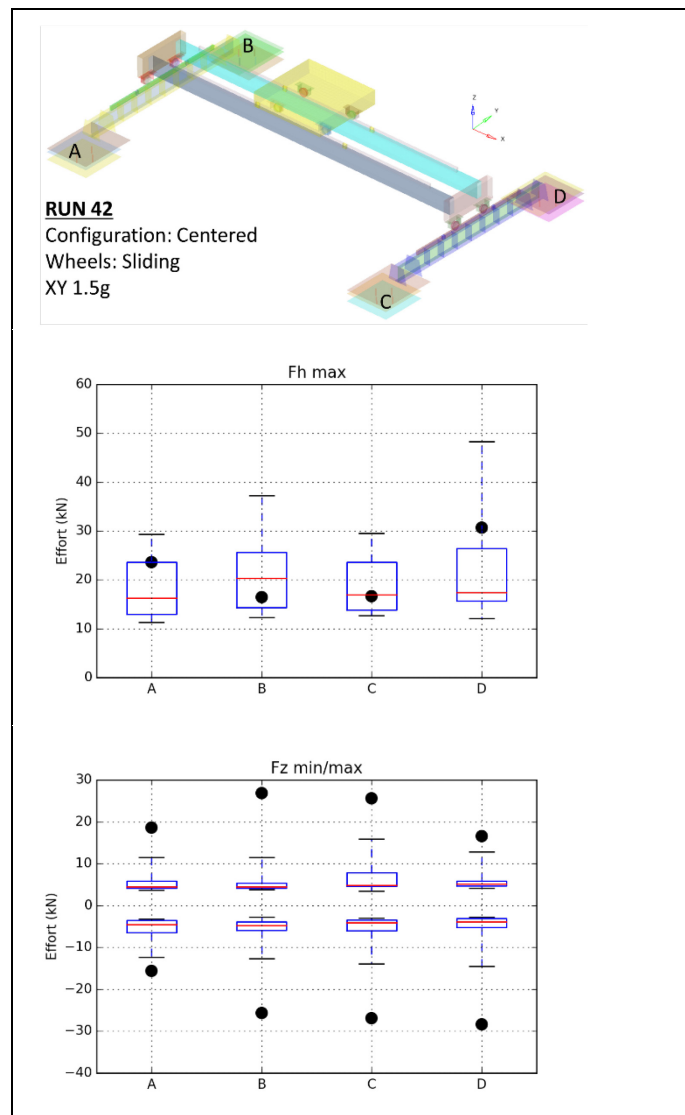
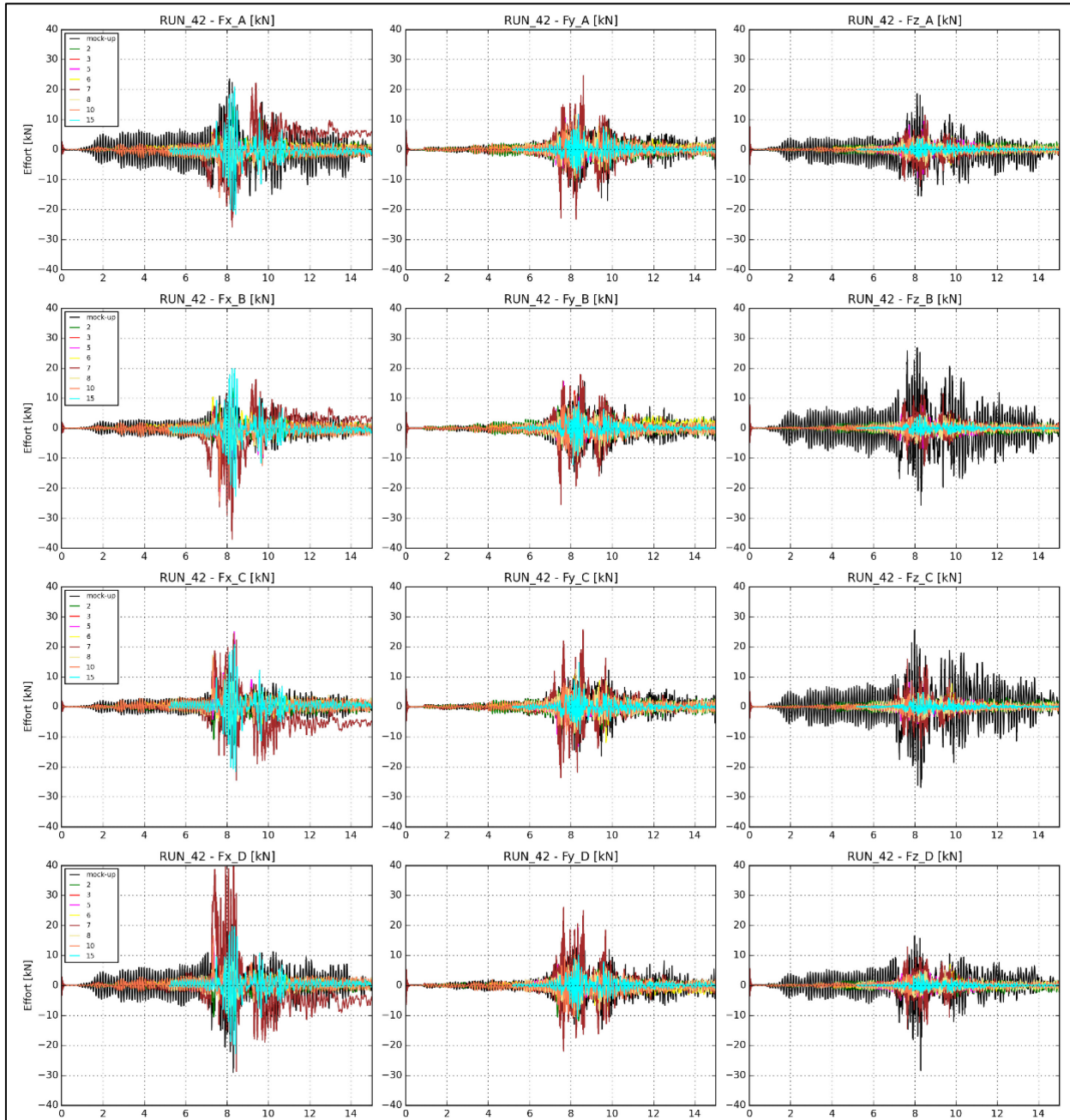


Figure 5.38. RUN 42 – Support reactions



5.4.3. Results for RUN 80 (Exercise 8)

Figure 5.39. RUN 80 – Support reactions – min/max

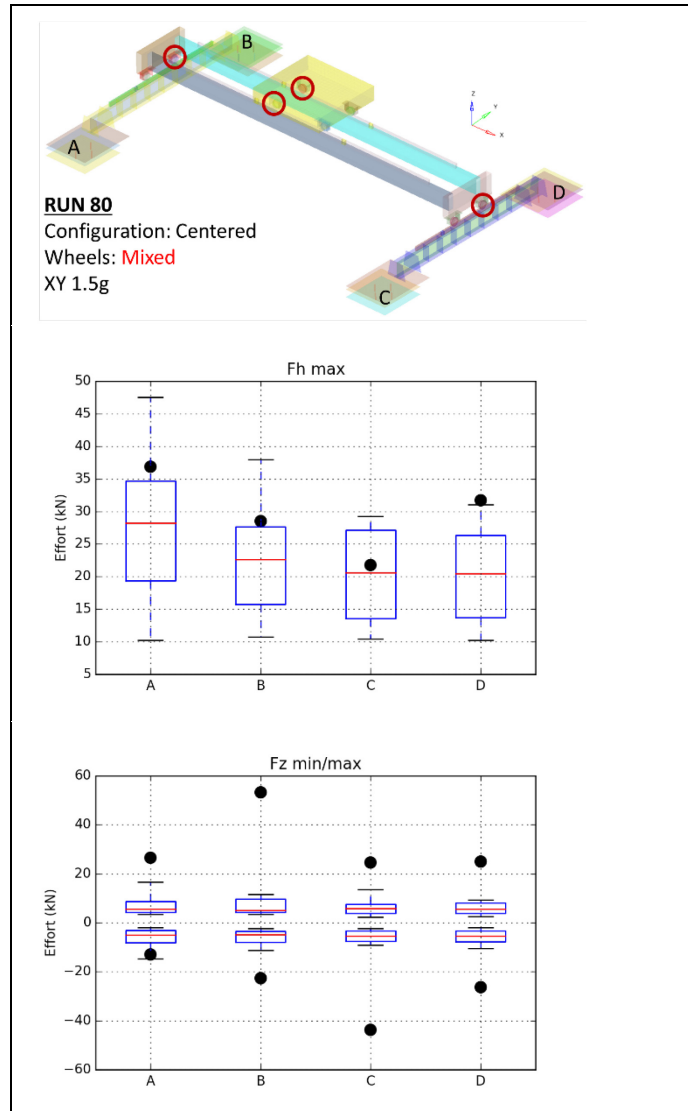
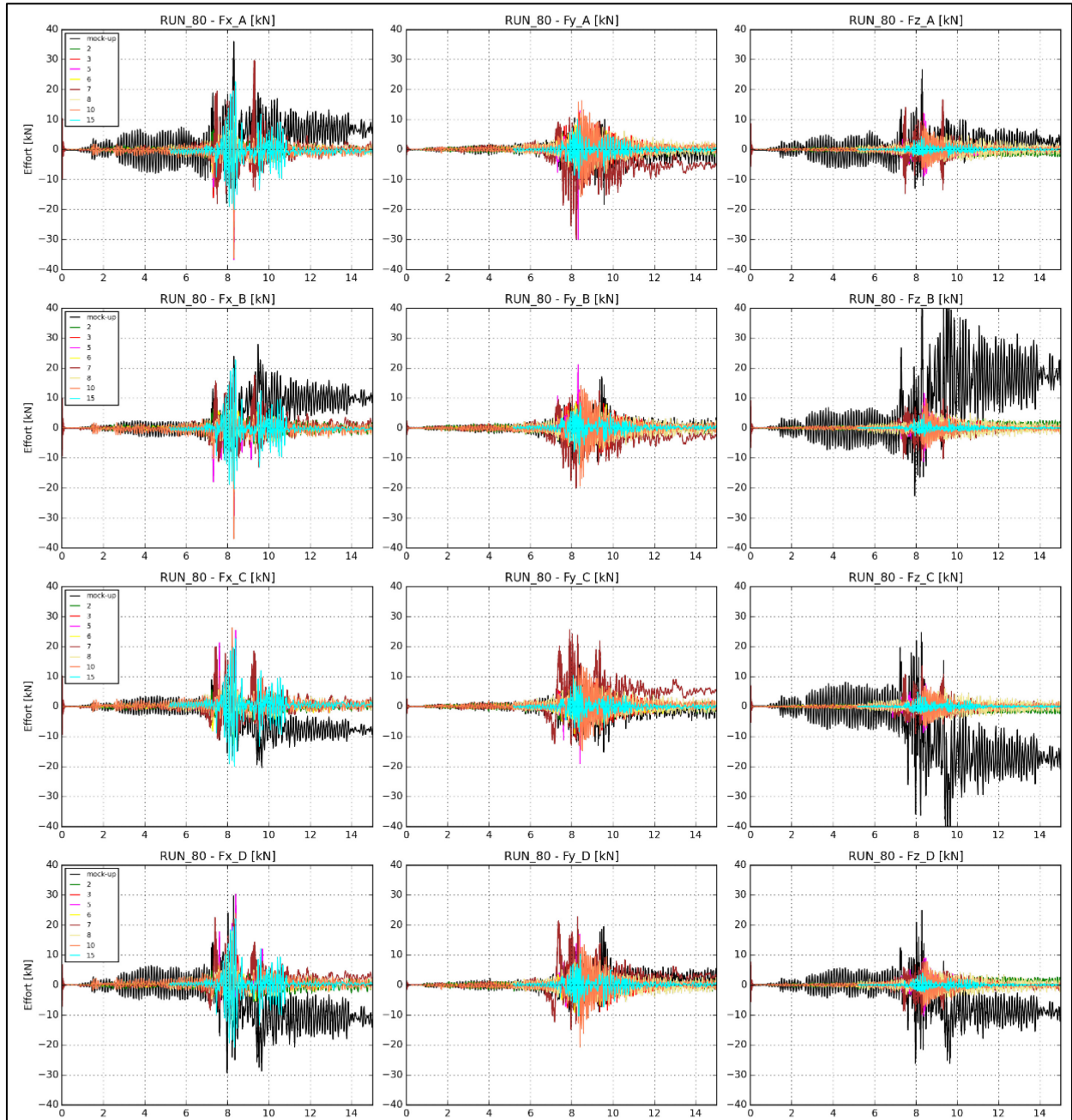


Figure 5.40. RUN 80 – Support reactions



5.4.4. Results for RUN 112 (Exercise 10)

Figure 5.41. RUN 112 – Support reactions – min/max

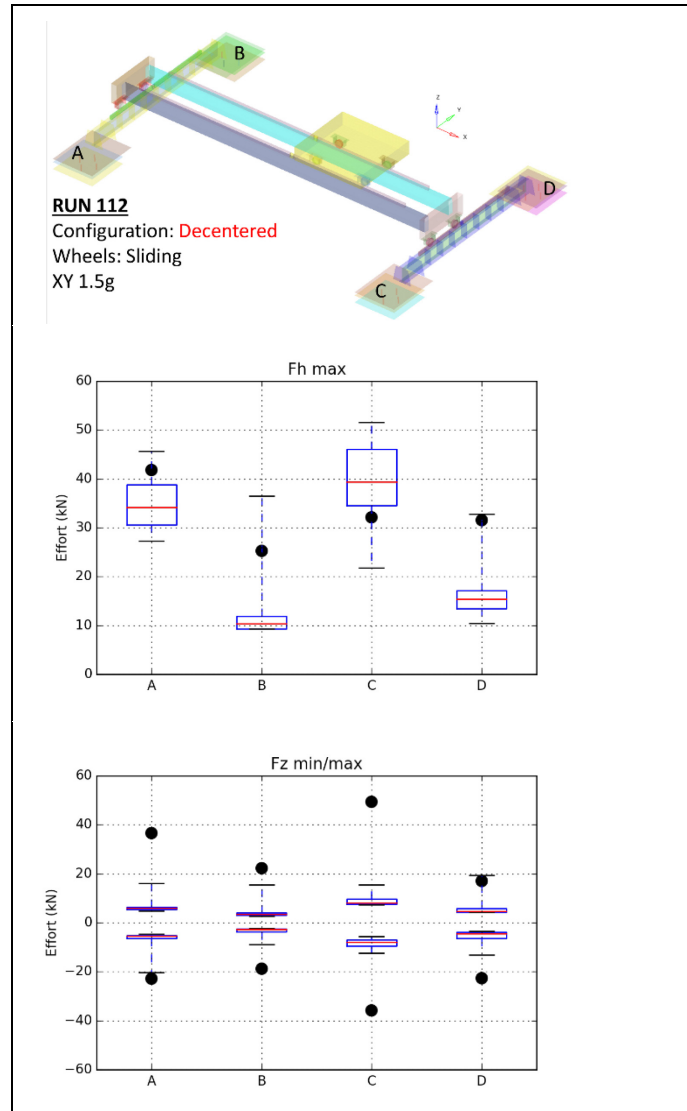
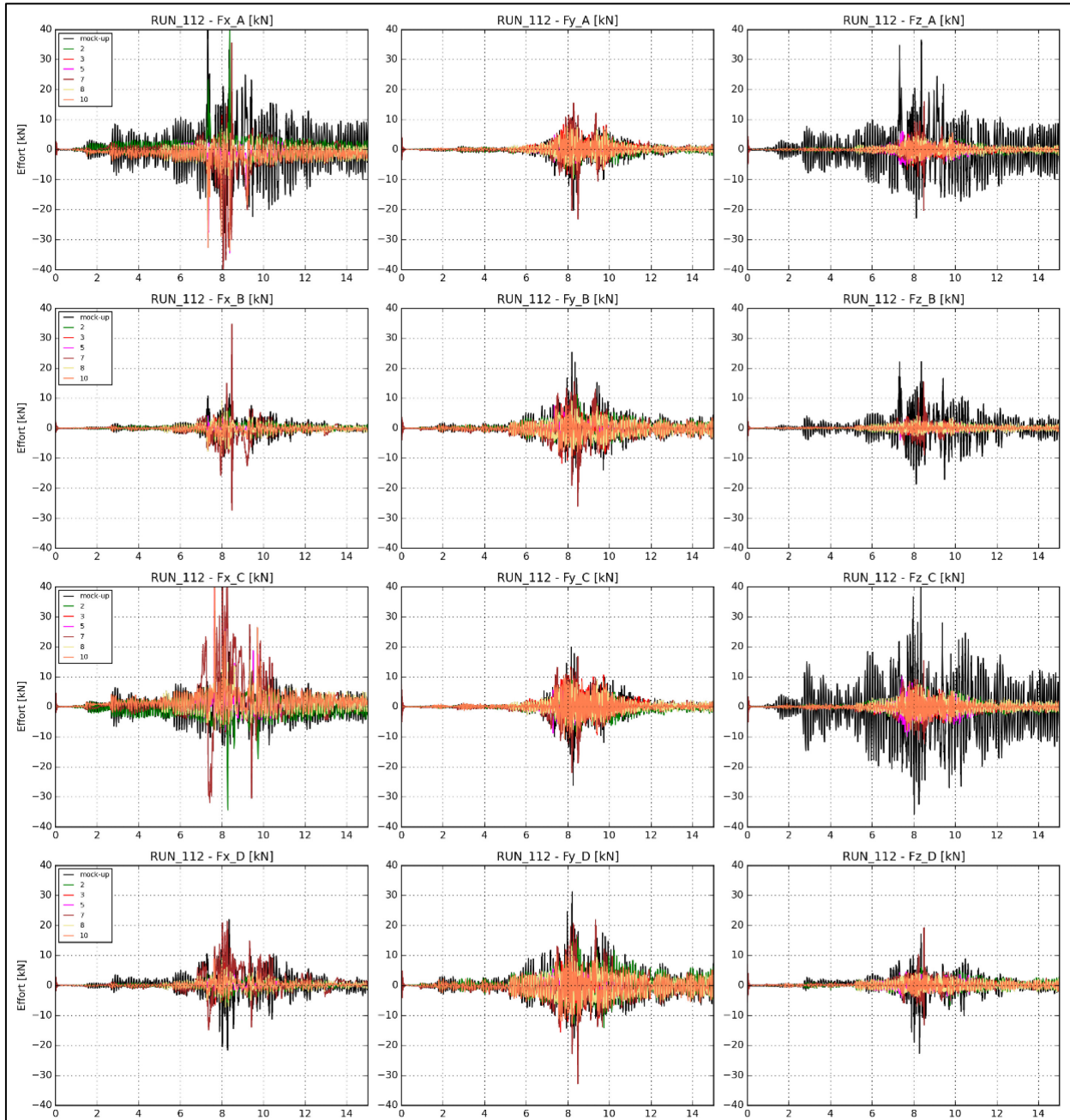


Figure 5.42. RUN 112 – Support reactions



5.4.5. Results for RUN 128 (Exercise 11)

Figure 5.43. RUN 128 – Support reactions – min/max

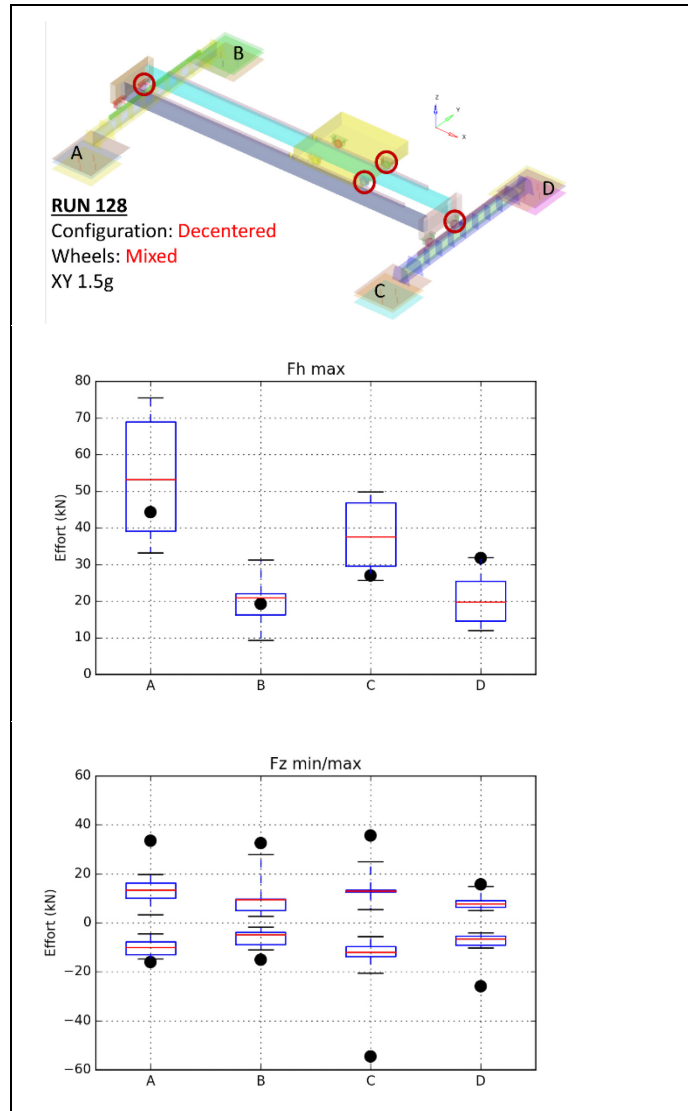
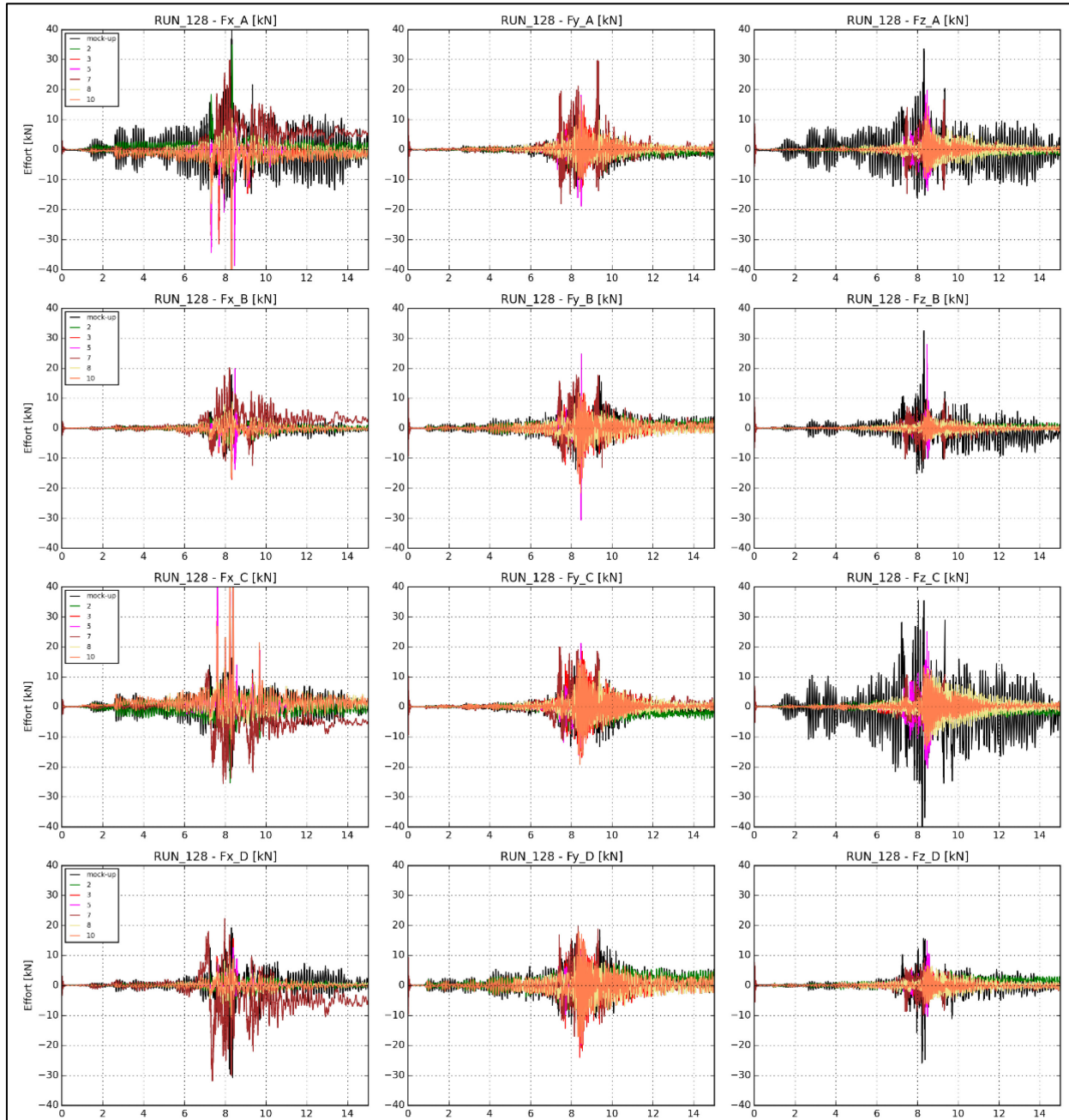


Figure 5.44. RUN 128 – Support reactions



5.4.6. Results for RUN 100 (Exercise 12)

Figure 5.45. RUN 100 – Support reactions – min/max

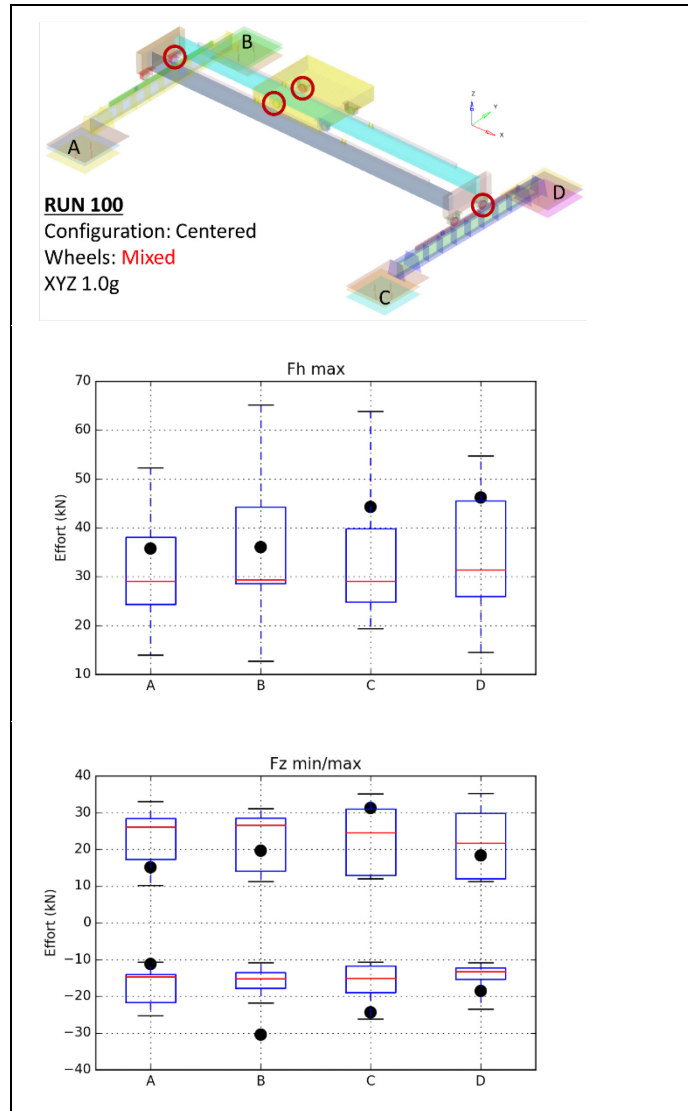
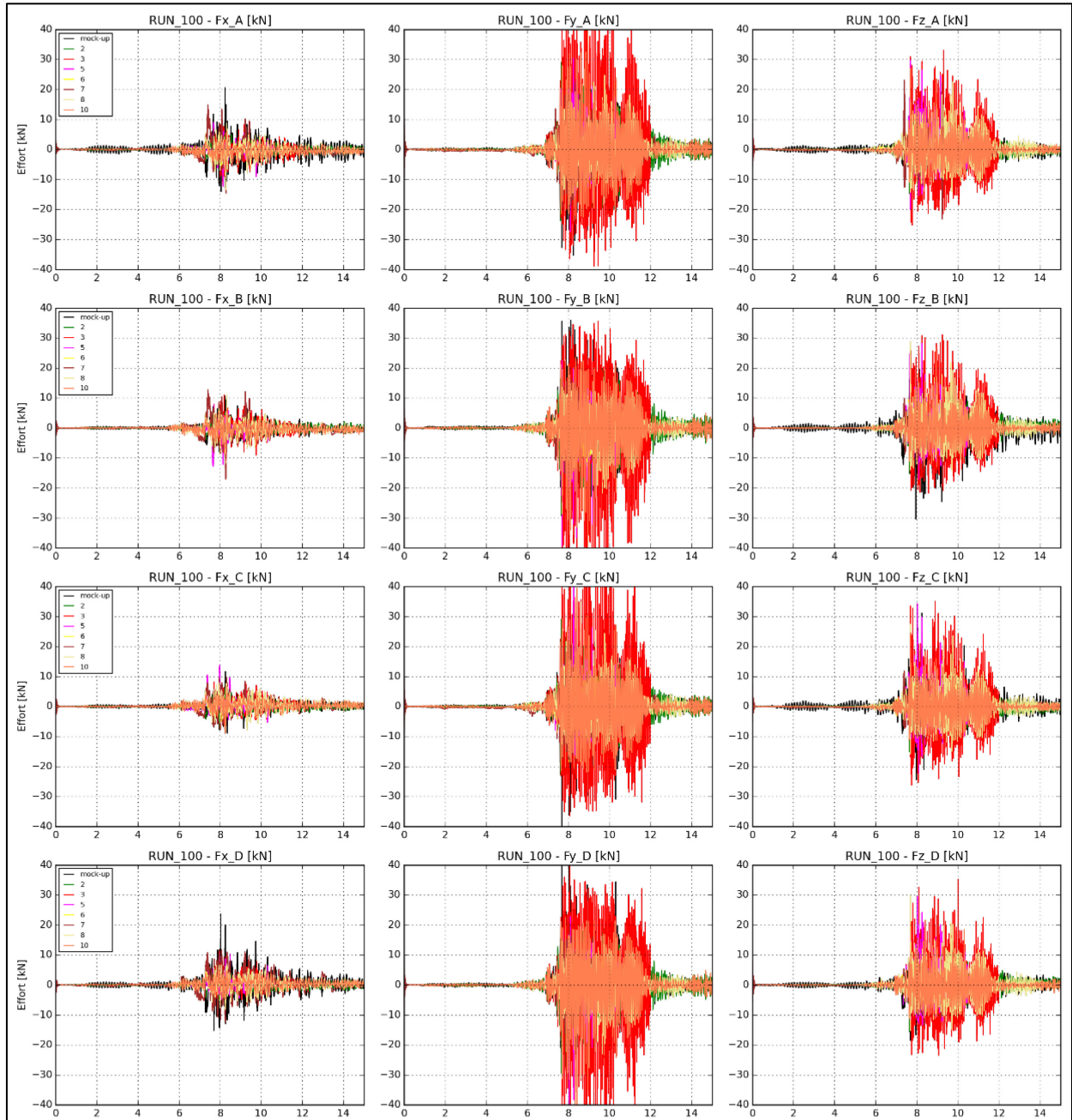


Figure 5.46. RUN 100 – Support reactions



5.4.7. Support reactions for all RUNs

Figure 5.47. All RUNs – Centred crane configurations - Support reactions

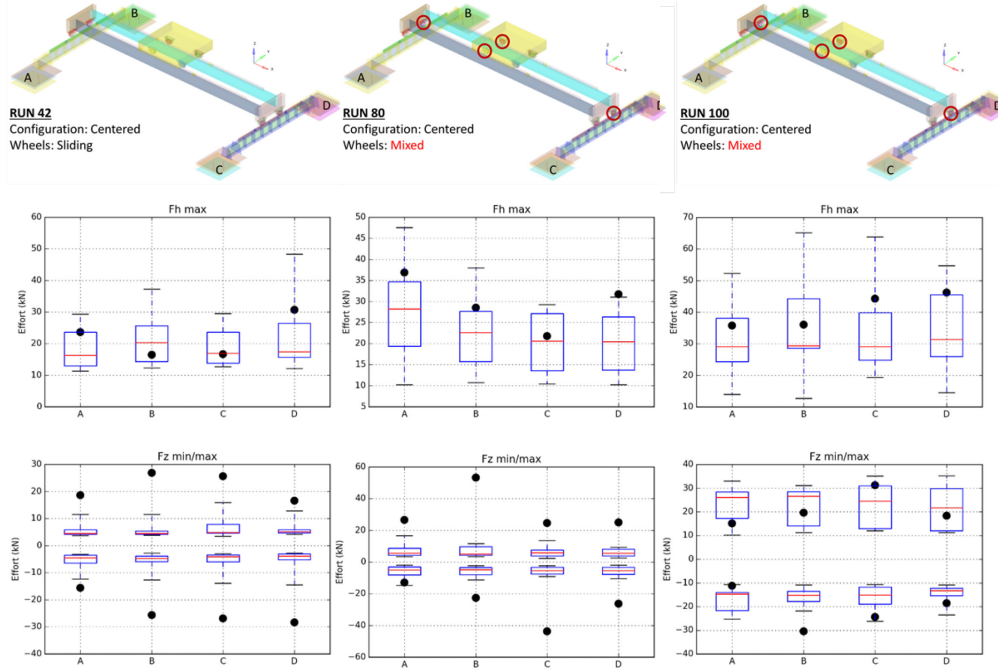
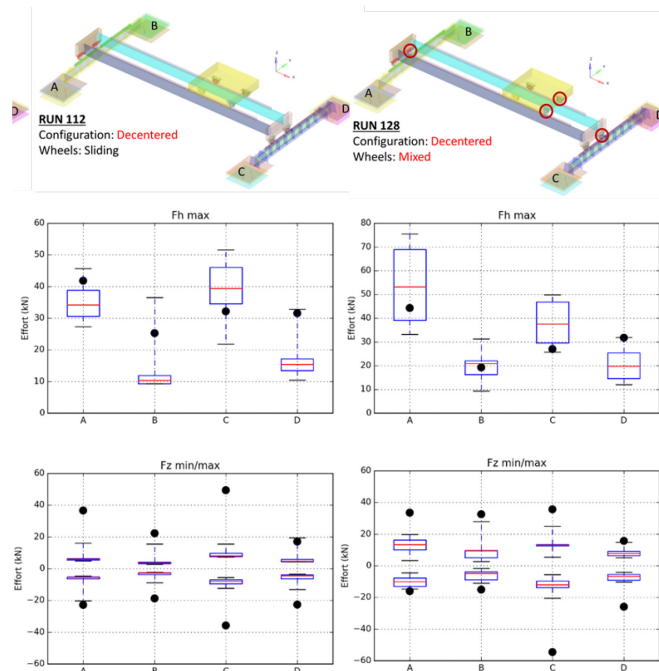


Figure 5.48. All RUNs – Decentred crane configurations - Support reactions



5.5. Comments on the results

5.5.1. Overall comments

For all the exercises, the horizontal reactions calculated by the participants are in great accordance with the one measured by the mock-up. The order of magnitude is the same and the mock-up value is sometimes inside the blue box (of the box plot graphs), which means it is between the 25th and the 75th percentiles (first and third quartiles) and always between the minimum and the maximum of the participants' values.

This cannot be said for the vertical reactions, among which two cases can be distinguished:

- For exercises with a two-dimensional input, meaning a horizontal input (every exercise except RUN 100), the mock-up values are almost always far from the min and the max values calculated by the participants. This leads to blue boxes (first to third inter-quartile space) that seem very thin.
- For RUN 100 with a three-dimensional input, vertical support reactions are in great accordance with the one measured by the mock-up.

As an explanation of this discrepancy between calculations and measurements concerning the vertical reaction, it can be helpful to take note of the horizontal RUNs; the participants imposed in their calculations a zero vertical movement at the four supports, and only a horizontal movement that was identical to the four supports. This does not correspond to the movement imposed on the bridge during the tests; besides, the setpoint signal imposed on the table is only along X-Y, but the movement of the bridge contains rotations and a slight vertical component that can differ at each support.

This discrepancy is less significant for RUN 100, where the vertical movement is imposed by the participants as well as during the test campaign.

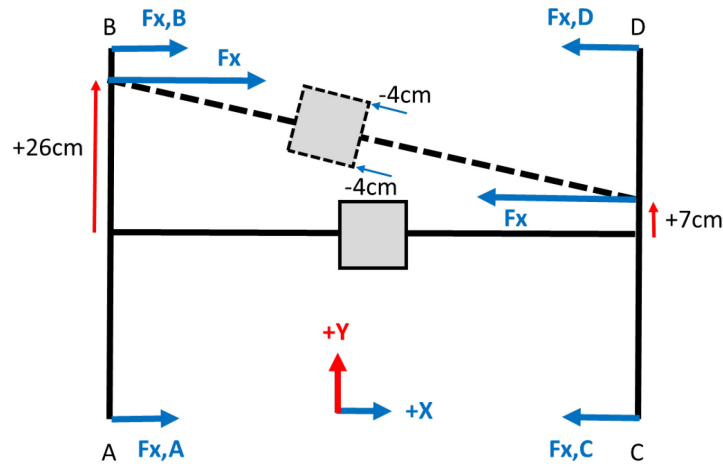
For the decentred configurations (RUN 112 and 128), the maximal reactions (in horizontal and vertical directions) of the mock-up are higher for the load cell blocks A and C than for B and D; see Figure 5.50. This is because in the decentred configuration girder beams are closer to the Load Cell Blocs A and C than B and D. This gap between values for load cell block A-C and B-D is even higher in the participants' results.

Focus on RUN 80

For RUN 80, mock-up reactions for each load cell blocks are not centred on 0 kN in the X and Z directions, after $t=9$ s (of course the sum of the reactions of the four load cell blocks is centred around 0 kN).

This is the effect of the large displacement of the trolley during the RUN 80 (see the Trolley's trajectory in Figure 5.8 or the displacements of the end-truck beams in Figure 5.7, indeed, after $t=9$ s):

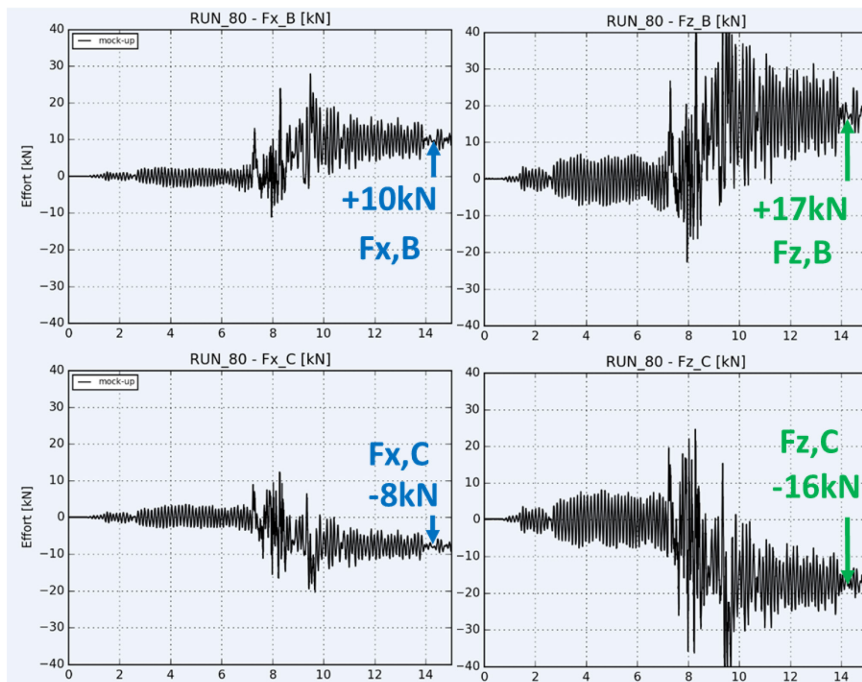
Figure 5.49. Final position of the crane for RUN 80



That means that the trolley, which was initially centred, has a final position that is near load cell block B and far from load cell block C. This leads to an increase of the support reaction in B of about +17 kN, and a decrease in C of about -16 kN (and no significant variations in A and D).

Moreover, given the fact that DySomA and DySomC are very different (+24 cm vs. +8 cm) after $t=9$ s, the girder beams have rotated and the cheeks of the end-truck's wheels are in contact with lateral faces of the girder rails. This leads to an internal effort along the X-axis which can be seen in the load cell block reactions (around +10 kN in A and B; around -10 kN in C and D, total reaction is 0 kN).

Figure 5.50. Support reactions in load cell blocks B and C in X and Z directions



6. Assessment of anchor capacity

The second objective of the benchmark was to identify relevant failure criteria. However, due to the tight schedule and heavy content of the benchmark, this second objective was in the end partially addressed by evaluating the forces transmitted to the anchor, as they appear to be one of the main causes of failure.

In this section, a comparison is made between the demand in terms of force at the anchorages of the crane and the resistant capacity of common types of anchors. The demand in terms of force comes directly from the calculations made by the participants. The resistance capacity is assessed in accordance with the methodological guide of the French Association of Earthquake Engineering (UIC and AFPS, 2014).

The demand is composed of:

- N_E : Anchor normal effort demand.
- V_E : Anchor shear demand.

The resistant capacity is calculated with:

- N_R : Resisting normal effort.
- V_R : Anchor shear resistance.

Three criteria are verified to ensure the resistance of the anchorage: one in pure tension, one in pure shear, and one in tension-shear interaction:

$$\frac{N_E}{N_R} < 1$$

$$\frac{V_E}{V_R} < 1$$

$$0.7 \cdot \frac{N_E}{N_R} + \frac{V_E}{V_R} < 1 \text{ for } 0.3 < \frac{V_E}{V_R} < 1$$

Normal resistance of the anchor is composed of the tensile steel resistance and the adhesion resistance of the bolt (the anchor rod is considered straight, which is conservative). Concrete cone failure resistance is neglected for this exercise.

$$N_R = \min(N_{R,S}; N_{R,C})$$

Where:

- $N_{R,S}$ is the steel resistance of the anchor:

$$N_{R,S} = \beta_p \cdot \min \left(\frac{0.9 \cdot f_{ub} \cdot A_s}{\gamma_{M2}}; \frac{f_{yb} \cdot A_s}{\gamma_{M0}} \right)$$

- $N_{R,C}$ is the adhesion resistance of the anchor:

$$N_{R,C} = \pi \cdot d \cdot l_b \cdot f_{bd}$$

With:

- β_p : manufacturing quality safety factor equal to 0.85
- A_s : resistant section of the bolt

- f_{ub} : ultimate traction resistance of the anchor rod
- f_{yb} : elastic limit of the steel
- γ_{M0} : partial security factor equal to 1.0
- γ_{M2} : partial security factor (traction) equal to 1.25
- d : diameter of the bolt
- l_b : length of the bolt (considered straight)
- f_{bd} : adhesion stress

The anchor shear resistance is composed of the shear steel resistance and a term relative to the pressure transferred to the concrete by the rod (diametral pressure due to shear effort on the rod). Concrete edge failure is neglected here.

$$V_R = \min(V_{R,s}; V_{R,c})$$

Where:

- $V_{R,s}$ is the shear steel resistance:

$$F_{vb,Rd} = \frac{(0.44 - 0.0003 \cdot f_{yb}) \cdot f_{ub} \cdot A_s}{\gamma_{M2}}$$

- $V_{R,c}$ is the concrete resistance to the pressure due to the shear effort:

$$V_{R,c} = 0.28 \cdot d^2 \cdot \frac{\sqrt{f_{ck} \cdot E_c}}{\gamma_c} \quad \text{if } 3 < \frac{l}{d} < 4.2$$

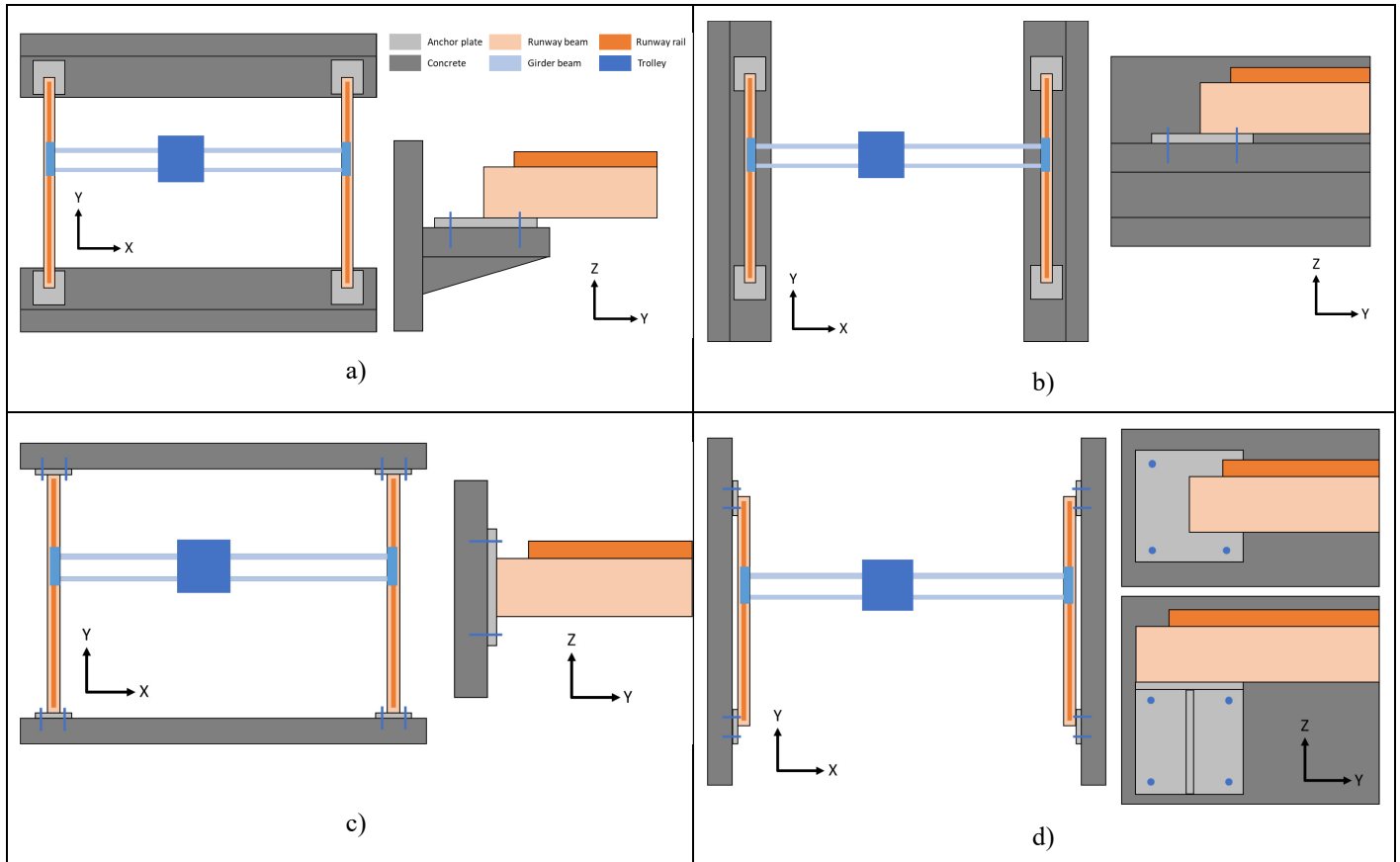
$$V_{R,c} = 0.36 \cdot d^2 \cdot \frac{\sqrt{f_{ck} \cdot E_c}}{\gamma_c} \quad \text{if } \frac{l}{d} \geq 4.2$$

With:

- f_{ck} : characteristic compression resistance of the concrete,
- E_c : concrete Young's modulus,
- γ_c : partial security factor for the concrete, equal to 1.3.

The common concrete anchoring configurations shown below are considered.

Figure 6.1. Types of anchoring



Note: a) horizontal plates – concrete wall perpendicular to runway beams, b) horizontal plates – concrete walls parallel to runway beams, c) vertical plates – concrete walls perpendicular to girder beams, d) vertical plates – concrete walls parallel to girder beams.

For horizontal anchorage plates, the shear demand is calculated by post-processing the forces along the X and Y directions, for both configurations a and b. The demand in terms of traction comes from the vertical force along the Z axis. Thus, both configurations a and b lead to the same N_E and V_E and only one verification covers these two configurations.

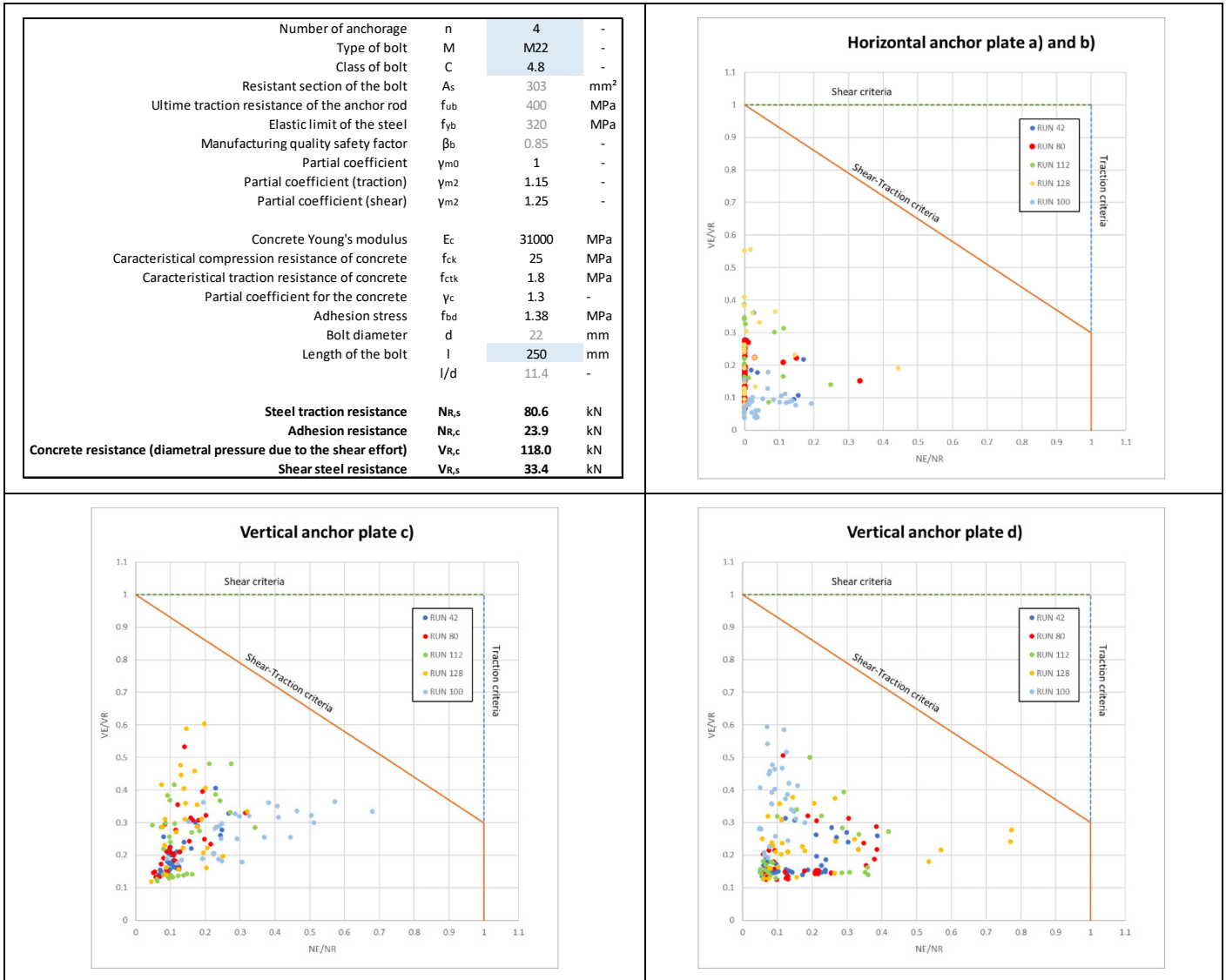
For vertical anchorage plates, the shear demand is calculated with the forces along the X and Z axes for configuration c, and along the Y and Z axes for configuration d. Thus, one verification is realised for each configuration.

The eccentricities of the forces with respect to the centre of the plate (and thus the bending moments) are neglected, as well as the lever arms.

Concerning configuration d, this leads to the simplification that is done between the top and the bottom scheme. The bottom scheme is a more realistic anchorage configuration where the bottom flange of the runway beam can be fixed to a first horizontal plate (which brings us back to configurations a or b), which is fixed to a second vertical plate that is anchored to the concrete wall.

Verifications are assessed considering four 22 mm diameter rods per anchoring plate. The length of these rods is equal to 250 mm. The results of the anchorage checks are presented in Figure 6.2 and show that the failure criteria are verified.

Figure 6.2. Anchorage verifications



It should be kept in mind that this comparison of the forces calculated in the load cell blocks by the participants to the resistant forces of standard anchorage configurations that have been retained is an exercise that aims to show what can be done. Nevertheless, the question of the robustness of the bridge crane is more complex; it is necessary to look at the anchoring of the rails since there are countless configurations.

Finally, it should be noticed that the configuration selected for this test campaign on the mock-up and then the forces measured on the load cell blocks remain difficult to extrapolate to any overhead crane configurations.

7. Concluding remarks and recommendations

7.1. Conclusions

The main conclusions that were made during the benchmark final workshop can be summarised as follows:

- The global dynamics of overhead cranes can be captured with different models, from the simplest to the most complex, and with different types of elements. Indeed, a detailed description of the crane geometry does not seem to be necessary if the physics of local impacts and frictional sliding are adequately represented. In addition, the model should capture the fundamental frequencies in all three directions.
- It is not possible to exactly reproduce (even experimentally) the dynamic response of the crane since this problem is highly nonlinear and small variations in the initial crane position and in the sliding parameters can disproportionately affect the response. The experiments showed that the initial conditions and the input signals are not the same even for repetitive tests. Considering the different models and methodologies used by participants, scattering on engineering demand parameters (EDPs) (max. accelerations, support reactions, displacements) were assessed, and appeared to be significant.
- The linear calculations are generally conservative with respect to the support forces since sliding is a significant source of energy dissipation. However, it is not easy to make general statements on the conservatism of linear models since the forces arising from horizontal and vertical impacts are sensitive to the input motion and gap widths and therefore afflicted with uncertainties.

7.2. Recommendations

Below are the recommendations for nonlinear dynamic analyses of bridge cranes that emerged from the SOCRAT benchmark.

- **R1:** Given the significant influence of friction between the wheels and the rails, it is recommended to carry out a sensitivity study considering:
 - a range of values for the friction coefficients;
 - an asymmetry in friction coefficients (between two facing rails, and between rails of the girder beams and of the runway beams);
 - a bi-axial sliding (longitudinal and transversal).
- **R2:** Given the significant influence of gaps between the wheels and the lateral faces of the rails, and the variability of the initial position of the crane, it is recommended to carry out sensitivity study considering the influence of:
 - different lateral gaps between the faces of the wheels and rails (symmetric and non-symmetric for two rails facing each other);
 - different initial positions of the crane (centred, decentred).

- **R3:** Since reduced models (less elements, discrete elements) provide relevant results in terms of general behaviour of the overhead crane, sensitivity/statistical studies should be performed considering the following uncertain quantities:
 - friction coefficients
 - gaps (wheels/rails)
 - initial position
 - material properties
 - damping
 However, to prove the load-bearing capacity of the components of the crane system, sufficiently fine modelling of the crane geometry is still required.
- **R4:** Given the fact that horizontal support excitations causing rocking movements in the bridge cranes (and thus different vertical excitations at each support) may lead to the wheels' uplift, it is recommended to consider the vertical motion imposed at the supports:
 - at least considering rigidly bound supports (rigid body) but imposing rotational motion and vertical motion (in addition to horizontal motion) to the rigidly bound supports;
 - at best by imposing the differential movement on each support (multi-supported).
- **R5:** If the calculation method retained is on a modal basis, it is necessary to consider both rigid body modes as well as the deformation modes. In this case it is important to not overdamp the rigid body modes. For calculations performed on a physical basis with Rayleigh global damping, it is important to remove the coefficient proportional to the mass matrix as soon as the system is allowed to slide, in order not to overdamp the rigid body modes.

Other remarks based on the discussions with the participants during the closing workshop deserve to be mentioned, e.g. the question of the loads' combination for a seismic verification, especially when a lifting load is considered. The clarification of these topics remains an important matter that should be investigated in the future.

References

- Bahr, L., J. Arndt and J. Sievers (2022), “Simulation of a crane bridge mock-up under seismic loading within the SOCRAT benchmark”, *26th International Conference on Structural Mechanics in Reactor Technology, Berlin/Potsdam, Germany, July 2022.*
- Bitar, I., B. Richard and E. Viallet (2021), “Dynamic behaviour of crane bridges - presentation of the OECD/NEA international benchmark 2020”, *17th World Conference on Earthquake Engineering, Sendai International Centre, Sendai, Japan, Oct. 2021.*
- Bitar, I., B. Richard and E. Viallet (2019), “Benchmark International sur le Comportement dynamique des ponts roulants”, Colloque National, AFPS’19, Strasbourg, France, Sept. 2019.
- Borgerhoff, M. et al. (2022), “Numerical Simulations of the Nonlinear Seismic Interaction of Bridge Crane Components in the SOCRAT Benchmark”, *26th International Conference on Structural Mechanics in Reactor Technology, Berlin/Potsdam, Germany, July 2022.*
- Brun, M., L. Sijia and A. Gravouil (2022), “Explicit/Implicit co-simulation of bridge cranes under earthquake using heterogeneous asynchronous time integrator for frictional contact/impact problems”, *26th International Conference on Structural Mechanics in Reactor Technology, Berlin/Potsdam, Germany, July 2022.*
- Colomb, J. et al. (2022), “Modelling of the seismic behaviour of nuclear overhead cranes – EGIS contribution to SOCRAT benchmark”, *26th International Conference on Structural Mechanics in Reactor Technology, Berlin/Potsdam, Germany, July. 2022.*
- EPRI (2005a), “Directives de vérification sismique des ponts roulants à partir de données historiques - Procédure de contrôle sismique - Rapport Final”, Note EPRI 1012022, vol. I. 2005.
- EPRI (2005b), “Directives de vérification sismique des ponts roulants à partir de données historiques - Comportement de quelques ponts roulants lors de tremblements de terre de forte amplitude - Rapport final”, Note EPRI 1012022, vol. II 2005.
- Feau, C. et al. (2015), “Experimental and numerical investigation of the earthquake response of crane bridges”, *Engineering Structures*, pp. 89-101, 2015.
- Ghadimi, S. et al. (2022), “SOCRAT Benchmark: Seismic Analyses of an Overhead Crane in LS-DYNA”, *26th International Conference on Structural Mechanics in Reactor Technology, Berlin/Potsdam, Germany, July 2022.*
- Rodriguez, J. et al. (2022), “Modelling of an Overhead Crane under Seismic Excitations (SOCRAT)”, *26th International Conference on Structural Mechanics in Reactor Technology, Berlin/Potsdam, Germany, July 2022.*
- UIC and AFPS (2014), “Guide Structures - Support”, DT 111, Union de Industries Chimiques (UIC) and Association Francais de Génie Parasismique (AFPS), May 2014.